

การสังเคราะห์โซเดียมซีโอไลต์จากไดอะตอมไมต์ลำปาง
เพื่อใช้ในการกำจัดไอออนแอมโมเนียม

นายอภิรักษ์ ชัยเสนา

วิทยานิพนธ์นี้เป็นส่วนหนึ่งของการศึกษาตามหลักสูตรปริญญาวิทยาศาสตรดุษฎีบัณฑิต

สาขาวิชาเคมี

มหาวิทยาลัยเทคโนโลยีสุรนารี

ปีการศึกษา 2547

ISBN 974-533-358-1

**SYNTHESIS OF SODIUM ZEOLITES FROM
LAMPANG DIATOMITE APPLIED FOR
AMMONIUM ION REMOVAL**

Mr. Aphiruk Chaisena

**A Thesis Submitted in Partial Fulfillment of the Requirements
for the Degree of Doctor of Philosophy in Chemistry**

Suranaree University of Technology

Academic Year 2004

ISBN 974-533-358-1

**SYNTHESIS OF SODIUM ZEOLITES FROM
LAMPANG DIATOMITE APPLIED FOR
AMMONIUM ION REMOVAL**

Suranaree University of Technology has approved this thesis submitted in partial fulfillment of the requirements for the Degree of Doctor of Philosophy.

Thesis Examining Committee

Malee Tangsathitkulchai

(Asst. Prof. Dr. Malee Tangsathitkulchai)

Chairperson

K. Kunwadee Rangriwatananon

(Asst. Prof. Dr. Kunwadee Rangriwatananon)

Member (Thesis Advisor)

Nurak Grisdanurak

(Assoc. Prof. Dr. Nurak Grisdanurak)

Member

Visit Vao-soongnern

(Asst. Prof. Dr. Visit Vao-soongnern)

Member

Tongraar An

(Asst. Prof. Dr. Anan Tongraar)

Member

Sarawut Sujitjorn

(Assoc. Prof. Dr. Sarawut Sujitjorn)

P. Suebka

(Assoc. Prof. Dr. Prasart Suebka)

Vice Rector for Academic Affairs

Dean of Institute of Science

อภิรักษ์ ชัยเสนา : การสังเคราะห์โซเดียมซีโอไลต์จากโคอะตอไมต์ลำปางเพื่อใช้ในการกำจัดไอออนแอมโมเนียม (SYNTHESIS OF SODIUM ZEOLITES FROM LAMPANG DIATOMITE APPLIED FOR AMMONIUM ION REMOVAL) อาจารย์ที่ปรึกษา : ผู้ช่วยศาสตราจารย์ ดร.กมลวิ รัมย์วัฒนานนท์, 161 หน้า. ISBN 974-533-358-1

ได้เตรียมโซเดียมซีโอไลต์จากโคอะตอไมต์ธรรมชาติและโคอะตอไมต์ที่คัดแปรโดยวิธีไฮโดรเทอร์มัลภายใต้ความดันไอของสารที่ใช้ ณ อุณหภูมิที่ศึกษา โซเดียมซีโอไลต์ที่สังเคราะห์ได้จะใช้ในการกำจัดไอออนแอมโมเนียมในน้ำ เพราะไอออนแอมโมเนียมมีอันตรายต่อสุขภาพของมนุษย์ในการศึกษาได้ใช้โคอะตอไมต์ที่แตกต่างกัน 6 ชนิด ปัจจัยที่ศึกษาคือ ความเข้มข้นของสารละลายโซเดียมไฮดรอกไซด์ อุณหภูมิ อัตราส่วนระหว่างของแข็งต่อสารละลายและเวลาที่ใช้ในการทำปฏิกิริยา ผลิตภัณฑ์ซีโอไลต์ที่ได้จากการทดลองคือ โซเดียมพี-1, อะนัลซิม, แคนคริไนต์ และไฮดรอกซีโซดาไลต์ ในการสังเคราะห์โดยใช้สภาวะเดียวกัน กรดซัลฟิวริกร้อนที่มีความเข้มข้น 6 โมลาร์ และ การเผาที่อุณหภูมิ 1100 องศาเซลเซียส จะช่วยให้เกิดผลิตภัณฑ์มากที่สุดในขณะที่อัตราส่วนของแข็งต่อสารละลายมีผลน้อยมาก สภาวะที่เหมาะสมสำหรับการสังเคราะห์ซีโอไลต์โซเดียมพี-1 คือ $12.5\text{Na}_2\text{O} : 1.4\text{Al}_2\text{O}_3 : 12\text{SiO}_2 : 552\text{H}_2\text{O}$ โดยโมล เวลาในการสังเคราะห์ 144 ชั่วโมงที่อุณหภูมิ 100 องศาเซลเซียส สำหรับการสังเคราะห์ซีโอไลต์อะนัลซิม คือ $12.5\text{Na}_2\text{O} : 1.4\text{Al}_2\text{O}_3 : 12\text{SiO}_2 : 552\text{H}_2\text{O}$ เวลาในการสังเคราะห์ 132 ชั่วโมงที่อุณหภูมิ 140 องศาเซลเซียส สภาวะดีที่สุดสำหรับการสังเคราะห์ซีโอไลต์แคนคริไนต์ คือ อัตราส่วนโดยโมล $75\text{Na}_2\text{O} : 1.4\text{Al}_2\text{O}_3 : 12\text{SiO}_2 : 1623\text{H}_2\text{O}$ เวลาในการสังเคราะห์ 72 ชั่วโมงที่อุณหภูมิ 180 องศาเซลเซียสและซีโอไลต์ไฮดรอกซีโซดาไลต์ $112.5\text{Na}_2\text{O} : 1.4\text{Al}_2\text{O}_3 : 12\text{SiO}_2 : 1579\text{H}_2\text{O}$ เวลาในการสังเคราะห์ 96 ชั่วโมงที่อุณหภูมิ 100 องศาเซลเซียส

ได้นำโซเดียมซีโอไลต์ที่ได้ไปศึกษาการกำจัดไอออนแอมโมเนียมด้วยกระบวนการดูดซับ ซึ่งพบว่าแลงเมียร์ไอโซเทอร์มมีความเหมาะสมกับข้อมูลของผลการทดลองซีโอไลต์อะนัลซิมในขณะที่ฟรอยด์ลิกไอโซเทอร์มจะใช้ได้ดีในการอธิบายข้อมูลการทดลองของซีโอไลต์โซเดียมพี-1 แคนคริไนต์ และ ไฮดรอกซีโซดาไลต์

สาขาวิชาเคมี
ปีการศึกษา 2547

ลายมือชื่อนักศึกษา _____
ลายมือชื่ออาจารย์ที่ปรึกษา _____
ลายมือชื่ออาจารย์ที่ปรึกษาร่วม _____

APHIRUK CHAISENA : SYNTHESIS OF SODIUM ZEOLITES FROM
LAMPANG DIATOMITE APPLIED FOR AMMONIUM ION REMOVAL.
THESIS ADVISOR : ASST. PROF. KUNWADEE RANGSRIWATANANON,
Ph.D. 161 PP. ISBN 974-533-358-1

Sodium zeolites were synthesized from natural and/or modified diatomites by conventional hydrothermal method under autogenous pressure. The synthesized sodium zeolites will be used for ammonium ion removal from water since the presence of ammonium ion will threaten human health. The study was carried out from 6 different sources of diatomites. Studied parameters were NaOH concentration, temperature, solid/liquid ratio and reaction time. Products of the reaction were Na-P1, analcime, cancrinite and hydroxysodalite. Under the same condition, hot 6M H₂SO₄ and calcination at 1100 °C would assist the reaction to maximize the products, while solid/liquid ratio did not show any production effect. Optimal conditions for each zeolite were 12.5Na₂O : 1.4Al₂O₃ : 12SiO₂ : 552H₂O with 144 hours 100 °C for Na-P1 zeolite, 12.5Na₂O : 1.4Al₂O₃ : 12SiO₂ : 552H₂O with 132 hours 140 °C for analcime zeolite, 75Na₂O : 1.4Al₂O₃ : 12SiO₂ : 1623 H₂O with 72 hours 180 °C for cancrinite zeolite, and 112.5Na₂O : 1.4Al₂O₃ : 12SiO₂ : 1579H₂O with 96 hours 100 °C for hydroxysodalite zeolite.

Application of ammonium ion removal was applied through the adsorption process. Langmuir isotherm could apply for analcime while Freundlich isotherm applied only to Na-P1, cancrinite and hydroxysodalite.

School of Chemistry

Student's Signature_____

Academic Year 2004

Advisor's Signature_____

Co-advisor's Signature_____

Acknowledgements

The success and culmination of this thesis is due to the help received from many people that I would like to express my gratitude.

I would like to thank my advisor, Assistant Professor Dr. Kunwadee Rangsiwatananon, who gave me the opportunity to enhance my knowledge, encouragement, guidance and support throughout this thesis. The true value of all I learned from her during my five years at Suranaree University of Technology goes far beyond what is presented here. I also owe debt of gratitude to Associate Professor Dr. Nurak Grisdanurak for serving as the co-advisor, and to all my thesis committee members, Assistant Professor Dr. Visit Vao-soongnern and Assistant Professor Dr. Anan Tongraar for their valuable and grateful direction, suggestion and criticism.

My thanks go to the Chairman of School of Chemistry, Assistant Professor Dr. Malee Tungsathikulchai for serving as the chairman of the committee and all lecturers at the School of Chemistry for their suggestions and encouragement. I wish to thank all the graduate students of the School of Chemistry for their invaluable professional guidance and friendly encouragement.

I also wish to thank Associate Professor Dr. Andrew Whittaker of The University of Queensland for access to the solid-state NMR spectrometer, and Associate Professor Dr. Ray L Frost of Queensland University of Technology for his kind suggestions on FT-IR and Peakfit program.

In addition, I wish to express my special thanks to the Office of Rajabhat Institute Council (ORIC) for the main offering the scholarship, Institute of research and

development at Suranaree University of Technology for their supporting and Lampang Rajabhat University support for providing a visiting scholarship at The University of Queensland and Queensland University of Technology, Australia.

Last but not least, I would like to thank my wife and children for their love, support, encouragement and patience. Mom and Dad, with all my heart, thank you.

Aphiruk Chaisena

Contents

	Page
Abstract in Thai	I
Abstract in English.....	II
Acknowledgements	III
Contents	V
List of Tables	IX
List of Figures.....	XI
List of Abbreviations	XVIII
Chapters	
I Introduction	1
1.1 General description of zeolite	3
1.2 General scheme of zeolite synthesis	10
1.2.1 Achievement of supersaturation	12
1.2.2 Nucleation.....	13
1.2.3 Crystal growth.....	13
1.3 Sodium zeolite	14
1.4 Sodium zeolite applications	14
1.4.1 Ion exchange	15
1.4.2 Molecular sieves	16
1.5 Diatomite.....	17
1.6 Characterization techniques	20
1.6.1 Powder X-ray diffraction	20

Contents (Continued)

	Page
1.6.2 X-ray fluorescence	21
1.6.3 Fourier transform infrared spectroscopy.....	22
1.6.4 Scanning electron microscope	23
1.6.5 Magic angle spinning nuclear magnetic resonance spectroscopy.....	24
1.6.6 Ultraviolet and visible spectrometry.....	26
1.7 Adsorption	27
1.7.1 Adsorption model.....	29
1.7.1.1 Langmuir adsorption model.....	30
1.7.1.2 Freundlich adsorption model	30
1.8 Ammonium ion	31
1.9 Research objectives.....	32
II Literature reviews.....	34
2.1 Synthesis of zeolites from diatomite.....	34
2.2 The ammonium ion removal by synthetic zeolites	37
III Materials, instrumentation and experimental procedures.....	41
3.1 Material lists	41
3.1.1 Chemical and materials.....	41
3.1.2 Glasswares	43
3.1.3 Apparatus	44
3.2 Instrumentation	45
3.2.1 Particle size analyzer.....	45
3.2.2 X-ray fluorescence spectrometer	45

Contents (Continued)

	Page
3.2.3 X-ray powder diffraction	46
3.2.4 Fourier transform infrared spectroscopy.....	47
3.2.5 Scanning electron microscope	48
3.2.6 Thermogravimetric analysis.....	48
3.2.7 Solid-state nuclear magnetic resonance spectroscopy	48
3.2.8 Ultraviolet and visible (UV-Vis) spectroscopy.....	49
3.3 Experimental methods	49
3.3.1 Diatomite preparation	49
3.3.2 Calcination and acid treatment.....	49
3.3.3 The sodium zeolites synthesis method.....	50
3.3.4 Analytical method for ammonium ion.....	51
3.3.5 Batch studies of ammonium removal	53
3.3.6 Cation exchange capacity	54
IV Results and Discussion	57
4.1 Morphology and particle size of diatomite	57
4.2 Diatomite composition analysis.....	58
4.3 Diatomite characterization	58
4.4 Calcination and acid treatment of diatomite	62
4.4.1 Calcination of diatomite.....	62
4.4.2 Acid treatment of diatomite	72
4.5 Starting diatomite materials for synthesis of sodium zeolites	78
4.6 The synthesis of sodium zeolite.....	87

Contents (Continued)

	Page
4.6.1 Effect of the starting materials	105
4.6.2 Effect of the alkalinity concentration, the solid/liquid ratio and the reaction temperature.....	109
4.7 Ammonium removal from aqueous solution by sodium zeolite obtained	122
4.8 Cation exchange capacity	132
V Conclusions	134
References.....	137
Appendices.....	146
Appendix A Simulated XRD powder patterns for zeolites.....	147
Appendix B Atlas of zeolite structure types	152
Curriculum Vitae	161

List of Tables

Table	Page
1.1 The seven groups of secondary building unit (SBU).....	7
4.1 The chemical compositions of natural diatomite sample determined by WDXRF	58
4.2 Identification of IR absorption bands to specific vibrations.....	61
4.3 Particle size distribution of calcined diatomite.....	64
4.4 The chemical compositions and Si/Al ratios of calcined diatomite.....	70
4.5 The total dissolution percentages of diatomite	74
4.6 The chemical compositions and Si/Al ratios of acid activation of diatomite compared to the natural diatomite determined by XRF	76
4.7 X-ray diffraction analyses of thermal and acid treatment natural diatomite samples.....	77
4.8 The mean particle size of starting diatomite materials	80
4.9 Chemical shift (ppm) ^{29}Si MAS NMR in diatomite samples	82
4.10 Percentage of Q^n (silicon coordination) in diatomite samples (results from ^{29}Si MAS NMR).....	82
4.11 Zeolitic phase synthesized from starting diatomite materials using NaOH as activation agents, with the chemical composition reported in collection of simulated XRD patterns for zeolites	87
4.12 Reflections (h, k, l), 2θ and $[I_{\text{rel}}]$ used in the integration procedure for each zeolite phase	88

List of Tables (Continued)

Table	Page
4.13 Experimental conditions used for synthesis experiments by natural diatomite material and sodium zeolites obtained.....	89
4.14 Experimental conditions used for synthesis experiments by calcined diatomite material at 900 °C and sodium zeolites obtained.....	90
4.15 Experimental conditions used for synthesis experiments by calcined diatomite material at 1000 °C and sodium zeolites obtained.....	92
4.16 Experimental conditions used for synthesis experiments by calcined diatomite material at 1100 °C and sodium zeolites obtained.....	93
4.17 Experimental conditions used for synthesis experiments by diatomite material treated with 6M H ₂ SO ₄ and sodium zeolites obtained.....	95
4.18 Experimental conditions used for synthesis experiments by diatomite material first treated with 6M H ₂ SO ₄ then calcined at 1100 °C and sodium zeolites obtained.....	96
4.19 Zeolitic material synthesized as a function of reaction parameters	110
4.20 Infrared absorption bands (cm ⁻¹) for each sodium zeolites from references and the experiments	117
4.21 Langmuir and Freundlich models parameters for best fit and corresponding correlation coefficients.....	130

List of Figures

Figure	Page
1.1 The primary building unit	6
1.2 The secondary building unit (SBU) in zeolite structures	6
1.3 The units linked to each other by sharing all of their oxygen atoms	7
1.4 Principle of zeolite synthesis	10
1.5 The solubility-supersolubility diagram	12
1.6 Structure of silica surface depicting the various types of bonds and silanol groups	18
1.7 The hydroxyl structure and the dehydration process of diatomite	19
1.8 The magic-angle spinning motion	25
1.9 Schematic of the Beer-Lambert Law	27
1.10 Types of equilibrium sorption; q_e = amount sorbed and C_e = amount in solution	29
4.1 SEM micrograph of diatomite samples with 10 kV 1000 and 5000 magnification	57
4.2 The thermogravimetric (DTA/TGA/TGD) curves for the natural diatomite	60
4.3 XRD pattern of the natural diatomite compared with the standard pattern from JCPDS database	60
4.4 FT-IR spectra of the natural diatomite	61
4.5 XRD patterns of calcined diatomite (a) natural diatomite calcined at 900 °C with a heating rate of 16 °C min ⁻¹ for 1,3,5 and 10 hours (b) natural diatomite calcined at 900 °C with a heating rate of 8 °C min ⁻¹ for 1, 3, 5 and 10 hours	65

List of Figures (Continued)

Figure	Page
4.6 XRD patterns of calcined diatomite (a) natural diatomite calcined at 1000 °C with a heating rate of 16 °C min ⁻¹ for 1,3,5 and 10 hours (b) natural diatomite calcined at 1000 °C with a heating rate of 8 °C min ⁻¹ for 1, 3, 5 and 10 hours	65
4.7 XRD patterns of calcined diatomite (a) natural diatomite calcined at 1100 °C with a heating rate of 16 °C min ⁻¹ for 1,3,5 and 10 hours (b) natural diatomite calcined at 1100 °C with a heating rate of 8 °C min ⁻¹ for 1, 3, 5 and 10 hours	66
4.8 IR transmission spectra for natural diatomite after calcination at 900 °C with a heating rate of 16 °C min ⁻¹ and 8 °C min ⁻¹ for 1, 3, 5 and 10 hours compared to the natural diatomite sample	68
4.9 IR transmission spectra for natural diatomite after calcination at 1000 °C with a heating rate of 16 °C min ⁻¹ and 8 °C min ⁻¹ for 1, 3, 5 and 10 hours compared to the natural diatomite sample	68
4.10 IR transmission spectra for natural diatomite after calcination at 1100 °C with a heating rate of 16 °C min ⁻¹ and 8 °C min ⁻¹ for 1, 3, 5 and 10 hours compared to the natural diatomite sample	69
4.11 IR transmission spectra for natural diatomite after calcination at 900, 1000 and 1100 °C with a heating rate of 16 °C min ⁻¹ for 5 hours compared to the natural diatomite sample	69
4.12 SEM micrographs of calcined diatomite obtained after calcination at 900, 1000 and 1100 °C with a heating of 16 °C min ⁻¹ for 5 hours.....	71
4.13 The total dissolution percentages of the material in cold acidic	75

List of Figures (Continued)

Figure	Page
4.14 The total dissolution percentages of the material in hot acidic.....	75
4.15 XRD patterns of diatomite treated with hot reflux (a) 6M HNO ₃ (b) 6M HCl and (c) 6M H ₂ SO ₄ for 24 hours.....	76
4.16 IR transmission spectra for diatomite after hot acid activation for 24 hours compared to the natural diatomite sample	77
4.17 SEM micrograph of acid activation (reflux 100 °C 24 hours) for (a) 6M H ₂ SO ₄ (b) 6M HCl (c) 6M HNO ₃ with 5000x and 1000x magnification.....	79
4.18 Particle size distribution of starting material for synthesise sodium zeolite	80
4.19 Experimental (A) and simulated (B) MAS ²⁹ Si-NMR spectra (arbitrary intensity unit) of the various diatomite samples (a) natural diatomite (b) diatomite calcined 900 °C, (c) diatomite calcined 1000 °C, (d) diatomite calcined 1100 °C, (e) diatomite treated with hot (reflux) 6M H ₂ SO ₄ and (f) diatomite treated with hot (reflux) 6M H ₂ SO ₄ and calcined at 1100 °C.....	83
4.20 The percentage of Q ² , Q ³ (total) and Q ⁴ (total) from simulation of the ²⁹ Si MAS NMR spectra of starting diatomite materials (1) natural diatomite (2) diatomite calcined at 900 °C (3) diatomite calcined at 1000 °C (4) diatomite calcined at 1100 °C (5) diatomite treated with hot 6M H ₂ SO ₄ and (6) diatomite first treated with hot 6M H ₂ SO ₄ then calcined at 1100 °C	84
4.21 Diatomite starting material	85
4.22 Diatomite calcined at 900 °C for starting material.....	85
4.23 Diatomite calcined at 1000 °C for starting material.....	85
4.24 Diatomite calcined at 1100 °C for starting material.....	86
4.25 Diatomite treated with hot 6M H ₂ SO ₄ for starting material	86

List of Figures (Continued)

Figure	Page
4.26 Diatomite first treated with hot 6M H ₂ SO ₄ then calcined at 1100 °C for starting material	86
4.27 Zeolite products obtained from natural diatomite starting material.....	99
4.28 Zeolite products obtained from diatomite calcined at 900 °C.....	100
4.29 Zeolite products obtained from diatomite calcined at 1000 °C.....	101
4.30 Zeolite products obtained from diatomite calcined at 1100 °C.....	102
4.31 Zeolite products obtained from diatomite treated with hot 6M H ₂ SO ₄	103
4.32 Zeolite products obtained from diatomite treated with acid and thermal	104
4.33 Na-P1 XRD peaks obtained from the reaction of each diatomite materials activated at 100 °C with 10 % NaOH concentrations, S/L=1/10 for 120 hours.....	106
4.34 Analcime XRD peaks obtained from the reaction of each diatomite materials activated at 140 °C with 10 % NaOH concentrations, S/L=1/10 for 120 hours.....	106
4.35 Cancrinite XRD peaks obtained from the reaction of each diatomite materials activated at 180 °C with 20 % NaOH concentrations, S/L=1/30 for 72 hours.....	107
4.36 Hydroxysodalite XRD peaks obtained from the reaction of each diatomite materials activated at 100 °C with 30 % NaOH concentrations, S/L=1/30 for 120 hours.....	107
4.37 XRD patterns of Na-P1 zeolite obtained in activated with 10 % NaOH concentration, S/L=1/10 and reaction temperature 100 °C for various times	111

List of Figures (Continued)

Figure	Page
4.38 XRD patterns of analcime zeolite obtained in activated with 10 % NaOH concentration, S/L=1/10 and reaction temperature 140 °C for various times	111
4.39 XRD patterns of cancrinite zeolite obtained in activated with 20 % NaOH concentration, S/L=1/30 and reaction temperature 180 °C for various times	112
4.40 XRD patterns of hydroxysodalite zeolite obtained in activated with 30 % NaOH concentration, S/L=1/30 and reaction temperature 100 °C for various times	112
4.41 The XRD intensity of Na-P1 zeolite obtained from the activated with 10 % NaOH concentration, S/L=1/10 and reaction temperature 100 °C for 96, 108, 120, 132, 144 and 156 hours	114
4.42 The XRD intensity of analcime zeolite obtained from the activated with 10 % NaOH concentration, S/L=1/10 and reaction temperature 140 °C for 84, 96, 108, 120, 132 and 144 hours	114
4.43 The XRD intensity of cancrinite zeolite obtained from the activated with 20 % NaOH concentration, S/L=1/30 and reaction temperature 180 °C for 48, 60, 72, 96 and 108 hours	115
4.44 The XRD intensity of hydroxysodalite zeolite obtained from the activated with 30 % NaOH concentration, S/L=1/30 and reaction temperature 100 °C for 84, 96, 108, 120, 132 and 144 hours	115
4.45 IR spectra of each sodium zeolite from diatomite starting material treated with maximum efficiency of synthesis	116

List of Figures (Continued)

Figure	Page
4.46 SEM micrograph of Na-P1 zeolite.....	119
4.47 SEM micrograph of analcime zeolite	119
4.48 SEM micrograph of cancrinite zeolite	120
4.49 SEM micrograph of hydroxysodalite zeolite	120
4.50 The particle size distributions of sodium zeolites obtained	121
4.51 Calibration curve of standard nessler reagent.....	122
4.52 Plot of initial ammonium concentration in the aqueous solution on the exchange capacity of diatomite at 25 °C and pH 6.5	124
4.53 Plot of initial ammonium concentration in the aqueous solution on the exchange capacity of Na-P1 zeolite at 25 °C and pH 6.5	124
4.54 Plot of initial ammonium concentration in the aqueous solution on the exchange capacity of analcime zeolite at 25 °C and pH 6.5	125
4.55 Plot of initial ammonium concentration in the aqueous solution on the exchange capacity of cancrinite zeolite at 25 °C and pH 6.5.....	125
4.56 Plot of initial ammonium concentration in the aqueous solution on the exchange capacity of hydroxysodalite zeolite at 25 °C and pH 6.5.....	126
4.57 Linearised Freundlich isotherm (a) and Linearised Langmuir isotherm (b) for ammonium removal by natural raw diatomite.....	128
4.58 Linearised Freundlich isotherm (a) and Linearised Langmuir isotherm (b) for ammonium removal by Na-P1 zeolite	128
4.59 Linearised Freundlich isotherm (a) and Linearised Langmuir isotherm (b) for ammonium removal by analcime zeolite.....	129

List of Figures (Continued)

Figure	Page
4.60 Linearised Freundlich isotherm (a) and Linearised Langmuir isotherm (b) for ammonium removal by cancrinite zeolite	129
4.61 Linearised Freundlich isotherm (a) and Linearised Langmuir isotherm (b) for ammonium removal by hydroxysodalite zeolite	129
4.62 The ammonium ion removal efficiency of natural diatomite material and each sodium zeolite material.....	132

List of Abbreviations

XRD	X-ray diffractometer
WDXRF	wavelength dispersive X-ray fluorescence
FT-IR	fourier transform infrared spectroscopy
SEM	scanning electron microscope
DTA	differential thermal analysis
TGA	thermogravimetric analysis
MAS NMR	magic angle spinning nuclear magnetic resonance spectroscopy
°C	degree celcius
Å	angstrom
µm	micrometer
cps	count per second
conc	concentrated
CEC	cation exchange capacity
cm ⁻¹	per centimeter
kV	kilovolt
w/v	weight by volume
ANA	analcime
CAN	cancrinite
HS	hydroxysodalite

Chapter I

Introduction

Sodium zeolites have been found as an important industrial application in many areas such as adsorption, separation, catalytic cracking, etc. They may be obtained from both natural deposits and laboratory synthesis. Generally, sodium zeolites are synthesized from freshly prepared sodium aluminosilicate gel, from various silica and alumina sources by a hydrothermal treatment. In the last decades, intensity research has focused on the use of other starting natural materials for zeolite synthesis. The rapid increase in the consumption of zeolites calls for further work aiming at still cheaper raw materials for its synthesis. Clay mineral is one that can constitute raw material. The synthesis of zeolites from kaolin is well-known and other raw materials such as high silica bauxites, halloysites, interstratified illite-smectite, montmorillonites, bentonite and diatomite are also used for the synthesis of zeolites (Sidneswaran and Bhat, 1997; Ruiz et al., 1997; Baccouche, Srasra and Maaoui, 1998; Biswajit, Dinesh and Subhash, 1994; Gualtieri, 2001; Boukadir, Bettahar and Derriche, 2002). Naturally occurring zeolites and their synthetic counterparts are an extremely important class of materials. They are products of reactions between volcanic ashes and the alkaline solutions associated with types of rock strata. Accordingly, the rate of zeolite formation is limited by the fact that reaction temperatures and pressures are quite low and soil solutions are only slight alkaline. However, the use of hydrothermal processing techniques, more concentrate solutions

and templating agents can shorten the synthesis times (Michaelw and Darryl, 1997; Anand and Michael, 1999). The first recorded attempt at zeolite synthesis was by St Clair Deville in 1862 who heated solutions of potassium silicate and sodium aluminate together at 170 °C, was to produce Levynite. Despite many preparations in the interim, it was Barrer who is usually credited for having first systematically synthesized zeolites in the early 1940s and made a push to those studies represented by developing the field of X-ray identification methods. In particular, Barrer and his co-workers combined SiO₂ and Al₂O₃ units using hydrothermal methods and obtained zeolites L, K, chabasite, mordenite and many others. Often overlooked was the fact that this work, in turn, depended on the first demonstration by Milton of Union Carbide (USA) in 1949, that zeolites could be synthesized using low temperature hydrothermal methods. At that time, a major emphasis was placed on mimicking those conditions under which the zeolites of volcanic origin were presumed to have been formed, i.e. high temperatures and salt concentrations and autogenous pressures. Preparing zeolites by simply loading a gel with components in pre-arranged proportions into sealed glass vials and then into a closed stainless steel ‘bomb’, or alternatively into a ‘bomb’ lined with inert material, now usually teflon at that time was a dramatic change. Such bombs are now commercially available and the turning of temperature and pressure is a routine.

The formation of zeolites from natural low-cost silica-alumina sources provides an opportunity for upgrading materials with high added value and possible utilization in a new application. Diatomite is an important source of silica-alumina, which, on leaching with sodium hydroxide, offers great potentialities for its use in the synthesis of sodium zeolites. However, the synthesis of zeolites from diatomite is a structurally

and chemically complicated problem and depends on a large number of factors. No efforts have been made in the part to use diatomite as a source of silica and alumina to synthesize zeolites. In Thailand, diatomite is easily available in large quantities at an extremely low cost. The Thailand's Department of Mineral Resources (DMR) has found 5,000,000,000 tons of natural raw diatomite mainly in Lampang Province (Thai ceramic directory, 2001 - 2003). It is commonly used as a filtering material, the production of thermal insulation bricks, pet litter and as absorbents.

Because the synthesis of sodium zeolites from diatomite depends on a large number of factors, there are a few reports on the synthesis with available diatomite. In Thailand, there is no report on the synthesis of sodium zeolites from Thai diatomite or the detail of diatomite after physical and chemical activation. In this study, we use Lampang diatomite as a source of silica and alumina to synthesize sodium zeolites which are expensive and applicable to many fields. The main question is whether Lampang diatomite can be used as the raw material for the synthesis of sodium zeolites. This research has been set to investigate the possibility of using Lampang diatomite as the starting material for the synthesis of sodium zeolites. Part of this research focused on the optimum conditions for the synthesis of sodium zeolites and may have a significant application in removal ammonium ion in aqueous solution. From my point of view, this work may provide high value industrial products and slightly pave the way for Thailand's large-scale sodium zeolites production industry.

1.1 General description of zeolite

Zeolites are crystalline, hydrated aluminosilicate minerals found in volcanic and sedimentary rocks. In 1756 the Swedish mineralogist, Cronstedt who discovered

zeolites, named them for the Greek roots means “boiling stones” for their peculiar bubbling characteristic (Dryer, 1988; Cheetham and Peter, 1992). Since that time, about 50 different natural species have been recognized, and at least 150 species have been synthesized in the laboratory. Zeolites consisting of three dimensional framework structure were composed of TO_4 tetrahedra where $T = Si, Al$ (framework of $[SiO_4]^{4-}$ and $[AlO_4]^{5-}$ tetrahedra) as shown in Figure 1.1. These tetrahedra are the primary building units in all zeolite structures. Each sub unit contains the pores and cavities within the frameworks which were called secondary building units (SBU) and illustrated in Figure 1.2. The SBU can be simple arrangements of tetrahedra such as four, six, or eight-membered ring or more complex structure. The following classification is based on seven groups of SBU is given in Table 1.1. These units link to one another by sharing all of their oxygen atoms and illustrated in Figure 1.3 (Breck, 1974; Khodabandeh and Davis, 1997). Zeolites have the general chemical formula (Roland and Kleinschmit, 1997):



When formula (1) expression enclosed in the square brackets shows the composition of the anionic framework in the crystallographic unit cell, M represents the nonframework metal cation, n is its charge, z is the number of water molecules per unit cell, x and y are the total number of tetrahedra per unit cell and the ratio y/x usually has values of 1 - 5. Formula (2) occurs frequently in the literature and, unlike formula (1) where y' is 2 to 10, n is the cation (M) valence, and z' represents the water contained in the voids of the zeolite. The frameworks are open containing channels and cavities where cations and water molecules are located. The cations generally

have a high degree of mobility rising to facile ion exchange. The water molecules are readily lost and regained; this accounts for the well-known desiccant properties of zeolites. The crystalline structure of zeolites is unique and easily characterized. The assemblages of tetrahedra creating the porous structure of zeolites produce regular arrays of apertures. These apertures of such a size are able to selectively take up some molecules into the porous structure, whilst rejecting others on the basis of larger effective molecular dimensions. This characteristic zeolite property of molecular sieve is unique and responsible for the first commercial application of zeolites. Some carbons and silicas have molecular sieve properties; therefore, some non-aluminosilicate materials have been described as zeolitic materials because of their sieving behaviors. However, activated carbons, activated alumina, and silica gel do not possess an ordered crystal structure. Consequently the pores are nonuniform (Breck, 1974). Zeolite has a reversible dehydration property. That is, when zeolites are heated, water molecules in channels or cavities will evaporate but frameworks will not be deformed or damaged. After dehydration, the channels and cavities can be refilled with water molecules (Tomlinson, 1998).

Zeolites have an uniform pore size (0.3 nm to 1.0 nm), which is uniquely determined by the unit structure of the crystal. The various zeolite structures differ not only in the type and dimensionality of their pore systems, but also in the size of the pore apertures. Narrow-pore, medium-pore, and wide-pore zeolites have different pore apertures formed by rings of 8, 10 or 12 T atoms, corresponding to crystallographic diameters of 0.35 - 0.45, 0.45 - 0.60 and 0.60 - 0.80 nm, respectively (Breck, 1974). The properties and uses of zeolites are being explored in many scientific disciplines: modern inorganic and organic chemistry, physical chemistry,

oceanography, biochemistry, catalysis and in all types of chemical engineering process technology (Breck, 1974). Zeolites have a wide variety of applications including: (1) the removal of radioactive wastes; (2) the enhancement of cleaning efficiency of detergents; (3) the softening of water; (4) as deodorizers and moisture control agents for animal manures; and (5) as dietary supplements for animals and fishes (Payan, 1999). Utilization of zeolites in most industrial applications requires certain specifications. In this context, synthetic zeolites can be tailored to meet the strict specifications imposed on an adsorption and catalytic process. Moreover, during zeolite synthesis, a constant composition of the products can easily be maintained, whereas natural zeolites usually display remarkable chemical and mineralogical variations (Chistidis, Paspaliaris and Kontopoulos, 1999).

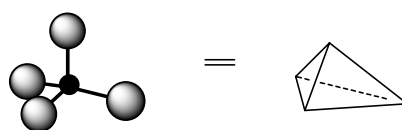


Figure 1.1 The primary building unit

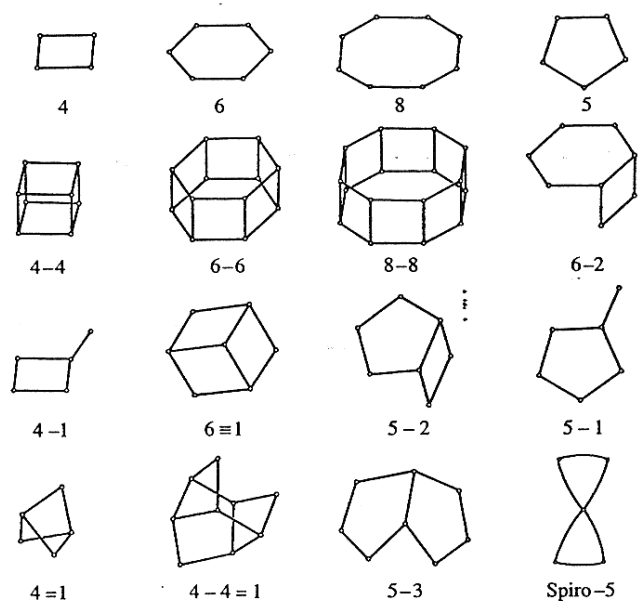
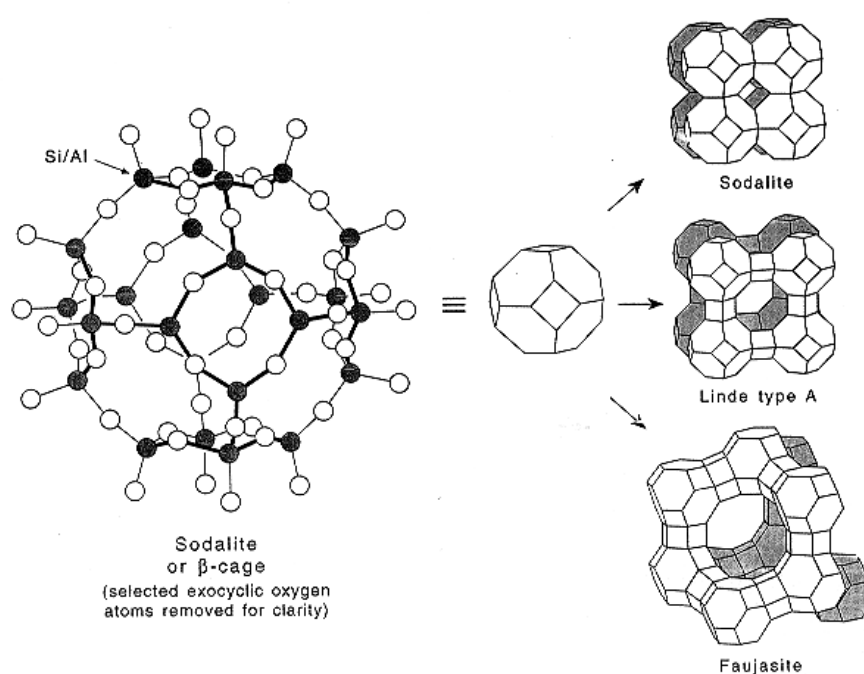


Figure 1.2 The secondary building unit (SBU) in zeolite structures

Table 1.1 The seven groups of secondary building unit (SBU)

Group	Secondary building unit (SBU)
1	Single 4-ring, S4R
2	Single 6-ring, S6R
3	Double 4-ring, D4R
4	Double 6-ring, D6R
5	Complex 4=1, T_5O_{10} unit
6	Complex 5-1, T_8O_{16} unit
7	Complex 4-1=1, $T_{10}O_{20}$ unit

**Figure 1.3.** The units linked to each other by sharing all of their oxygen atoms.

Natural zeolite minerals generally occur in regions of high temperatures, salt concentrations and autogenous pressures. These regions include saline alkaline lakes, cavities of basaltic and volcanic rocks. The less hydrous and denser zeolites such as laumontite and analcime were found in regions of higher temperatures and pressures. On the other hand, the more hydrous and less dense zeolites, such as chabazite and stilbite, occur at the temperatures below 100 °C. With an increasing pressure, as a result of increasing burial depth, the less dense zeolite becomes unstable and transformed into more dense zeolites. When burial depth increases anhydrous aluminosilicates, such as feldspars, rather than dense zeolites are found (Breck, 1974). In natural environments, the zeolite minerals are formed by the reaction of a solid phase with water solution. The volcanic glass is more reactive in zeolite mineral formation than crystalline materials because it is relatively more soluble. The hydroxyl ion can catalyze the crystallization of amorphous silica to quartz and consequently diminish the availability of silica (Breck, 1974). Generally, the solubility of silica-rich glass increases with increasing pH. Although pure zeolites are colorless, some mineral zeolites may be colored because of the presence of the finely divided oxides of metals or impurities. The natural zeolite structure has more acid resistant, so, it does not mildly break down acidic the environment. Therefore, the natural zeolites are broadly used in an agro-industry. The most commonly found natural zeolites are analcime, chabazite, clinoptilolite, erionite, heulandite, laumontite and phillipsite and these are not suitable for commercial applications. Therefore, synthetic zeolites have been developed for the commercial applications by mimicking the formation conditions of mineral zeolites.

Zeolites can be synthesized from reactive starting materials (e.g. freshly co-precipitated gels or amorphous solid) by controlling the condition to form uniform growth of crystal, such as (a) a relatively high pH (introduced in the form of an alkali metal hydroxide or other strong base, including tetraalkylammonium hydroxides) (b) low temperature hydrothermal conditions with concurrently low autogenous pressure at a saturated water pressure and (c) a high degree of supersaturation of the gel components so that a large number of crystals will nucleate (Breck, 1974; Tomlinson, 1998). Zeolites are formed under the hydrothermal conditions. The factors operating in the crystalline mixture after mixing and before formation of the final crystalline phase (Tomlinson, 1998) are as follows:

- (1) precipitation of an initial gel phase,
- (2) dissolution with time of the gel,
- (3) an event or series of events leading to nucleation of zeolite structures from either the gel or solution phase,
- (4) continued crystallization and crystal growth of these structures again either from the gel or from the solution,
- (5) dissolution of any initial metastable phase,
- (6) continued crystallization and crystallisation and crystal growth of new, more stable crystalline phases while the initial metastable crystals are dissolving,
- (7) dissolution of further metastable phases,
- (8) nucleation of the equilibrium phases,
- (9) crystallization and crystal growth of the final crystalline phases.

There are too many types of zeolite to have a general synthesis rule. Zeolite formation is sensitive to many factors such as temperature, kinds of cations, nature and history of reactants, pH, seed, aging prior to crystallization and stirring. The examples of synthetic zeolites are zeolite A, X, Y, analcime, Na-P1, hydroxysodalite, hydroxycancrinite, etc.

1.2 General scheme of zeolite synthesis

The synthesis mechanism is generally described as involving solution-mediated crystallization of the homogeneous gel at a relatively high pH value (Pfenninger, 1999). In the early alkali aluminosilicate synthesis of the low-silica zeolites, it was proposed that the hydrated alkali cation acts as a “template” - a forming agent - in the formation of zeolite structural sub-units. Water and hydroxide ions were the mineralizing agents. Crystallization of the zeolite was performed at a temperature close to 100 °C. The synthesis was varied according to raw materials changed, composition and reaction conditions, but the principal lay-out of the reaction was still valid (Figure 1.4).

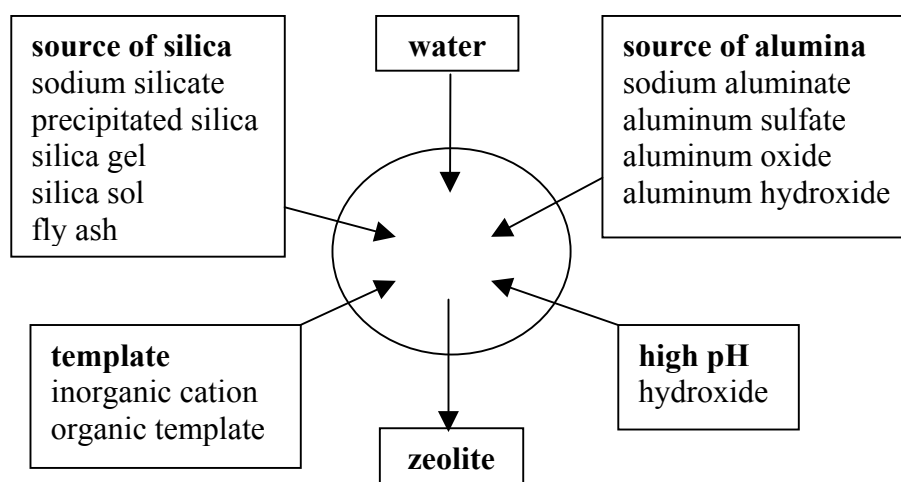


Figure 1.4 Principle of zeolite synthesis

Each of the reagents used in the zeolite synthesis has its particular role. The synthesis is normally performed in water as a solvent, which does not only dissolve the starting materials but also is a guest molecule as it hydrates the cations and thus leading to the hydrated template. The silica source acts as a primary building unit of the whole zeolite framework, each silica being connected with four oxygen atoms to form a tetrahedral network. Alumina acts as the second primary building unit and is connected to four oxygen atoms like silica, again contributing to the tetrahedral network. As aluminum is trivalent, it becomes the origin of the negative charge of zeolite framework. According to Lowen-stein's rule, it is not possible to get two alumina centers as neighbors in the zeolite framework. This is because the two negative charges would destabilize the whole system. Due to this fact, the $\text{SiO}_2/\text{Al}_2\text{O}_3$ ratio is always ≥ 2 . Hydroxide acts as a mineralizing agent and has a big influence on the result of the zeolite synthesis. The kinetics of zeolite formation is partly controlled by the hydroxide, but the size of the zeolite crystals is also influenced by the basic compound. The alkaline or alkaline earth cation will counterbalance the negative charge of the alumina built into the framework and acts as the template for the structure-forming process.

The formation process of zeolite is thermally activated and usually takes place at elevated temperatures in order to achieve high yield of crystals in an acceptable period of time. On the basis of the chemical phenomena occurring during zeolite genesis, the process can be divided into three basic steps: achievement of supersaturation, nucleation and crystal growth (Feijen, Martens and Jacobs, 1994).

1.2.1 Achievement of supersaturation

A solution with specific concentration and temperature can be in a stable, metastable or labile conditions as depicted in Figure 1.5. The stable and metastable areas are separated by the normal solubility curve, determining the normal equilibrium saturation concentration of a component c^* . The boundary between the metastable and labile region is not always well defined, as indicated by the shaded area. The degree of supersaturation S is defined as the ratio of the actual concentration to the normal equilibrium concentration ($S = c/c^*$). In the stable region, no nucleation or crystal growth can occur, while in the labile region nucleation as well as crystal growth are possible. In the metastable area, only crystal growth can occur. During aging, especially at the increased temperature, the concentration of adequate aluminosilicate precursor species increases with time by dissolution of the amorphous solid phase and interconversions of dissolved aluminosilicate oligomers in solution. This increasing concentration of solute, occurring usually at a constant temperature, will transform a stable solution into a metastable solution, and finally into a labile one. This transformation is indicated with an arrow in the solubility-supersolubility diagram of Figure 1.5.

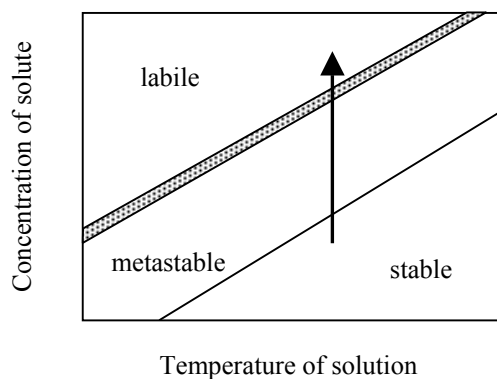


Figure 1.5 The solubility-supersolubility diagram

1.2.2 Nucleation

The primary nucleation from a supersaturated solution can be either homogeneous or heterogeneous. The latter is induced by impurities or foreign particles in the solution, while the former occurs spontaneously. It is evident that the heterogeneous nucleation can be suppressed by filtration of the different solutes. The secondary nucleation is induced by crystals and is relevant to the technique of seeding. During the period preceding the formation of viable nuclei, different kinds of germ nuclei (embryos) form by chemical aggregations of the aluminosilicate precursor species and disappear again through depolymerization. As a result of such fluctuations, the germ nuclei will grow in time and form, eventually, different kinds of nuclei with dimensions of the critical size to become viable, i.e. nuclei on which crystal growth occurs spontaneously. The concentration of these species is the highest in the boundary layer surrounding the amorphous solid particles resulting from the enhanced local concentration by dissolution. Presumably, nucleation occurs preferentially in these boundary regions. The rate of nucleation could be derived from crystal size distribution measurement in the final crystallization product and size increment measurement of the large crystals during the crystallization. As nucleation and crystal growth are assumed to consume the same precursor species, the nucleation rate is expected to go through the maximum and decline again after a certain period of time when the consumption of precursor species by crystal growth limits the forming of new nuclei.

1.2.3 Crystal growth

After nucleation, crystal growth can start. It occurs at the crystal-solution interface

by condensation of dissolved species (the secondary building unit or more extended species) onto the crystal surface. A direct transition of the solid phase of the gel into crystalline product through solid-solid transformation seems very unlikely. Likewise, nuclei grow into crystals by multiple addition of precursor species. Experimental crystallization curves, giving the yield of crystalline material in time, usually exhibit an S-shape profile. The inflection point of these sigmoid curves separates an autocatalytic growth period from a stage of delayed crystal growth owing to a depletion of the solution with precursor species. The autocatalytic nature of the first stage of the crystallization reflects the intrinsic property of self-acceleration of a crystallization process, provided that the source of nutrients is not limited.

1.3 Sodium zeolite

Most of the sodium zeolites crystallize from sodium aluminosilicate gels below 150 °C. The rate of crystallization and the stability of the sodium zeolite phases are optimum in the vicinity of 100 °C. The crystallization of sodium zeolites depends on the various starting reactants and temperatures (Breck, 1974).

1.4 Sodium zeolite applications

Sodium zeolite is one of the first industrial applications of ion exchange. The primary purpose of sodium zeolite is to remove the scale forming ions of calcium and magnesium. This ion exchanger consists of an exchange medium (zeolite resins) that has an ability to exchange sodium ions for hardness ions (calcium and magnesium) upon contact. The structure of zeolite consists of many channels, cavities and

interconnected voids that are occupied by cation and water molecules. Some properties of zeolite are very interesting such as (a) high degree of hydration (b) low density and large void volume when dehydrated (c) stability of crystal structure (d) cation exchange properties (e) uniform molecular sized channels (f) special physical properties, i.e. high surface area, molecular sieve (g) adsorption for gas and vapor and (h) catalytic properties. As a consequence of the peculiar structural properties of zeolites, they have a wide range of industrial applications. Sodium zeolites became very attractive materials for many applications. These zeolites have a high potential for application in ion exchange and molecular sieve (Bekkum, Mflanigen and Cjansen, 1991).

1.4.1 Ion exchange

The high Al (III)/Si (IV) ratio of sodium zeolites accounts for the high cation exchange capacity (CEC) such as Na-P1, hershelite, faujasite and zeolite 4A. The largest-scale industrial production of zeolite has been devoted to the production of the sodium form of zeolite A (LTA) for use in the detergent industry. Zeolite A (NaA) is added to washing powders and other household detergents or cleansing powders as a water softener. It has a high selectivity for Ca^{2+} (less so for Mg^{2+}). The advantage of zeolite builders comes in their use as a replacement for sodium tripolyphosphate, hence reducing the release of phosphates to the environment (Dryer, 1988). Sodium zeolites have been used for many years to remove Cesium and Strontium radioisotopes from nuclear waste. Sodium zeolites are very resistant to the high doses of radiation and are very selective ion exchangers, causing to remove dangerous isotopes which may be present in only minute concentrations (e.g. conc. $\text{Sr}^{2+} \approx 1$

microgram per litre) relating to other ions present (e.g. Na^+ conc. \approx 150 milligrams per litre). Treatment is usually carried out by placing spent fuel rods under water for long periods. This contaminated water is cleaned by the zeolites, which take up the Cs and Sr isotopes. The sodium zeolites are then placed in cement and sealed in steel drums before being stored. Sodium zeolites are used to remove ammonia and ammonium ions from wastewater, and they can reduce the concentration by over 90 %. Once the zeolite has been used, it can be regenerated and cleaned for re-use. Sodium zeolites have been proved to be even more efficient for treatment, with higher exchange capacities and as the cost of synthesized sodium zeolites decreases, these may be more widely used.

1.4.2 Molecular sieves

The channels in different zeolites are of different sizes and shapes, allowing zeolites to be used as selective molecular sieves. Some of the denser zeolites have pores which are too small to allow molecular sorption and some may have a lower density and high pore volume but may only have small pore openings. It is necessary to select an appropriate pore size. The crystallographically determined pore sizes offer only an approximate correlation to the effective pore size because all factors including temperature, type of cation, hydration have large effects on molecular sieve properties. The use of sodium zeolites as molecular sieves for flue gas treatment and separation and recovery of gases such as CO_2 , SO_2 and NH_3 has been tested (Anand and Michael, 1999). The most interesting sodium zeolites are A and X zeolites, and followed by Na-P1 (Querol, Moreno, Umana, Alastuey, Hernandez, Lopez-soler and Plana, 2002). The sodium zeolites are well known as general laboratory and industrial

drying agents in the form of extruder or beads. The success of these materials as desiccants arises from several possible reasons as follows: a) their abilities to exclude other molecules on the basis of size; b) the strong affinity of water for the internal zeolite surfaces; c) accommodation of water molecules in voids containing cations; d) ease of regeneration; e) long useful life (natural gas drying towers have a five year lifetime).

1.5 Diatomite

The term diatomite refers to sedimentary rocks that are mainly composed of the skeleton of single-celled diatoms. Diatomite, a soft and light rock, consists of amorphous silica skeletons and has a pale colour. It (also known as diatomaceous earth, kieselguhr, tripolite, etc.) is easily available in large quantities at an extremely low cost. The low density, high porosity and thus high absorption capacity for liquid, low thermal conductivity and outstanding filtration properties make diatomite versatile raw materials. Diatomite first appeared in the geological record about one hundred million years ago during the Upper Cretaceous. It is often associated with volcanic terraces as airfall ash, run-off waters and spring water replenish silica content of an aquatic environment. This association is of potential value in identifying areas of occurrence. During deposition, the purity of a diatomite deposit is chiefly controlled by clastic and/or volcanoclastic input. Calcareous microfossils, prevalent in equatorial marine environments, can also affect purity by introducing biogenic calcite (Inglethorpe and Morgan, 1992). A formation of diatomite of considerable thickness also occurs in marine coastal areas with continual subsidence, a periodical barrier to the open sea, and a regular supply of nutrients. In addition, diatomite of brickish

origin is formed in former saltwater lakes. Apart from water and organic substances, most frequently additional components of diatomite are quartz, calcium carbonate and clay minerals. The content of water and organic substances is only of minor significance for quality assessment since they can be removed by drying or calcination (Bibliothek, 1998). The type of silica found in diatomite is a hydrous form of opaline silica, which contains between 3 - 8 % of structural water.

Figure 1.6 Structure of silica surface depicting the various types of bonds and silanol groups

Several types of opaline silica are defined by their different X-ray diffraction (XRD) characteristics. They are composed of (1) opal C (well-order β -cristobalite), (2) opal CT (disordered cristobalite tridymite) and (3) opal A (poorly-ordered, almost amorphous). Diatomite is composed of biogenic opal A silica which is diagnosed from XRD analysis by a broad peak in the vicinity of the β -cristobalite at 4.05 Å

(Inglethorpe and Morgan, 1992). The silica surface contains silanol groups that spread over the matrix of silica as shown in Figure 1.6 (Al-Ghouti, Khraisheh, Allen and Ahmad, 2003). There are two types of silanols i.e. isolated and H-bonded silanols, on diatomite surface. At room temperature, both of the two types of silanols are H-bonded with water. With the increase of temperature of 200 - 1000 °C, five dehydration processes are assumed, shown as scheme I - IV in Figure 1.7 (Yuan, Wu, He and Lin, 2004). At first, the desorption of water more increases when the temperature raises (Figure 1.7, scheme I and II). Some strongly H-bonded silanols are condensed to form siloxane bridges (Figure 1.7, scheme III and IV) while most of the isolated silanols have not condensed. At 1000 °C, the amount of isolated silanols reaches the maximum and some weakly H-bonded silanols remain on the surface. At 1100 °C, most of isolated silanols condense as shown in scheme V.

Figure 1.7 The hydroxyl structure and the dehydration process of diatomite

In Thailand, the Department of Mineral Resources (DMR) found 500,000,000 tons of raw diatomite materials (Thai ceramic directory, 2001 - 2003). It is mainly found in Lampang, approximately 600 km north of Bangkok. The total areas are found in three districts which are Muang District, Ko Kha District and Mae Tha District. The Lampang Basin is a post-oligocene, intermontane basin occupying an area of approximately 100 km². Diatomite-bearing sequence of up to 50 m thick is found in the Ko Kha Formation, which is underlain by cyclotherms of mudstone, oil shale and lignite of the Mae Sot Formation. Overlying are Quaternary-to-Recent fluvial gravels, sands and clays, are generally capped by laterite. Dominants *Melosira granulata* and rare *Navicula* and *Fragilaria* diatom species of post-Miocene age indicate a freshwater, eutrophic, stagnant lacustrine environment. The high quality of the diatomite in Lampang Basin has the following compositions: silica (SiO₂) 75 - 80; alumina (Al₂O₃) 10 - 12; iron oxide (Fe₂O₃) < 5.0 wt.% (Inglethorpe, Utha-aroon and Chanyavanich, 1997).

1.6 Characterization techniques

1.6.1 Powder X-ray diffraction

X-ray diffraction (XRD) is a powerful technique used to uniquely identify the crystalline phases present in materials and to measure the structural properties (strain state, grain size, phase composition, preferred orientation and defect structure) of these phases. The X-ray region is normally considered to be the part of the electromagnetic spectrum lying between 0.1 and 100 Å bounded by the γ -ray region to the short-wavelength side and the vacuum ultraviolet region to the long-wavelength side. In terms of energy, the X-ray region covers the range from about 0.1 to 100 keV.

An X-ray diffraction has been used in two main areas; the fingerprint characterization of crystalline materials and the determination of their structures. Each crystalline solid has its unique characteristic X-ray powder pattern, which may be used as a “fingerprint” for its identification. Once the material has been identified, an X-ray crystallography may be used to determine its structure, i.e. how the atoms packed together in the crystalline state and what the inter-atomic distance and angle are. These unique properties make X-ray diffraction one of the most important characterization tools used in solid state chemistry and material science.

An important equation for X-ray diffraction is Bragg’s equation which shows the relationship between X-ray wavelength (λ) with lattice point distance (d) and incident diffraction angle (θ).

$$n \lambda = 2d \sin \theta \quad (1.1)$$

The different crystal plane in the crystal will diffract X-ray at different angles according to the Bragg’s equation. Therefore, by rotating the sample plane with respect to the incident X-ray, the diffracted angles can be recorded by a detector and the diffraction pattern is obtained. The identification of the sample structure can be done by comparing the spectrum with the pattern stored in the database.

1.6.2 X-ray fluorescence

Today, the X-ray fluorescence (XRF) is widely accepted as a versatile method of instrumental element analysis. XRF analysis is fast, non-destructive and accurate. In the XRF, the sample is irradiated by an X-ray beam consisting of a broad band of continuous radiation. In return, the chemical elements in the sample produce secondary (fluorescent) X-rays. These secondary X-rays are the characteristic for each

specific elements. The intensity of the secondary radiation is proportional to the concentration of the element. In this way the concentrations of all elements of interest can be calculated by measuring the intensity of the secondary radiation. XRF can handle a great variety of sample types: liquids, powders, solids, plant-tissue, metals, clay, soil and rock. Basically, there are two methods for sample preparation: borate-disk and pressed tablet. Borate-disk, compared to pressed tablets, has the main advantage that effects of particle size and mineralogy are eliminated, while inter-element effects are minimized. A disadvantage is the (high) dilution. This can be a problem for the analysis of trace elements with low concentrations. Therefore, we use borate-disk for routine quantitative analysis of major, minor and trace element, while the pressed tablet is used for qualitative analysis.

1.6.3 Fourier transform infrared spectroscopy

Fourier transform infrared (FT-IR) spectroscopy is a characterization method about the infrared radiation, which is passed through a sample. FT-IR techniques may be used for qualitative observations or quantitative measurements if used in conjunction with the Beer-Lambert relationship. The atoms in a molecule constantly oscillate around average positions. Bond length and bond angles are continuously changed due to this vibration. A molecule absorbs on infrared radiation when the vibration of the atoms in the molecule produces an oscillating electric field with the same frequency as the incident IR radiation when they are in resonance. Each molecule has its own characteristic spectrum. The bands that appear depend on the types of bonds and the structure of the molecule. FT-IR spectroscopy measures dominantly vibrations of functional groups and highly polar bonds. Thus, these

chemical fingerprints are made up of the vibration features of all the sample components. FT-IR spectrometer records the interaction of the IR radiation with experimental samples, measuring the frequencies at which the sample absorbs the radiation and the intensities of the absorptions. Determining these frequencies allows the identification of the sample's chemical makeup, since chemical functional groups are known to absorb light at specific frequencies.

Samples may be prepared in a solid, liquid or gas form. The nature of the sample determines which technique should be used. A common sample preparation method includes: the salt pellet technique (sample powder is diluted in an IR-transparent salt like KBr); Nujol Mull method (sample powder is diluted in an IR-transparent oil); thin sample technique; attenuated total reflectance (the sample is sandwiched between two IR-transparent crystals); and diffuse reflectance infrared FT (optics focus beam on the top surface of the sample).

1.6.4 Scanning electron microscope

Scanning electron microscope (SEM) is a type of microscope that uses electrons rather than light to form an image. There are many advantages to use SEM instead of a light microscope. SEM has a large depth of field, which allows a large amount of sample to be in focus at one time. SEM also produces images of high resolution, which means that small spaced features can be examined at a high magnification. The preparation of samples is relatively easy since most SEM instruments only require the sample to be conductive. The combination of higher magnification, larger depth of focus, greater resolution and ease of sample observation make SEM one of the most heavily used instruments in present-day research.

By using the wave-particle duality, SEM creates the magnified images by using electrons instead of light waves. The SEM shows very detailed 3-dimensional images at a much higher magnification than is possible with a light microscope. The images created without light waves are rendered black and white. By the nature of an electron beam, the vacuum is required during the operation; therefore, the sample has to be prepared carefully to withstand the vacuum inside the microscope. The samples must be a conductive material in order to be able to interact with an electron; SEM samples are coated with a very thin layer of gold by a machine called a sputter coater. The sample is placed inside the microscope's vacuum column through an airtight door. After the air is pumped out of the column, an electron gun emits a beam of high energy electrons. This beam travels downward through a series of magnetic lenses designed to focus the electrons to a very fine spot. Near the bottom, a set of scanning coils moves the focused beam back and forth across the specimen, row by row. As the electron beam hits each spot on the sample, the secondary electrons and the back scattered electrons are knocked loose from its surface. A detector counts these electrons and sends the signals to an amplifier. The final image is built up from the number of electrons emitted from each spot on the sample. By this way, the morphology of the sample can be seen directly from the micrograph.

1.6.5 Magic angle spinning nuclear magnetic resonance spectroscopy

Nuclear magnetic resonance (NMR) spectroscopy measures transitions between the spin states of nuclei in the presence of strong magnetic fields. Nuclear magnetic resonance is achieved by matching the energy of electromagnetic radiation (in the radio frequency region of the spectrum) to the energy separation of the nuclear spin

states. In solution NMR, spectra consist of a series of very sharp transitions, due to averaging of anisotropic NMR interactions by rapid random tumbling. By contrast, solid-state NMR spectra are very broad, as the full effects of anisotropic or orientation-dependent interactions are observed in the spectrum. High-resolution NMR spectra can provide the same type of information that is available from corresponding solution NMR spectra, but a number of special techniques/equipment are needed, including magic-angle spinning, cross polarization, etc. An important method has been developed and considered in order to minimize the large anisotropic NMR interactions between nuclei and increase S/N in rare spin NMR spectra is magic-angle spinning. The magic-angle spinning introduces an artificial motion by placing the axis of the sample rotor at the magic angle (54.74°) with respect to B_0 - the term $3\cos^2\theta - 1 = 0$ when $\theta = 54.74^\circ$. The rate of MAS must be equal to or greater than the magnitude of the anisotropic interaction to average it to zero. The samples are finely powdered and packed tightly into rotors, which are then spun at the rates from 1 to 35 kHz, depending on the rotor size and type of experiment being conducted. If the sample is spun at a rate less than the magnitude of the anisotropic interaction, a manifold of spinning side bands becomes visible. These bands are separated by increasing the rate of spinning (in Hz). Solid state NMR is clearly a very powerful technique capable of looking at a variety of materials. It does not require crystalline materials like diffraction techniques, and can still determine local molecular environments.

B_0

Figure 1.8 The magic-angle spinning motion

1.6.6 Ultraviolet and visible spectrometry

Ultraviolet and visible spectrometers have been in general use for the last 35 years and over this period have become the most important analytical instrument in modern day laboratory. In many applications, other techniques could be employed but none rival UV-Visible spectrometry for its simplicity, versatility, speed, accuracy and cost-effectiveness. Radiation is a form of energy and we are constantly reminded of its presence via our sense of sight and ability to feel radiant heat. It may be considered in terms of a wave motion where the wavelength, λ , is the distance between two successive peaks. The frequency, ν , is the number of peaks passing a given point per second. These terms are related so that:

$$c = \lambda \nu \quad (1.2)$$

where c is the velocity of light in a vacuum.

The full electromagnetic radiation spectrum is continuous and each region merges slowly into the next. Besides the sun, the most conveniently available source of visible radiation we are familiar is the tungsten lamp. For the UV region itself the most common source is the deuterium lamp. The UV-Visible spectrometer will usually have both lamp types to cover the entire wavelength range.

The Beer-Lambert Law states that the concentration of a substance in solution is directly proportional to the absorbance (A) of the solution.

$$\text{Absorbance (A)} = \text{constant} \times \text{concentration} \times \text{cell length} \quad (1.3)$$

When the monochromatic radiation passes through a homogeneous solution in a cell, the intensity of the emitted radiation depends upon the thickness (l) and the concentration (C) of the solution.

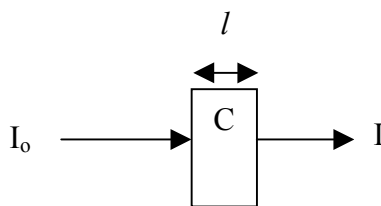


Figure 1.9 Schematic of the Beer-Lambert Law

I_0 is the intensity of the incident radiation and I is the intensity of the transmitted radiation. The ratio I/I_0 is called transmittance. This is sometimes expressed as a percentage and referred to as percentage transmittance. Mathematically, absorbance is related to the percentage transmittance (%T) by the expression:

$$A = \log_{10}(I_0/I) = \log_{10}(100/T) = kcl \quad (1.4)$$

Where l is the length of the radiation path through the sample, c is the concentration of adsorbing molecules in that path, k is a constant extinction coefficient dependent only on the nature of the molecule and the wavelength of the radiation.

1.7 Adsorption

The adsorption phenomena are widely used for industrial applications and for purification of water and wastewaters. The process of adsorption involves separation of a substance from one phase accompanied by its accumulation or concentration at the surface of another. The adsorbing phase is the adsorbent, and the material concentrated or adsorbed at the surface of that phase is the adsorbate. Electromagnetic interactions control the adsorption processes, because they are the result of binding forces between the atoms, ions or molecules of an adsorbate and the surface. Four principal types of adsorption are exchange (ion exchange), physical, chemical and

specific adsorption. The exchange adsorption involves electrostatic attachment of ionic species to sites of opposite charge at the surface of an adsorbent. The physical adsorption is resulted from the action of Van der Waals forces. The chemical adsorption involves a reaction between an adsorbate and an adsorbent resulting in a change in the chemical form of the adsorbate and the specific adsorption is the interaction between adsorbate and adsorbent without any adsorbate changes. A number of parameter specific to a given system will, therefore, affect an adsorption. The important parameters of adsorbate include: concentration, molecular weight, molecular size, molecular structure, molecular polarity, configuration and competitive adsorbates. The most important parameters of the adsorbent are: surface area, the availability of that surface to adsorbate molecules or ions and the physical size and shape of the adsorbate particles.

The removal of compounds in water treatment is often determined by the rate of adsorption while having a contact with the adsorbent. The process of adsorption can be categorized as a set of sequential steps with individual rate laws: (1) transport of solute from bulk solution phase to the boundary layer or surface film surrounding the adsorbent particle; (2) transport of solute across boundary layer to the exterior surface of the adsorbent particle; (3) diffusion of solute within the pores, from the exterior of the particle to the interior surface of the particle and; (4) physical or chemical binding of the adsorbate to the internal surface of the adsorbent. The four steps work as resistances against the mass transport of adsorbate solution to adsorbent. If the resistance of one of the four steps is much larger than the others, therefore, controls the reaction and the other can be neglected. In most cases of the water treatment, the rate of adsorption is controlled by either film diffusion or pore diffusion or both.

1.7.1 Adsorption model

During the adsorption, some molecules are adhered while others are detached. Once the rate of molecules adhered is equal to the rate of the molecules detached, the net adsorption is zero. Then the adsorbent material is exhausted and the equilibrium is reached. At this moment, the amount of the substance absorbed per unit weight of adsorbent, q_e , is a function of the residual equilibrium concentration of substance remaining in the solution, C_e . An expression using dose terms is called an adsorption isotherm, which describes the equilibrium adsorption with a concentration of the adsorbate in solution at constant temperature. Figure 1.10 shows the different patterns of adsorption isotherms. An experimental isotherm is useful to describe the adsorption capacity and is used to evaluate the feasibility of this process for the given application, for the selection of the most appropriate adsorbent, and for the preliminary determination of the adsorbent dosage requirements. Moreover, the isotherms play a crucial functional role in predictive modeling procedures for an analysis and a design of the adsorption systems.

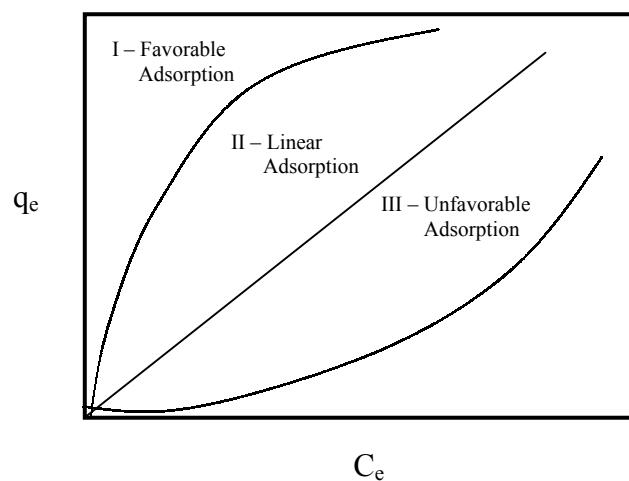


Figure 1.10 Types of equilibrium sorption; q_e = amount sorbed and C_e = amount in solution

Several equilibrium models have been developed to describe adsorption isotherm relationships such as Langmuir and Freundlich models.

1.7.1.1 Langmuir adsorption model

The Langmuir isotherm adsorption model is based on the fundamental principles: (1) adsorption energy is constant and independent for all locations of adsorption in the surface of the particle; and (2) monomolecular deposition is attained at equilibrium. The Langmuir adsorption model for solid-liquid systems is:

$$Q = \frac{abC_e}{1 + aC_e} \quad (1.5)$$

Where: Q = Quantity of solute adsorbed per unit weight of adsorbent.

C_e = Equilibrium concentration of solute.

a and b are Langmuir model parameters. a is a constant related to the area occupied by a monolayer of sorbate, reflecting the sorption capacity, b is a direct measure for the intensity of the sorption process.

Equation 1.5 can be written in a linear form to facilitate fitting the experimental data

as:
$$\frac{1}{Q} = \frac{1}{abC_e} + \frac{1}{b} \quad (1.6)$$

Plotting $1/Q$, versus $1/C_e$, yields a straight line, thus the parameters a and b can be determined from its slope and ordinate intercept, respectively.

1.7.1.2 Freundlich adsorption model

The Freundlich model is an empirical equation and is not based on fundamental principles. Freundlich found that some adsorption equilibrium data were best described by the equation:

$$Q = K_f C_e^{1/n} \quad (1.7)$$

Where K_f and n are indicative isotherm parameters of sorption capacity and intensity, respectively. Freundlich equation linearize in logarithmic form:

$$\text{Log}Q = \text{log}K_f + \frac{1}{n} \text{log}C_e \quad (1.8)$$

This adsorption isotherm yields a straight line for plotting $\log Q$ versus $\log C_e$. The slope of the line will be $1/n$, and it is an indicator of sorption intensity, and once the value $1/n$ is known, the value of K_f may be determined. K_f is an indicator of sorption capacity.

1.8 Ammonium ion

Ammonium ion, NH_4^+ , is an ionized form of nitrogen. There are many naturally occurring forms of nitrogen, including the nitrogen gas that comprises nearly 80 % of the atmosphere. Nitrogen compounds dissolved in water are usually classified as organic or inorganic. Soluble inorganic nitrogen compounds include ammonia, nitrite, and nitrate. Nitrate is related to ammonia in that nitrifying bacteria convert ammonia to nitrate, which is less toxic to animal life. The principal source of ammonium ion in the aquatic environment may be classified into biogenic, agricultural, industrial, residential and urban, atmospheric deposition. In the aqueous solution, ammonia can exist in either un-ionized form (NH_3) and/or ionized form (NH_4^+). These form depend on pH, with ammonium predominating when the pH is below 8.75, and ammonia predominating above pH 9.75. The forms are freely interconverted during a change in pH. Nitrogen is an essential nutrient for all forms of life, including all levels of aquatic organisms. Biologically available nitrogen is found in both suspended solids

and dissolved compounds in natural waters. Many natural waters are nitrogen-limited, meaning that nitrogen compounds are the limiting nutrients. Thus even small changes in biologically available nitrogen levels can dramatically affect the levels of microbiological, plant, and eventually, animal life. High levels of accessible nitrogen, of which total ammonia is one form, can lead to an over abundance of microorganisms, a situation which often results in mortality to higher organisms (such as fish and shrimp) because of the depleted dissolved oxygen. Excessive total ammonia can also result in mortality of the higher organisms, especially when high pH favour dissolved ammonia gas, which is more toxic than the ammonium form.

1.9 Research objectives

The overall objective of this research was to evaluate the natural raw Lampang diatomite and modified Lampang diatomites as starting materials for synthesis of sodium zeolites and remove ammonium ion from aqueous solution by obtained zeolitic products. The specific objectives were:

1. to study the influence of physical and chemical treatment on diatomite by calcination and acidic activation.
2. to synthesize sodium zeolites from natural raw Lampang diatomite and modified diatomites treated from (1).
3. to study the factors affecting the synthesis of sodium zeolites including: starting diatomite material. (natural raw diatomite and modified diatomites), ratio of diatomite to solution (solid/liquid), concentrations of alkalinity (NaOH), reaction temperatures and reaction time.

4. to find the formation condition which is most favourable for the synthesis of each sodium zeolite.
5. to remove ammonium ion in aqueous solution by sodium zeolite products.

Chapter II

Literature reviews

2.1 Synthesis of zeolites from diatomite

The synthesis of zeolites from low-cost silica-alumina sources has been the aim of many experimental investigations during the last two decades. Starting materials are natural materials such as volcanic, glasses, volcanic vitric ashes, rocks and clay minerals. Natural materials have been frequently used for the formation of zeolites, due to their high contents of silica and aluminum, which are easily dissolved and recombined to transform into zeolites under the alkali hydrothermal conditions.

The attempts to prepare zeolites from diatomite have been developed continually leading to the formation of various types of zeolites. However, the synthesis of zeolites from diatomite is a structurally and chemically complicated problem, and it depends on a large number of factors. The natural diatomite can be used as a starting material to synthesize zeolites both pretreatment and without pretreatment. In most studies, silica and/or alumina was used to adjust Si/Al ratio of natural diatomite before synthesized. The synthesis of zeolite X from diatomite was first reported in 1975 by Hotta, Torii and Asaka. Hotta and his co-workers prepared zeolite X from diatomite by the treatment with NaOH-NaCl solution and found that the diatomite from Showa-mura (Fukushima) can be used as a starting material without pretreatment such as heating. In the reaction between diatomite and NaOH-NaCl solution at 100 °C to give mainly zeolite X and a few of hydroxysodalite.

In following year, Midivnishvili, Uridiya and Ya prepared the NaA, faujasite NaX, philipsite and hydroxysodalite zeolite from natural diatomite by adding Al into the reaction mixture to adjust the different Si/Al ratios and synthesized at low temperature (90 - 100 °C).

Tsanov, Pavlova and Karamisheva (1979) studied the possibilities of producing zeolite products from diatomites. They used diatomite from 3 deposits in Bulgaria as a raw material. Before hydrothermal process, they treated natural diatomite material by thermal treatment at 650, 750 or 850 °C. Stilbite-type zeolite was obtained at high temperature (140 °C).

Sakamoto, Nishido and Doi (1981) prepared the mordenite, analcime and Na-P1 zeolite from natural diatomite deposits in Hiruzen district (Okayama). They found that the optimum conditions to get a mixture of well crystallinity of mordenite, analcime and Na-P1 zeolite were treatment with NaOH and Na₂CO₃ at the temperature in the range of 100 - 250 °C. In the following year, this researcher group modified the molar ratio Si/Al by adding NaAlO₂ solutions. They found that the crystallization of zeolite A, X, S and P depended on Si/Al ratio in solution and reaction temperature (80 - 100 °C). The zeolite S and P were found to be the stable crystallinity state in prolonged experiments. In 1984, Miyamoto prepared the pure phase zeolite A with good crystallinity from Noto diatomite (Ishikawa Prefecture). He synthesized zeolite A in NaOH solution by modifying natural raw diatomite with leaching and adjusted the conditions as follow: 1.8 - 2.2 for Na₂O/SiO₂, 1.9 - 2.3 for SiO₂/Al₂O₃ and 40 - 49 for H₂O/Na₂O in mole ratios, at 90 °C for 4 - 6 hours. In 1994, Biswajit et al. studied the optimum condition of synthesis of zeolite A from calcined diatomite by using a high-pressure Parr reactor. They found that the molar ratio of SiO₂/Al₂O₃ = 1.31,

$\text{Na}_2\text{O}/\text{SiO}_2 = 3.61$ and temperature of hydrogel formation of $37\text{ }^\circ\text{C}$ gave the maximum crystallinity of 92 % at the crystallization temperature $110\text{ }^\circ\text{C}$ and reaction time of 51 hours. Boukadir et al. (2002) synthesized zeolite 4A and hydroxysodalite from natural diatomite. The natural diatomite material was activated by NaOH solution. They suggested that the formation of zeolite 4A and hydroxysodalite depended on the concentration of aluminium.

Nowadays, some researchers prefer to use organic template instead of inorganic template for synthesizing novel zeolites. Vilma, Ursula and Ruby (2003) studied the synthesis of mordenite zeolite from natural diatomite. A high mordenite product was obtained from a natural diatomite material, either with or without the presence of diethanolamine. The synthesis process took 2 days and was carried out under hydrothermal conditions at autogenous pressure and at a temperature of $180\text{ }^\circ\text{C}$. It was essential that the reaction mixture was stirred before its introduction into the stove. Without stirring there was no reaction.

As mentioned earlier, in the introduction and the literature reviews, the synthesis of zeolites from diatomite material depends on a lot of factors, such as nature of starting diatomite material, type of base or template, base concentration, $\text{SiO}_2/\text{Al}_2\text{O}_3$ ratio, temperature and duration of the synthesis. The advantage of diatomite is the amorphous state of silica skeletons; this silica is in highly reactive state. Therefore, diatomite is an important source of silica, which offers a great potentiality for synthesizing zeolite. Unfortunately, there are no reports on zeolite synthesis from Thai diatomite, especially from Lampang, the details of the diatomite transformation into crystalline zeolite and also the details of the diatomite after physical and chemical activation. Furthermore, it is well-known that diatomite from Lampang is mainly used

in filter and ceramic industry, thus it is useful to utilize diatomite from Lampung as a starting material to produce new materials which are expensive and applicable to many industrial organizations such as in environmental sectors, agricultural sectors and catalyst industry. Therefore, the purpose of this study was to synthesize the sodium zeolite from the natural raw diatomite and modified diatomite (acid and thermal treatments) and to study the influence of the starting diatomite materials, solid to liquid ratio, the concentrations of alkalinity, reaction temperature and reaction time under constant ratio of the $\text{SiO}_2/\text{Al}_2\text{O}_3$.

2.2 The ammonium ion removal by synthetic zeolites

Ammonium ion removal from the wastewater is very important in order to maintain proper quality for a normal aquacultural life. Various methods of ammonium removal from aqueous solution have been developed. Synthetic zeolites gained significant interest in the scientific community over the last two decades. The favoured zeolites used as adsorbent for ammonium removal are sodium zeolites (activated with NaOH solution) and potassium zeolites (activated with KOH). Generally, fly ash used as starting material to synthesizes these zeolites for ammonium removal but sometime used natural material such as clays, volcanic rock. A small collection of early studies as follow:

Christopher et al. (1996) studied ammonium removal by zeolites Na-P1 and zeolite Pc from coal fly ash. They used these zeolites to remove ammonium ion in wastewater. They found that all of the fly ash zeolites had a high affinity for ammonium ion in low pH solution but did not favor in high pH solution.

Querol, Alastuey, Lopez-soler and Plana (1997) studied the ammonium ion removal by Na-P1, hydroxysodalite, cancrinite, analcime, tobermorite, nepheline hydrate, KM-phillipsite and F linde zeolite from fly ash by conventional and microwave-assisted hydrothermal alkaline activation. The interesting zeolites synthesized were Na-P1, KM-phillipsite and F linde zeolite since the ammonium ion retention capacities (20 - 30 mg of NH_4^+ g^{-1}). The experiments performed also showed that high ammonium ion retention capacities were attained after a few minutes of equilibrium with ammonium ion rich solution.

In 1997, Ruiz et al. synthesized zeolites with bentonite clay by alkaline treatment in distilled and seawater media. They found that cation exchange capacity and ammonium ion removal were increased by alkaline treatment. Ammonium ion is removed more efficiently from distilled water solutions where there were no competitive ions. The products generated by alkaline treatment in seawater media were more selective for ammonium ion removal. This may be related to the size of particles and the specific effluent. In the same year, Singh and Prasad studied 13X, ZSM-5 and 5A zeolite to remove ammonium ion from coke-plant secondary wastewater. They indicated that the ammonium adsorption rate increases with an increase in the contact time of zeolite with solution. Also, the different crystalline structures of the zeolites as well as the different channel diameters and pore diameters may be responsible for the difference in the ammonium ion removal. 13X zeolite has good efficiency to remove ammonium from effluent.

Hollman, Steenbruggen and Janssen-Jurkovicova (1999) studied zeolite Na-P1 and zeolite NaX with synthesized from fly ash for removal of ammonium ion in wastewater. The cation exchange capacities ranged from 3.6 to 4.3 meq g^{-1} for pure

zeolites and from 2.0 to 2.5 meq g⁻¹ for the zeolite containing residual fly ash. It appeared that the pure zeolite Na-P1 and NaX can be used for removal of ammonium ion from wastewater.

Poole, Prijatama and Rice (2000) studied hydroxysodalite zeolite and zeolite F that synthesized from fly ash for removal of ammonium ion from solution. Zeolite F can be removed ammonium ion more than hydroxysodalite zeolite. The maximum ammonium ion removal for these zeolites was 65 - 80 % after 60 minutes.

Michihiro, Chikashi and Motohide (2002) converted waste incineration fly ash to zeolitic compounds by hydrothermal treatment in the presence of NaOH solution. The major zeolite products were zeolite A and Na-P1. The removal reactions of ammonium ion by these zeolites proceeded rapidly, reaching individual equilibrium within 1 hours, where as fly ash showed no uptake behavior. The maximum uptake amount of ammonium was estimated to be 1.1 mmol g⁻¹. In the same year, Juan, Hernandez, Querol, Andres and Moreno synthesized zeolitic material (Na-P1 zeolite as the main component) from fly ash. Their study showed that Na-P1 had a high retention capacity, in this case, the ion exchange seemed to be influenced by diffusion through channels in the zeolite. They found that the highest ammonium ion retention capacity was 0.7 meq g⁻¹. In the following year, Otal et al. synthesized zeolitic materials (mainly Na-P1) from fly ash with NaOH activation. Also, they studied the effects of the zeolite dose on the ammonium ion adsorption of synthetic zeolites. They found that the uptake of ammonium ion by zeolite increased with zeolite dose and the maximum elimination percentages ranged from 16.7 to 45.0 % in the case of the landfill leachate and from 32.2 % to 43.4 % in the case of the pig slurry for the different types of zeolites tested.

As mentioned above, different kinds of synthetic zeolites are most frequently suggested as ammonium ion removal for wastewater treatment. It was felt that the sodium zeolites that synthesized from Lampang diatomite might be offered as a suitable medium for ammonium ion treatment due to its high affinity for cations.

Chapter III

Materials, instrumentation and experimental procedures

3.1. Material lists

3.1.1 Chemical and materials

- (a) Diatomite sample of Ban Keuw Mae Tha District, Lampang Province, Thailand (Sriphum Wattana Ltd.)
- (b) Anhydrous sodium hydroxide pellets (NaOH), Analytical reagent, Merck, Germany
- (c) Reference Material Kaolin, MBH Analytical Ltd., UK
- (d) Standard Reference Materials from NIST (National Institute of Standard and Technology, Department of commerce, USA)
 - Standard Reference Material 600 (Bauxite)
 - Standard Reference Material 98b (Plastic clay)
 - Standard Reference Material 679 (Brick clay)
 - Standard Reference Material 2709 (Soil)
- (e) Lithium tetraborate anhydrous, $\text{Li}_2\text{B}_4\text{O}_7$; Claisse 252, Chemin Saite-Foy, Canada
- (f) Lithium bromide, LiBr; Claisse 252, Chemin Saite-Foy, Canada
- (g) Mercury (II) iodide (HgI_2), Analytical reagent, Univar, Australia
- (h) Potassium iodide (KI), Analytical reagent, Univar, Australia

- (i) Nessler reagent: dissolved 100 g HgI_2 and 70 g KI in a small quantity of water and added this mixture slowly, with stirring, to a cool solution of 160 g NaOH dissolved in 500 mL water. Diluted to 1000 mL.
- (j) Ammonium chloride (NH_4Cl), Analytical reagent, Fisher Scientific, UK
- (k) Stock ammonium solution: dissolved 3.819 g anhydrous NH_4Cl , dried at 100 °C, in water, and diluted to 1000 mL; 1.00 mL = 1.00 mg N = 1.22 mg NH_3 .
- (l) Standard ammonium solution: diluted 10.00 mL stock ammonium solution to 1000 mL with water; 1.00 mL = 10.00 μg N = 12.2 μg NH_3 .
- (m) Hydrochloric acid 37 %; Analytical reagent, Merck, Germany
- (n) Hydrochloric acid, 1 N: in a 1000 mL volumetric flask, pipetted 83 mL of concentrated HCl, diluted to volume, and mixed well.
- (o) Sulfuric acid 96 %; Analytical reagent, Merck, Germany
- (p) Nitric acid 65 %; Analytical reagent, Merck, Germany
- (q) Aluminium hydroxide ($\text{Al}(\text{OH})_3$), Analytical reagent, Aldrich Chemical, Milwaukee, USA
- (r) Ammonium acetate (NH_4OAc), BDH, England
- (s) Sodium chloride (NaCl), Analytical reagent, Merck, Germany
- (t) Ammonium acetate (NH_4OAc), 1 N: dissolved 77.08 g NH_4OAc into 1000 mL volumetric flask and made up to volume with deionized water.
- (u) Isopropyl alcohol ($\text{CH}_3\text{CH}(\text{OH})\text{CH}_3$), 99 %, BDH, England
- (v) Methanol (CH_3OH), 99.8 %, Merck, Germany
- (w) Magnesium oxide (MgO), 98 %, Acros, Belgium
- (x) Boric acid (H_3BO_4), 99.8 %, Riede-de Haen

- (y) 4 % boric acid solution, dissolved 40.00 g H_3BO_4 in deionized water and diluted to 1000 mL
- (z) Bromocresol green indicator, dissolved 40.00 mg of bromocresol green in ethanol 95 % and diluted to 100 mL
- (aa) Ammonium chloride, 1 *N* neutral: in a 1000 mL volumetric flask, added approximately 500 mL deionized water. Dissolved 53.49 g ammonium chloride in it. Adjusted the pH to 7.0 with ammonium hydroxide, and diluted to the volume with deionized water and mixed.
- (bb) Ammonium chloride, 0.25 *N* neutral: in a 1000 mL volumetric flask, added approximately 500 mL DI water. Dissolved 13.37 g ammonium chloride. Adjusted the pH to 7.0 with ammonium hydroxide. Filled up to the volume with deionized water and mixed.
- (cc) Sodium chloride, acidified 10 %: in a 2000 mL volumetric flask, added approximately 1000 mL deionized water. Added 200 g NaCl and 10 mL 1 *N* HCl. Mixed well and diluted to volume with deionized water.

3.1.2 Glasswares

- (a) Watch glass
- (b) Utility clamp
- (c) Glass stirring rod
- (d) Breakers 50, 100, 250, 500, 1000 mL
- (e) Erlenmeyer flasks, 125, 500 mL
- (f) Volumetric flasks 50,100, 250, 500, 1000, 2000 mL
- (g) Mortal and pestle

- (h) Platinum crucible and mold
- (i) Round bottom flask 250 mL
- (j) Condenser for reflux procedure
- (k) Porcelain crucible
- (l) Conical flask 125 mL
- (m) Volumetric pipets 1, 5, 10, 25, 50 mL

3.1.3 Apparatus

- (a) Thermometer
- (b) Heating mantle with stirrer (Horst)
- (c) Vacuum filtration apparatus
- (d) Oven for drying sample (Memmert)
- (e) Furnace chamber (Carbolite CWF 12/23)
- (f) Fusion machine for sample preparation XRF analysis, (Claisse, Fluxer Bis)
- (g) Desiccator
- (h) Digestion bomb
- (i) pH meter, (Mettler Delta 320)
- (j) Shaking water bath, (Maxi-Shake, Heto Lab Equipment, Denmark)
- (k) Standard sieve 230 mesh (63 μ m), (Analysensieb, Retsch, USA)
- (l) Spatular
- (m) Analytical balance, (Model 250A, Precisa, Switzerland)
- (n) Sieve Shaker, (Octagon digital, Endecotts, England)
- (o) Glass microfiber filters, Whatman GF/C diameter 47 mm

3.2 Instrumentation

3.2.1 Particle size analyzer

Diatomite particle size distribution was measured by Malvern Mastersizer S Ver. 2.15 laser light-scattering-based particle sizer (for grain size determination of powder in suspension, ranging from 0.1 to > 600 μm). For this purpose, the wet method of particle size distribution analysis was used. Water was used as the medium to dispersion of the samples. The solution was ultrasonicated for 45 min in order to break down the flocculates before the run was performed. All samples were run twice to ensure the accuracy of the measurements.

3.2.2 X-ray fluorescence spectrometer

X-ray fluorescence (XRF) is one of the techniques, which are widely used to determine elemental compositions of solid samples especially in soil or powder samples. Highly accurate measurements of total silica content in diatomite can be determined by using X-ray fluorescence spectrometry. This technique is also useful to determine the total of other elements in diatomite, such as aluminum, iron and sodium (Shiuh, 1997). In this work, XRF (Philips, PW 2404, MagiX Pro) was used to measure the composition of diatomite materials. The samples were prepared for the measurement by Borate-fusion technique as follow:

- Mixed 1.00 g of the sample with 7.00 g of $\text{Li}_2\text{B}_4\text{O}_7$ in the platinum crucible.
- Added LiBr 0.03 g to mixed sample in the platinum crucible using a clean spatula.
- Placed the platinum crucible with mod in fusion machine.

-The fusion machine was pre-programmed for power and fusion time according to the instruction manual.

-After cooling, solidification, and casting, weighed and recorded the weight of disk, which was used for WDXRF analysis.

-Prepared the disk of all the standard reference materials with the same procedure as sample.

The tube high voltage was 40 kV with the tube current of 30 mA. Each sample was measured using standard procedure suggested by the instrument manufacturer. The measurement time was about 10 min per sample. The results were reported in the form of oxide percentage.

3.2.3 X-ray powder diffraction

X-ray powder diffraction (XRD) is a popular technique used for the structural properties and the identifications of mineral in solid state and material science. The instrument used in the experiments of current research is Bruker D5005 powder X-ray diffractometer. The D5005 is equipped with a Ni filter in conjunction with the Cu radiation (wavelength = 1.5406 Å). Prior to the measurement, each sample was prepared using a standard method for powder sample preparation. The phase identification was done by comparing with the diffraction patterns (JCPDS-ICDD) data base and collection of simulated XRD powder patterns for zeolite (Treacy and Higgins, 2001). However, only qualitative results were obtained for this research. The procedure for powder XRD sample preparation was described as following:

-Dried the sample in oven at 110 °C

-Ground about 1.00 g of each solid sample to fine powder as homogeneous as

possible, then load into the polymethyl metaacrylate (PMMA) sample holder.

-Tapped the powder gently and evenly to uniformly cover the holder cavity.

-Gently pressed the powder sample into the cavity using a glass slide.

-Gently lifted up glass slide to reveal the sample surface.

Each diffraction spectrum was recorded with the condition: 2θ angle of between 5° and 50° , Cu-target, 35 kV, 35 mA., and scan speed of 0.3 degree/0.02 second. Typically, the data was expressed in the plot between intensity of diffraction peaks and 2θ angle. The positions of diffraction peaks were compared with a reference database and the identifications of compounds could be obtained.

3.2.4 Fourier transform infrared spectroscopy

Fourier transform infrared spectroscopy (FT-IR) is used to study structural features and examine the adsorption of many species. Spectroscopy is the study of the interaction of electromagnetic radiation with matter. Several spectroscopic techniques correspond to different regions in the electromagnetic radiation spectrum. Infrared spectroscopy studies the mid-infrared region (from 4000 to 370 cm^{-1}) where vibrational and rotation bands are observed. The instrument used for this analysis was a Perkin-Elmer spectrum GX FTIR Spectrophotometer with KBr pellet technique. The solid sample and KBr pellet were dried at 120°C for 1 hour before using. Approximately 0.5 mg of each sample was mixed with 300 mg dried KBr powder and ground to very fine powder with a mortar and pestle. The ground powder was pressed into a transparent disk using a hydraulic pressing machine with an equivalent weight of about 10 tons for 1 minute. The spectra were obtained using an average of 5 scans with 4 cm^{-1} resolution.

3.2.5 Scanning electron microscope

Morphology of the solid sample could be seen through the use of scanning electron microscope (SEM). Crystal shape and size of the crystalline solid phase could be identified from the micrograph. The observation was done using scanning electron microscope model JSM 6400. To prepare for the observation, the solid sample was placed on a brass stub sample holder using double stick carbon tape. Then, the sample was dried using infrared light for ten minutes. After that, the sample was coated with a layer of gold approximately 20 - 25 Å thick using a Balzer sputtering coater to make them conductive. The micrographs were recorded with an accelerating voltage of 10, 15, 20 kV and 500x - 10,000x magnification.

3.2.6 Thermogravimetric analysis

The thermogravimetric analysis (DTA/TGA/TGD) was used to measure the weight lost of solid samples at different temperatures and the temperature difference of sample and standard. The thermogravimetric analyses were carried out by Analyzer Simultaneous TGA-DTA Instrument model SDT-2960 at a heating rate of 16 °C min⁻¹ under a flow of oxygen of 20 mL min⁻¹ with Al₂O₃ as a reference. The thermal analyses curves were recorded simultaneously along with temperature increment.

3.2.7 Solid-state nuclear magnetic resonance spectroscopy

Solid-state nuclear magnetic resonance spectroscopy (NMR) was performed on a Bruker MSL 300 spectrometer. Samples were packed into 8 mm ZrO₂ rotors and spun in the air. ²⁹Si NMR spectra were obtained by magic angle spinning (MAS) at spinning rates of 4.5 kHz, pulse widths of 2.5 μs (30°), and recycle delay times of 60

seconds. Kaolin was used as the external reference material for ^{29}Si NMR chemical shift determination. All chemical shifts were reported in ppm relative to kaolin. Spectral simulation was performed with Peakfit software and the relative peak areas obtained by curve-fitting procedures.

3.2.8 Ultraviolet and visible (UV-Vis) spectroscopy

The ammonium ion was determined by UV-Vis spectrophotometer (Model Cary 1E, Varian). The concentration of ammonium ion in solution was determined by measuring the absorbance at the wavelength 420 nm and 1-cm light path by developed colour with Nessler reagent.

3.3 Experimental methods

3.3.1 Diatomite preparation

Diatomite sample was collected from Ban Keuw in Mae Tha District of Lampang Province, Thailand (Sriphum Wattana Ltd.). It was crushed to aggregate-size pieces in roller mills with air-drying and was ground to less than 63 μm (230 mesh) by hand. The fraction measuring less than 63 μm in size was used as starting material for further experimental. The diatomite sample was characterized by WDXRF to find the composition prior to the calcination and acid treatment and the zeolitization experiments.

3.3.2 Calcination and acid treatment

The diatomite material was submitted to activation treatment by different methods as follows:

- (1) Diatomite was only activated by calcination at temperature 900, 1000 and 1100 °C. Calcination was carried out under air atmosphere in a heating rate of 16 °C min⁻¹ and 8 °C min⁻¹ for 1, 3, 5, 7 and 10 hours at the calcination temperature.
- (2) Diatomite was only activated by acid (6M HCl, 6M H₂SO₄, 6M HNO₃) at room temperature, for different contact times (24, 72, 120 and 168 hours) and under reflux condition at 100 °C, for different contact times (1, 6, 12 and 24 hours); 10 g of diatomite was mixed with 50 mL of the acid solutions (solid: liquid = 1:5) and stirred during the times indicated above. Then the product was washed with water to pH 7 and dried. The decrease in mass of the samples was recorded as the dissolved mass; wt %.
- (3) The best result of diatomite thermal treatments at 900, 1000 and 1100 °C from (1) was activated with acid treatment selected from the best result of (2) to provide the sample with high eliminated some impurities.
- (4) The best result of diatomite acid treatment from (2) was activated with thermal treatments at 900, 1000 and 1100 °C selected from the best result from (1).

3.3.3 The sodium zeolites synthesis method

The procedures for hydrothermal reaction of diatomite in alkaline medium were described as follows.

-Each diatomite sample (natural diatomite, treated diatomite) was reacted with 10 %, 20 % and 30 % w/v of sodium hydroxide (NaOH) with the ratio (in g:mL) of solid to liquid 1:10 and 1:30. The reaction mixture was carried out in digestion

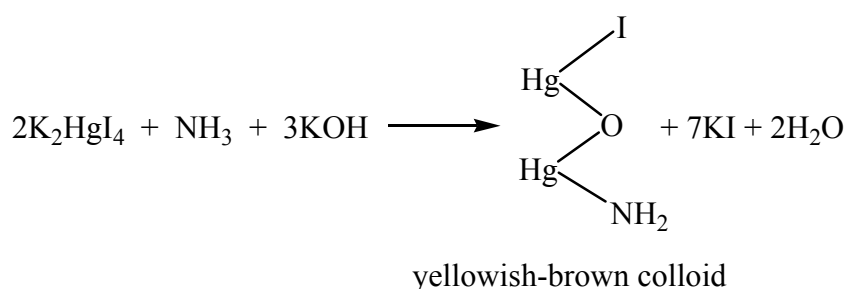
bombs at autogenous pressures of the temperature at 100, 140 and 180 °C with various reaction periods from 24 to 168 hours. In addition, Al(OH)₃ was used to adjust the SiO₂/Al₂O₃ molar ratio of treated diatomite for the same composition as the natural diatomite.

-The experiments were performed in an oven at 100, 140 and 180 °C with controller (± 1 °C). Once the activation time was reached, the digestion bomb was quenched in cold water to stop the reaction. The solid product was filtered and washed with deionized water to remove excess alkali until the pH of the filtrate became 7. Then, the sample was dried at 110 °C for 24 hours and stored in a desiccator.

-The solid products were characterized by XRD, FT-IR, particle size analyzer and SEM techniques.

3.3.4 Analytical method for ammonium ion

The ammonium ion concentration of the samples was determined by the standard nesslerization method (APHA, 1992) using a UV-Vis spectrophotometer (Model Cary 1E, Varian). Nesslerization is the oldest of the colorimetric techniques and at one time was also the most widely applied. It is possible to obtain a measure of the amount of ammonia nitrogen by treatment with nessler's reagent, which is a strongly alkaline solution to potassium mercuric iodide. It is combines with NH₃ in alkaline solution to form a yellowish-brown colloidal dispersion, the color intensity of which is directly proportional to the amount of NH₃ originally present. The reaction may be represented by the equation:



The reaction is fast and requires no temperature control. The procedure was as follows:

-From the standard solution, prepared a series of nessler standards by diluting the volumes given in the following chart to 50 mL in deionized water and adding 1 mL of nessler reagent.

mL standard	0	1	2	3	4	5	6	7	8	9	10
mg/L (ppm)	0	0.2	0.4	0.6	0.8	1.0	1.2	1.4	1.6	1.8	2.0

-Mixed thoroughly. Keep such conditions as temperature and reaction time the same in blank, samples and standards. Let reaction proceed for at least 10 min after adding nessler reagent. After 30 minutes, read the absorbance at 420 nm against a blank for 1-cm light path.

-Alternate the samples and blanks, readjusting the blank to zero each time.

-Plot a calibration curve of absorbance against with mg/L.

-Pipetted 1.00 mL of the sample and added 1.00 mL of the nessler reagent to develop the color. Measured the absorbance after 30 minutes, and from the calibration curve, read the mg/L.

-Deducted amount of $\text{NH}_3\text{-N}$ in water used for diluting original sample before computing final nitrogen value. Computed total $\text{NH}_3\text{-N}$ by the following equation:

$$\text{mg NH}_3\text{-N/L} = A \times 50 \quad (3.1)$$

Where: A = mg $\text{NH}_3\text{-N/L}$ read from curve

3.3.5 Batch studies of ammonium removal

The ammonium removal process was carried out using a batch method.

-Ammonium removal was determined in 125 mL conical flasks. An equal weighted (1.00 g) of samples were introduced into each conical flask to which 100 mL of ammonium solution concentrations of between 10 and 120 mg/L were added. The pH value of ammonium solution was adjusted to 6.5 using 0.1 N HCl (to decrease the pH) or 0.1 N NaOH (to increase the pH value).

-Ammonium adsorption experiments were performed at 25 °C under 200 rpm with orbital shaking Water Bath for 96 hours and samples were taken periodically for measurement of aqueous-phase ammonium concentration. Preliminary tests confirmed that 96 hours contact time was enough to reach a steady-state ammonium concentration.

-The ammonium concentration of the samples was determined by the standard nesslerization method. It should be noted that no more than 1.0 mL of sample was taken for measurement of ammonium, and hence the total volume of the aqueous solution was effected insignificantly by sampling.

3.3.6 Cation exchange capacity

Cation exchange capacity (CEC) is a reversible chemical reaction. The cations held on the surface of the soil minerals and within the crystal framework of some mineral species and those which are a part of certain organic compounds can be reversibly replaced by those of salt solutions and acids. Cation exchange capacity is reported as milliequivalents per 100 g sample or more recently as cmol (+)/kg sample (S.I. unit). In this study, the CEC of raw diatomite was determined by the ammonium acetate method according to Maria (1997) and the CEC of zeolite products was determined by modified ammonium acetate method according to Molina and Poole (2004). The procedures for CEC were described as follows:

(1) Ammonium acetate method

- 10.00 g of sample was weighed into 500 mL erlenmeyer flask.
- 250 neutral 1 *N* ammonium acetate was added to the flask.
- The flask was covered with parafilm and the contents were later mixed thoroughly.
- The sample was kept overnight.
- The sample was filtered and kept wet.
- The sample was rinsed for 3 times with 25 mL aliquots of neutral 1 *N* ammonium chloride.
- The sample was, then, rinsed for 3 times with 25 mL aliquots of neutral 0.25 *N* ammonium chloride.
- Next, the sample was washed with 150 to 200 mL of 99 % isopropyl alcohol.
- The liquid of isopropyl alcohol was disposed with deionized water.
- The ammonium-saturated sample was washed with 10 % acidified NaCl

solution until 225 mL passed through the sample. Then, the NaCl was added in small portions allowing each portion to pass through sample before adding the next portion. The liquid was stored in wide mouth soil jars in the refrigerator until time for the analysis.

-Finally, the ammonia was analyzed with Kjeldahl method (the sample must be Diluted about 1:50 before analysis). The result is calculated as milliequivalents per 100 g sample:

$$\text{CEC} = \text{Reading} \times \text{DF (dilution factor)} \times 1/14.0067 \times 0.225 \times W_{\text{sample}} \quad (3.2)$$

(2) Modified ammonium acetate method

This property consists in the exchange of cations, slightly attached to the structure of the zeolite, with ammonium ions in the solution. Then, under a basic aqueous environment, the ammonium ions are released as ammonia by distillation. In order to demonstrate the CEC of the synthetic sodium zeolite, the following procedure steps were used.

-5.00 g of the sample (m_s) was weighed and leached for 20 minutes with 100 mL of 1 N ammonium acetate solution.

-The solid was then filtered under vacuum and rinsed with small portions of methanol (to avoid hydrolyzation), until no free ammonia could be detected on the filtrate.

-Ammonia in solution was determined by a colour indicator (nessler's reagent).

-The sample was filtered and transferred the powder to a 250 mL distilling flask filled with 100 mL of deionized water and 1 g of MgO.

-The mixture was distilled for about 25 minutes and during this time the liquid

was put into a beaker containing 25 mL of 4 % H_3BO_4 solution and few drops of bromocresol green indicator, which turned blue during the process.

-At the end of the distillation, the contents of the beaker were transferred to a 250 mL volumetric flask (V_f) and filled to the mark.

-The ammonia exchanged was determined by an aliquot of about 20 mL (V_a) of the solution was taken and titrated directly with a solution 0.1 N HCl (T), until the solution changed from blue to green. The results are expressed as milliequivalents per 100 grams (meq/100 g) of solids as they were calculated directly from the following expression:

$$CEC = \frac{T \times (V_f / V_a) \times 0.1 \times 100}{m_s} \quad (3.3)$$

Chapter IV

Results and discussion

4.1. Morphology and particle size of diatomite

The study of morphology of diatomite was performed by scanning electron microscope (SEM). Since the powders were non-conductive, a thin coating of gold was sputtered on the powder surface in order to observe the fine detail of the diatomite skeletons. The morphology of the natural diatomite shown in Figure 4.1 was typical, showing dominant *A. granulata* species (Inglethorpe, et al., 1997; Owen and Utha-aroon, 1999). The particle size distribution of the natural diatomite determined by laser scattering particle size analyzer had an average particle size of 9.88 μm .

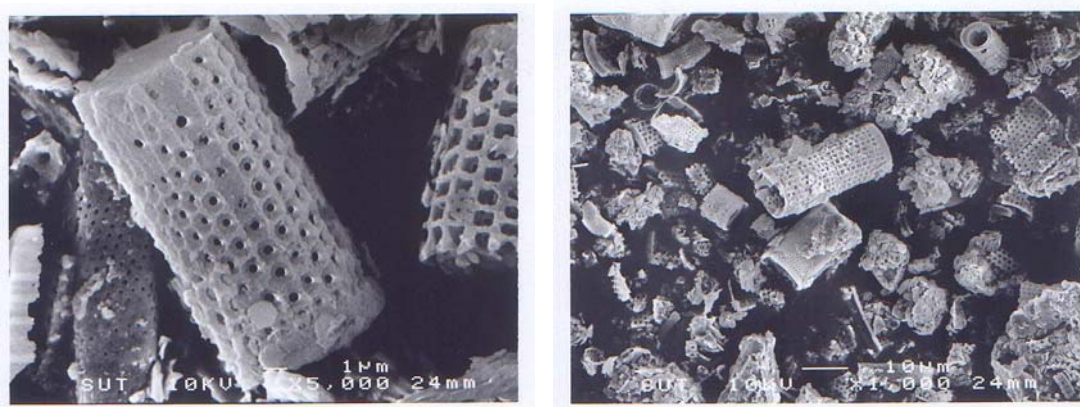


Figure 4.1 SEM micrograph of diatomite samples with 10 kV 1000 and 5000 magnification

4.2. Diatomite composition analysis

The chemical compositions of natural diatomite was determined by wavelength dispersive X-ray fluorescence (WDXRF) as given in Table 4.1. The main compositions of diatomite sample were oxides of Si, Al and other mineral impurities of Fe, K, Ca, Mg, etc. The Si/Al ratio of Lampang diatomite was 4.35. Therefore sodium zeolites prepared from natural diatomite material were always contaminated with these elements. Those impurities may also effect the crystallization mechanism of zeolites.

Table 4.1 The chemical compositions of natural diatomite sample determined by WDXRF.

Composition	SiO ₂	Al ₂ O ₃	Fe ₂ O ₃	K ₂ O	CaO	MgO	MnO	TiO ₂
(wt %)	71.90	14.60	5.78	1.95	0.17	0.69	0.01	0.51

4.3. Diatomite characterization

The thermogravimetric analyses (DTA/TGA/TGD) of the natural diatomite are shown in Figure 4.2. The DTA curve showed three endothermic effects at 76.7 °C, 496.2 °C and 1086.0 °C, accompanied the weight loss of TGA curve. The endothermic peak centered at 76.7 °C and a shoulder around 165 °C were assigned to the loss of water absorbed on the diatomite. The small peak at 496.2 °C might be due to the liberation of water caused by dehydroxylation of some associated silanol groups on the external surface of diatomite. In the high temperature region, the large endothermal peak with a centre at 1086.0 °C has been assigned to a formation of siloxane bridges resulting from dehydroxylation of isolated silanol groups on the

internal surface of diatomite. These were a great deal that may enable to treat diatomite by thermally, which several other variables would effect. The most important reason in selecting the calcination at 900, 1000 and 1100 °C was the evaporation of water due to dehydroxylation on surface of the particle and it's network. As the results of the evaporation, (1) new voids appear, and (2) defects occur in the crystalline structures (Goren, Baykara and Marsoglu, 2002). During this process the diatomite loses the hydroxyl units from its structure and an amorphous product is formed (Biswajit et al., 1994). The powder spectra of natural diatomite are recorded in Figure 4.3. The identification of diatomite phases was realized by using diffraction pattern files provided by Joint Committee on Powder Diffraction Standards (JCPDS). The sample showed clear diffraction pattern peaks exhibiting some degrees of crystallinity. Significantly, the major composition of natural diatomite was biogenic hydrous silica that can be grouped as Opal-A (A-amorphous) mixed with a minority amount of quartz, kaolinite, montmorillonite and illite. It produced an X-ray diffraction pattern of single diffuse band centered at approximately $22^{\circ} 2\theta$ (4.1 Å d-spacing). IR spectra of natural diatomite are also recorded as shown in Figure 4.4. In general, an absorption bands is related to the vibration at specific configuration of chemical bonding. The interpretation of the spectra has been guided by the data published in literatures (Van der marel and Beutelspacher, 1976; Hassan, Ibrahim and Ismael, 1999; Weng, Shen, Yuan, Guo and Chen, 1999; Al-Degs, Khraisheh and Tutunji, 2001; Yuan, Wu, Lin, Diao, Peng and Wei, 2001; Aicha, Thibaud, Jocelyne, Francois and Jacques, 2003). The identifications of IR absorption bands to the related vibrations are shown in Table 4.2.

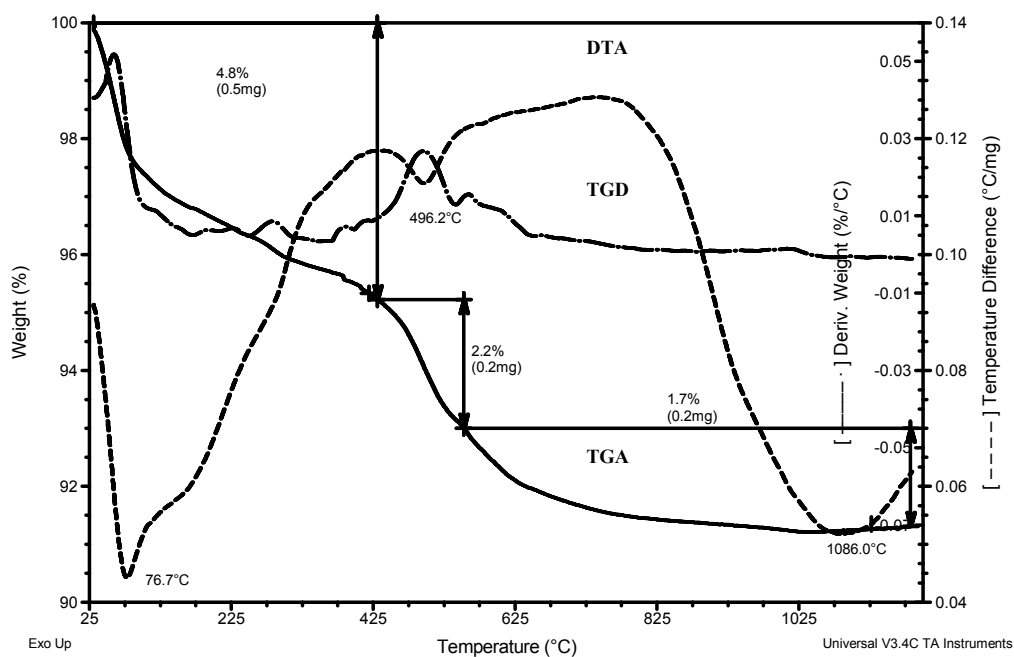


Figure 4.2 The thermogravimetric (DTA/TGA/TGD) curves for the natural diatomite

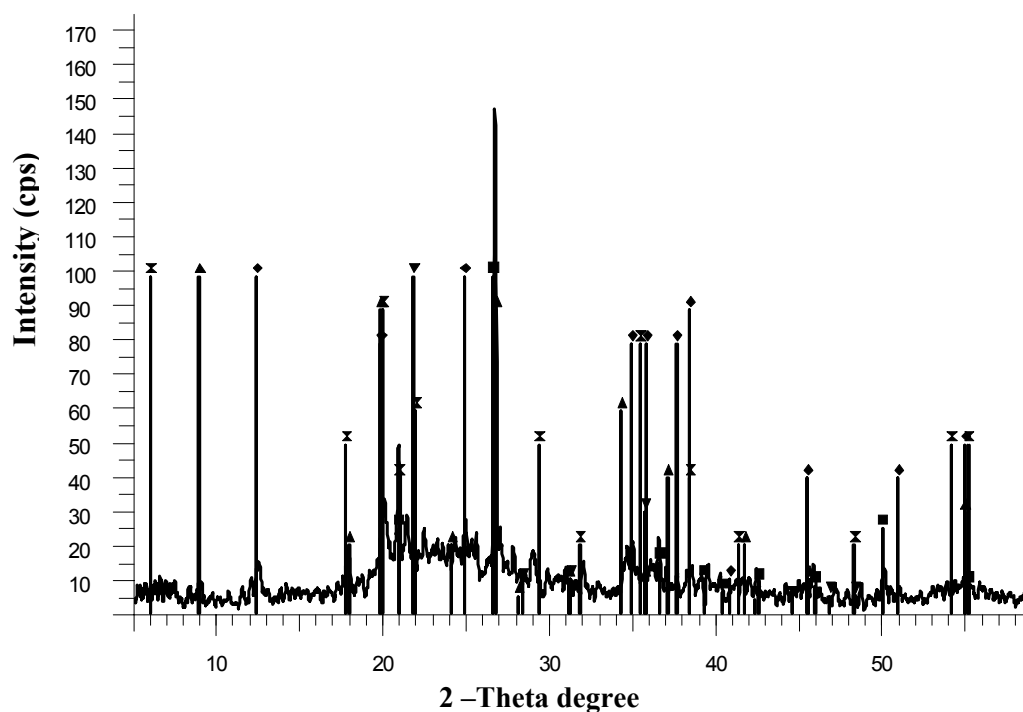


Figure 4.3 XRD pattern of the natural diatomite compared with the standard pattern from JCPDS database (■ quartz, ◆ kaolinite, × montmorillonite, ▲ illite and ▼ opal)

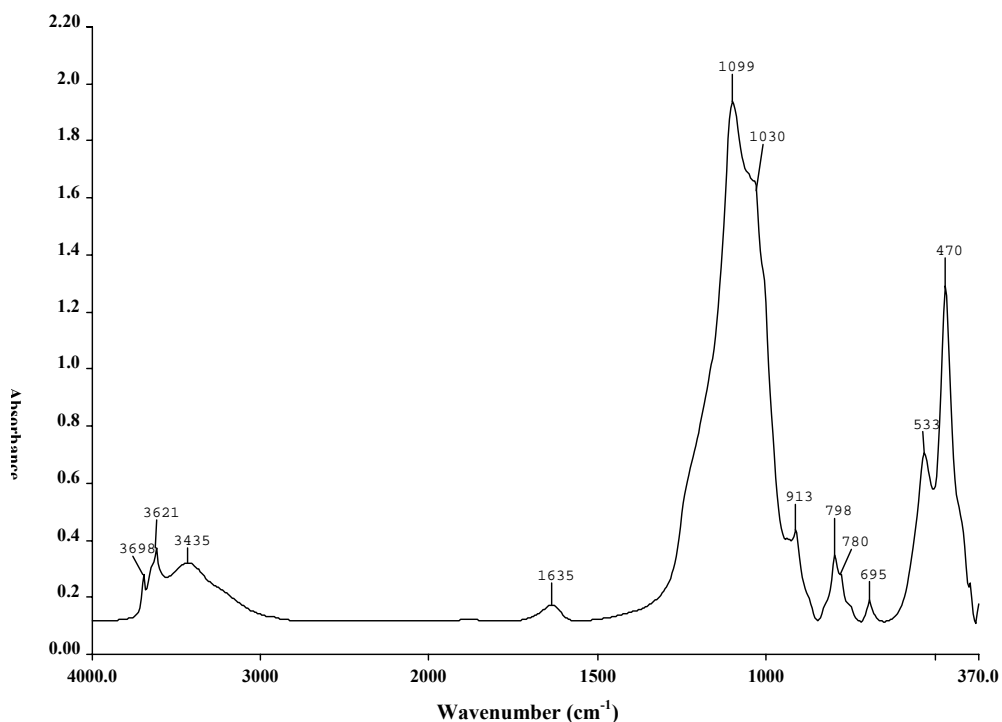


Figure 4.4 FT-IR spectra of the natural diatomite

Table 4.2 Identification of IR absorption bands to specific vibrations

Wavenumber (cm ⁻¹)	Vibrations
3698, 3621	O-H stretching of kaolinite
3435	O-H stretching of water
1635	H ₂ O bending
1099, 1030	Si-O-Si stretching
913	Si-OH stretching, Al-Al-OH bending (kaolinite)
798, 780	Intertetrahedral Si-O-Si bending
695, 470	O-Si-O bending
533	Si-O-Al bending

Since the major composition of diatomite sample is oxide of Si, therefore the IR spectra exhibit the similar series of absorption bands as expected. The FT-IR spectral band intensities of the natural diatomite were at 3698, 3621, 3435, 1635, 1099, 1030, 913, 798, 780, 695, 533 and 470 cm^{-1} . The bands at 3698 and 3621 (weak and narrow) were due to OH stretching vibration of kaolinite, and the band at 3435 assigned to OH stretching of water forming H-bonds. The band at 1635 assigned to bending vibration of adsorbed water. In the region of low wave numbers, there were up to 8 characteristic bands of natural diatomite, the bands at 1099 and 1030 cm^{-1} (strong and broad) were mainly attributed to siloxane (Si-O-Si) stretching of amorphous silica and kaolinite, respectively. The bands at 798 and 780 cm^{-1} correspond to an inter-tetrahedral Si-O-Si bending vibration, while 695 and 470 cm^{-1} bands were due to (O-Si-O) bending, and 913 cm^{-1} (weak and broad) band may be due to Si-OH stretching and Al-Al-OH bending of kaolinite.

4.4. Calcination and acid treatment of diatomite

There is a great deal that may enable us to treat diatomite by calcination and acid as starting material for synthesis of zeolites in order to know the effect of calcination and acid treatment.

4.4.1 Calcination of diatomite

The natural diatomite less than 63 μm was submitted to calcination at 900, 1000 and 1100 $^{\circ}\text{C}$. The particle size distribution of the calcined diatomite with heating rate of 16 $^{\circ}\text{C min}^{-1}$ and 8 $^{\circ}\text{C min}^{-1}$ for 1, 3, 5 and 10 hours is shown in Table 4.3. Calcined at the same temperature, the mean particle sizes differ slightly but quite different in

three temperatures. It showed that the mean particle size decreased with increasing temperature. In addition, the particle size seems to be less effective after 5 hours. The X-ray diffraction patterns of natural diatomite after calcination at different temperatures are shown in Figure 4.5 - 4.7. From the XRD results, it could be expected that natural diatomite remained amorphous pattern at approximately $22^\circ 2\theta$ (4.1 \AA d-spacing) and the presence of quartz at approximately $26.65^\circ 2\theta$ and $20.86^\circ 2\theta$. The calcined diatomite at 1000°C showed only the amorphous silica and quartz. In addition, the diatomite calcined at 900°C also shows tectosilicates ($19.8^\circ 2\theta$) and at 1100°C crystal of cristobalite ($21.8^\circ 2\theta$). The XRD patterns of 900°C and 1000°C show only slightly different after 5 hours. However, the XRD pattern of 1100°C was more effective than 900°C and 1000°C after 5 hours. It indicates that amorphous (Opal-A) can be easily transformed into crystalline structure (cristobalite) by calcination at 1100°C . Not only the natural diatomite altered by the calcination but also some chemical bondings as shown by FT-IR measurement.

FT-IR spectra for diatomite samples after calcination with heating rate of $16^\circ \text{C min}^{-1}$ were compared to the natural diatomite with heating rate of $8^\circ \text{C min}^{-1}$ for 1, 3, 5 and 10 hours, shown in Figure 4.8 - 4.10. The dehydroxylation of the natural diatomite samples (elimination of the OH stretching) from Si-OH and Al-Al-OH bond at 913 cm^{-1} was attained at any conditions of calcination (Belver, Munoz and Vicente, 2002; Shawabkeh and Tutunji, 2003). At the same calcination temperature and time, the IR spectra of the heating rate of $16^\circ \text{C min}^{-1}$ were similar to the heating rate of $8^\circ \text{C min}^{-1}$ for all samples. In the region of OH stretching vibration of water, it shows a band at 3436 cm^{-1} , which is typical of water forming hydrogen bond on the diatomite and remained in all samples after the calcination.

Table 4.3 Particle size distribution of calcined diatomite

Condition	Particle size (μm)
1. Calcined at 900 °C (heating rate 16 °C min ⁻¹) for 1 h	19.14
2. Calcined at 900 °C (heating rate 16 °C min ⁻¹) for 3 h	18.55
3. Calcined at 900 °C (heating rate 16 °C min ⁻¹) for 5 h	18.15
4. Calcined at 900 °C (heating rate 16 °C min ⁻¹) for 10 h	18.17
5. Calcined at 900 °C (heating rate 8 °C min ⁻¹) for 1 h	18.52
6. Calcined at 900 °C (heating rate 8 °C min ⁻¹) for 3 h	18.52
7. Calcined at 900 °C (heating rate 8 °C min ⁻¹) for 5 h	18.34
8. Calcined at 900 °C (heating rate 8 °C min ⁻¹) for 10 h	18.36
9. Calcined at 1000 °C (heating rate 16 °C min ⁻¹) for 1 h	17.82
10. Calcined at 1000 °C (heating rate 16 °C min ⁻¹) for 3 h	17.52
11. Calcined at 1000 °C (heating rate 16 °C min ⁻¹) for 5 h	17.16
12. Calcined at 1000 °C (heating rate 16 °C min ⁻¹) for 10 h	17.42
13. Calcined at 1000 °C (heating rate 8 °C min ⁻¹) for 1 h	17.70
14. Calcined at 1000 °C (heating rate 8 °C min ⁻¹) for 3 h	17.74
15. Calcined at 1000 °C (heating rate 8 °C min ⁻¹) for 5 h	17.55
16. Calcined at 1000 °C (heating rate 8 °C min ⁻¹) for 10 h	17.88
17. Calcined at 1100 °C (heating rate 16 °C min ⁻¹) for 1 h	18.22
18. Calcined at 1100 °C (heating rate 16 °C min ⁻¹) for 3 h	16.84
19. Calcined at 1100 °C (heating rate 16 °C min ⁻¹) for 5 h	16.82
20. Calcined at 1100 °C (heating rate 16 °C min ⁻¹) for 10 h	16.16
21. Calcined at 1100 °C (heating rate 8 °C min ⁻¹) for 1 h	15.52
22. Calcined at 1100 °C (heating rate 8 °C min ⁻¹) for 3 h	18.14
23. Calcined at 1100 °C (heating rate 8 °C min ⁻¹) for 5 h	17.69
24. Calcined at 1100 °C (heating rate 8 °C min ⁻¹) for 10 h	17.43

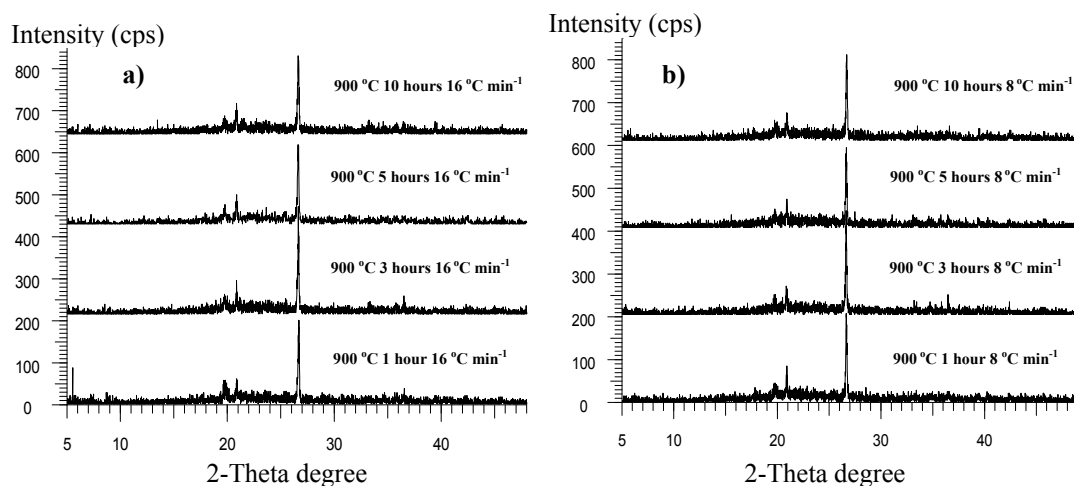


Figure 4.5 XRD patterns of calcined diatomite (a) natural diatomite calcined at 900 °C with a heating rate of 16 °C min⁻¹ for 1, 3, 5 and 10 hours (b) natural diatomite calcined at 900 °C with a heating rate of 8 °C min⁻¹ for 1, 3, 5 and 10 hours

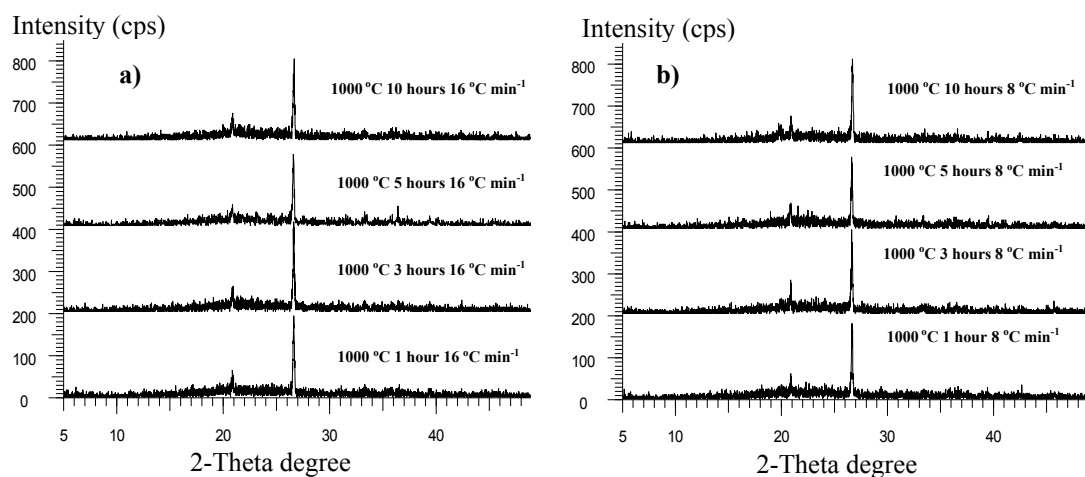


Figure 4.6 XRD patterns of calcined diatomite (a) natural diatomite calcined at 1000 °C with a heating rate of 16 °C min⁻¹ for 1, 3, 5 and 10 hours (b) natural diatomite calcination at 1000 °C with a heating rate of 8 °C min⁻¹ for 1, 3, 5 and 10 hours

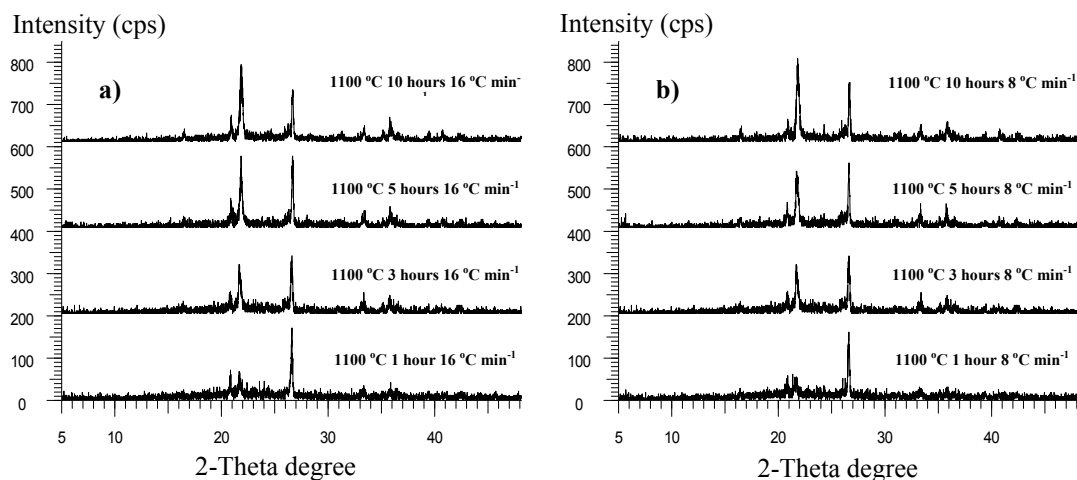


Figure 4.7 XRD patterns of calcined diatomite (a) natural diatomite calcined at 1100 °C with a heating rate of 16 °C min⁻¹ for 1, 3, 5 and 10 hours (b) natural diatomite calcined at 1100 °C with a heating rate of 8 °C min⁻¹ for 1, 3, 5 and 10 hours

A weak additional band, assigned to the H-O-H bending vibration mode of H₂O adsorbed molecules, can be seen at 1635 - 1623 cm⁻¹. The OH stretching bands of kaolinite at 3698 and 3621 cm⁻¹ were eliminated in all samples after the calcination. The absorption band at 533 cm⁻¹, which related to Al at octahedral sheet (Si-O-Al bending) of kaolin (Belver et al., 2002), was not observable even after being calcined at 900, 1000 and 1100 °C. This is because the octahedral sheet changed into tetrahedral sheet of metakaolin (Belver et al., 2002). According to the calcination at 900 °C, it showed mullite structure and a part of metakaolin with a band at 553 cm⁻¹ (Ojima, 2003). The appearance of a new band at 616 cm⁻¹ when calcined at 1100 °C shows the typical of cristobalite. Generally, the calcination temperature condition was chosen in the range that enable the complete transformation of natural diatomite. According to the results of particle size distribution, XRD and FT-IR, the calcination temperature of 900, 1000 and 1100 °C with a heating rate of 16 °C min⁻¹ for 5 hours

were chosen for further experiment because at these calcination temperatures the structural transformation was quite well and the mean particle size was very slightly different after 5 hours either with $16\text{ }^{\circ}\text{C min}^{-1}$ or $8\text{ }^{\circ}\text{C min}^{-1}$. In addition, the mean particle size of heating rate of $16\text{ }^{\circ}\text{C min}^{-1}$ trended to be smaller than the heating rate of $8\text{ }^{\circ}\text{C min}^{-1}$. The IR spectra of calcined diatomite at 900, 1000 and 1100 $^{\circ}\text{C}$ with a heating rate of $16\text{ }^{\circ}\text{C min}^{-1}$ for 5 hours was given in Figure 4.11. After calcination, the intensities of these bands (3698, 3621, 913 and 533 cm^{-1}) disappeared. The appearance of a new band at 553 cm^{-1} of 900 $^{\circ}\text{C}$ gave a characteristic tectosilicates structure of mullite and metakaolin. A band at 616 cm^{-1} appeared during the calcination of 1100 $^{\circ}\text{C}$ and progressed continuously with increasing heating time, this band is attributed to the typical band of cristobalite. The chemical compositions of diatomite sample after calcination at 900, 1000 and 1100 $^{\circ}\text{C}$ with a heating rate of $16\text{ }^{\circ}\text{C min}^{-1}$ for 5 hours was determined by XRF as given in Table 4.4. The Si/Al ratio of natural diatomite and calcined diatomite for 900, 1000 and 1100 $^{\circ}\text{C}$ was 4.35, 4.37, 4.40 and 4.38, respectively. Therefore, Si/Al ratio of natural diatomite slightly differ from the calcined diatomite. The calcination of diatomite at 900, 1000 and 1100 $^{\circ}\text{C}$ with a heating rate of $16\text{ }^{\circ}\text{C min}^{-1}$ for 5 hours were determined by SEM. The micrographs are shown in Figure 4.12. Each micrograph was taken at the electron energy of 10 kV with a magnification of 1000 and 5000 times, respectively. From the SEM micrograph of the calcined diatomite at 900 and 1000 $^{\circ}\text{C}$ gave details of diatomite structure, which was still original geometry. After calcined at 1100 $^{\circ}\text{C}$, the material still showed signs of its original diatomite structure, but the concave and convex surfaces were almost gone, and smoother surfaces were formed instead.

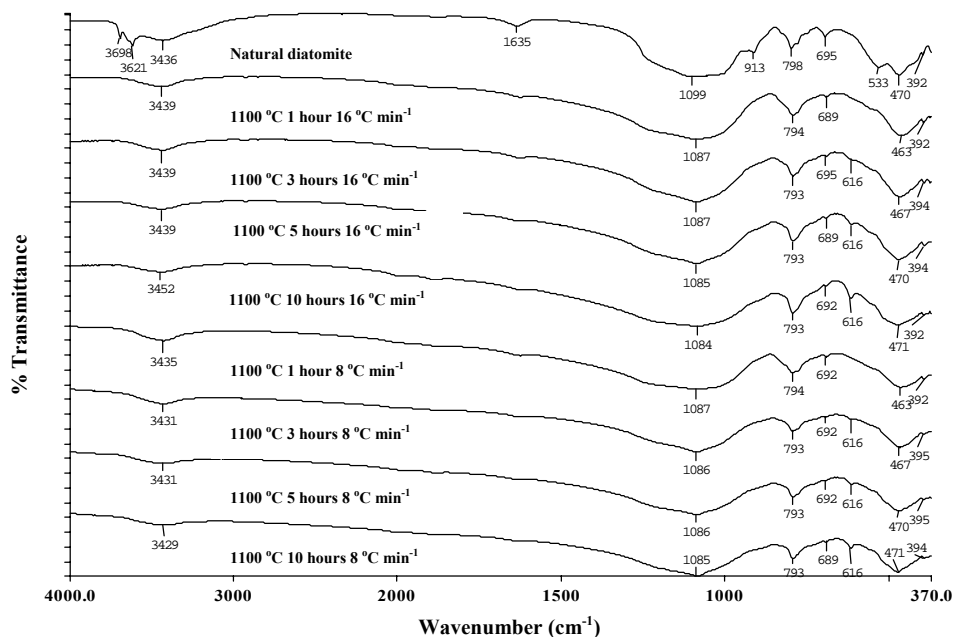


Figure 4.10 IR transmission spectra for natural diatomite after calcination at 1100 °C with a heating rate of 16 °C min⁻¹ and 8 °C min⁻¹ for 1, 3, 5 and 10 hours compared to the natural diatomite sample.

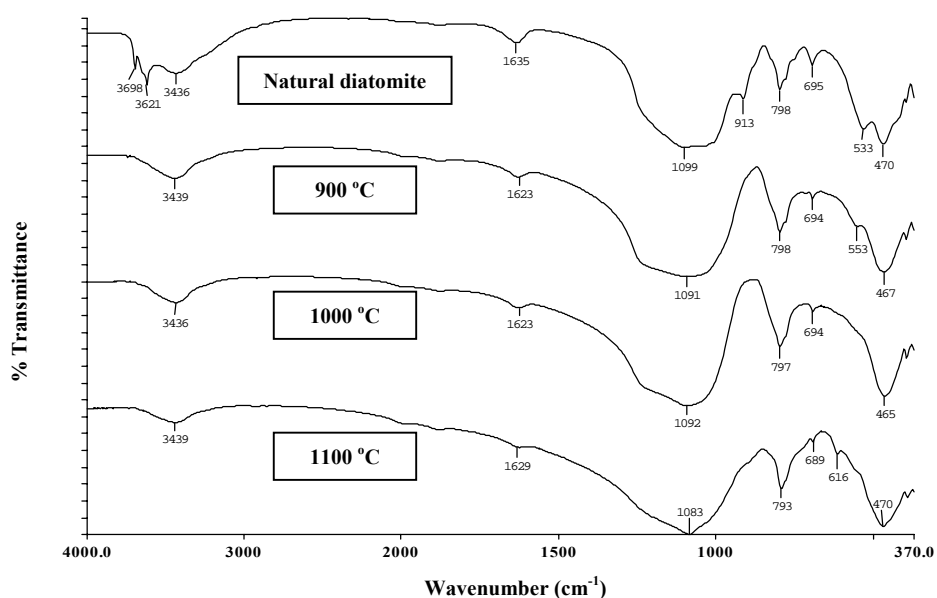


Figure 4.11 IR transmission spectra for natural diatomite after calcination at 900, 1000 and 1100 °C with a heating rate of 16 °C min⁻¹ for 5 hours compared to the natural diatomite sample.

Table 4.4 The chemical compositions and Si/Al ratios of calcined diatomite

Chemical content (% weight)	Natural diatomite	Calcination at 900 °C	Calcination at 1000 °C	Calcination at 1100 °C
SiO ₂	71.90	76.34	76.24	76.73
Al ₂ O ₃	14.60	15.43	15.26	15.48
Fe ₂ O ₃	5.78	6.08	6.08	6.18
K ₂ O	1.95	1.96	1.91	1.92
CaO	0.17	0.17	0.23	0.17
MgO	0.69	0.75	0.79	0.75
MnO	0.01	0.01	0.01	0.01
TiO ₂	0.51	0.53	0.52	0.52
Si/Al ratio	4.35	4.37	4.40	4.38

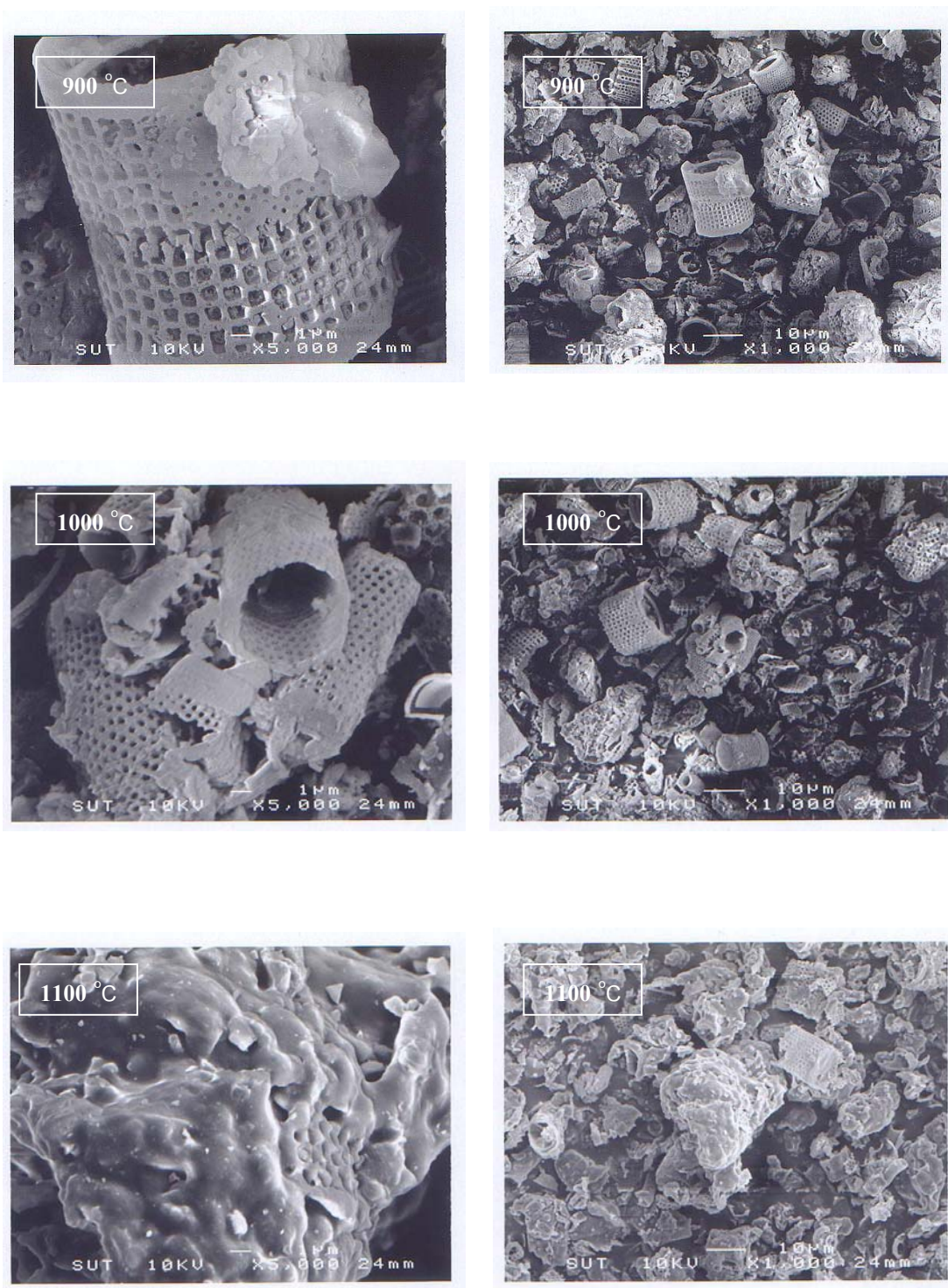


Figure 4.12 SEM micrographs of calcined diatomite obtained after calcination at 900, 1000 and 1100 °C with a heating rate of $16\text{ }^{\circ}\text{C min}^{-1}$ for 5 hours

4.4.2 Acid treatment of diatomite

The results of acid activation experiment in total dissolution percentage as a function of time are tabulated in Table 4.5 and plot between these values are shown in Figure 4.13 - 4.14. The values for the total dissolution percentages of the material in Table 4.5 and Figure 4.13 - 4.14 were calculated from the difference in weight between the starting and undissolved materials (filter cake). After diatomite samples were contacted with acid (6M HCl, 6M H₂SO₄ and 6M HNO₃), they great influence on the brightness. The weight percentage of dissolved substances in diatomite was effected by both the cold and hot (reflux 100 °C) conditions. The weight percentage of dissolved substances changed more rapidly by the hot condition rather than the cold condition. There was also a much greater difference between cold and hot treatment. In the conditions of cold acid treatments after 120 hours, the percentage of total dissolution trend to decrease. This may be the limit of solubility of impurities, and occur some insoluble metallic oxide complexes of SO₄²⁻, Cl⁻ and NO₃⁻. In contrast, the weight percentage of dissolve substances raised enormous by reflux when increasing treatment time. The maximum extents of dissolution were obtained using hot acid solutions. It is well known that many acids dissolve certain substance in diatomite and alter their chemical compositions (Hassan et al., 1999; Goren et al., 2002). The chemical composition of the acid activation was determined by WDXRF as given in Table 4.6. The obtained dissolution treated with 6M hot acid for 24 hours contained great amounts of the soluble oxides. The high solubility may be resulted from the appearance of the soluble oxides in contact with the solvent acid due to the destruction of the physical structure of diatom and other particles. Again, significant

amounts of amorphous silica may be dissolved together with alumina when the activation time was increased (Goren et al., 2002). The hot acid activation for 24 hours was chosen for the following experiment because it took long enough time for the purification. Figure 4.15 shows the XRD patterns of the diatomite treated with hot acid and amorphous silica and quartz. This suggests that the acid activation does not change the diatomite structure and quartz. FT-IR spectra of hot acid treatment samples are shown in Figure 4.16. The IR band intensities of Si-OH or Al-Al-OH at 913 cm^{-1} and Si-O-Al which is related to Al octahedral sheet found at 533 cm^{-1} , decreased more rapidly when the diatomite was activated with hot 6M HCl rather than with hot 6M HNO₃. These bands were eliminated with hot 6M H₂SO₄ for 24 hours. This trend can be seen in the region of OH stretching vibration of kaolinite (3698 and 3621 cm^{-1}) as well. The results indicated that clay minerals can be more easily removed with hot H₂SO₄ than with others. The SEM micrograph of the acid activation diatomite in Figure 4.17 shows that the original geometry of the pores was preserved but there was a collapse of the skeletal structure.

X-ray diffraction analyses of diatomite were calcined at 900, 1000 and 1100 °C for 5 hours and the diatomite sample treated first with calcination at 900, 1000 and 1100 °C for 5 hours, then followed with hot 6M H₂SO₄ for 24 hours as well as the samples treated at first with hot 6M H₂SO₄, then with calcination at 900, 1000 and 1100 °C, are shown in Table 4.7. The first treated with hot 6M H₂SO₄ and, then calcined samples remained amorphous even though at the temperature of 1100 °C. On the other hand the samples calcined at 1100 °C and first calcined at 1100 °C, then treated with hot 6M H₂SO₄ material caused crystallization at 1100 °C. This suggested

that the samples contained some impurities, which caused crystallization of cristobalite.

Table 4.5 The total dissolution percentages of diatomite

Type of acid	Condition	The leaching time (hours)	Dissolve mass, wt-%
6M HCl	Cold	24	6.58
		72	7.52
		120	8.14
		168	7.84
	Hot (reflux 100 °C)	1	14.7
		6	18.24
		12	21.15
		24	22.05
6M H ₂ SO ₄	Cold	24	4.95
		72	6.79
		120	7.81
		168	6.26
	Hot (reflux 100 °C)	1	15.99
		6	22.54
		12	24.09
		24	27.40
6M HNO ₃	Cold	24	3.35
		72	4.61
		120	5.52
		168	4.70
	Hot (reflux 100 °C)	1	12.44
		6	14.67
		12	17.99
		24	19.86

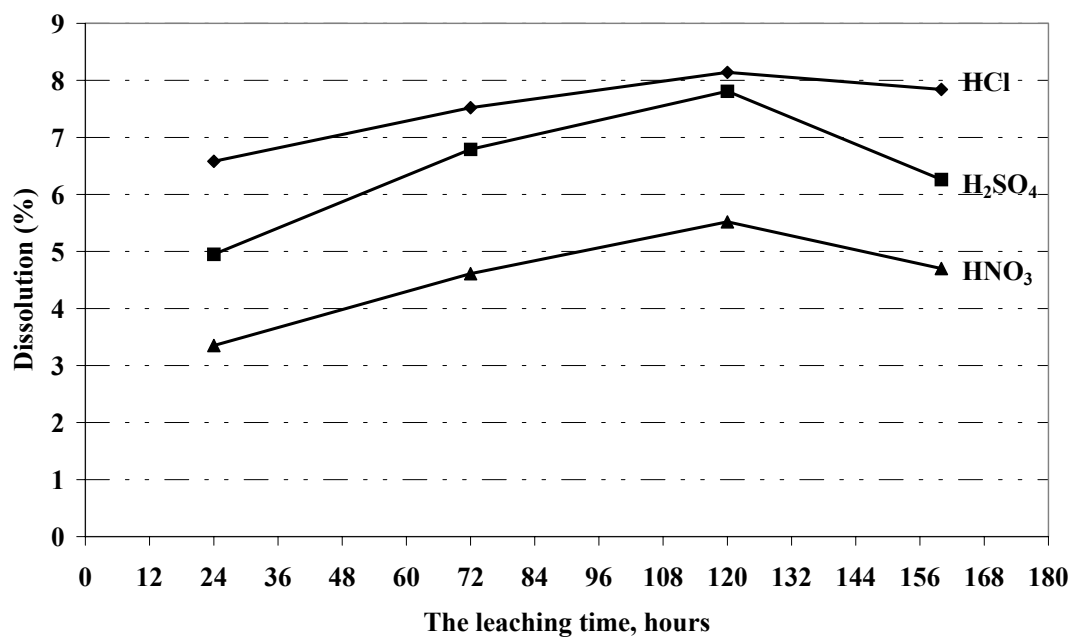


Figure 4.13 The total dissolution percentages of the material in cold acidic

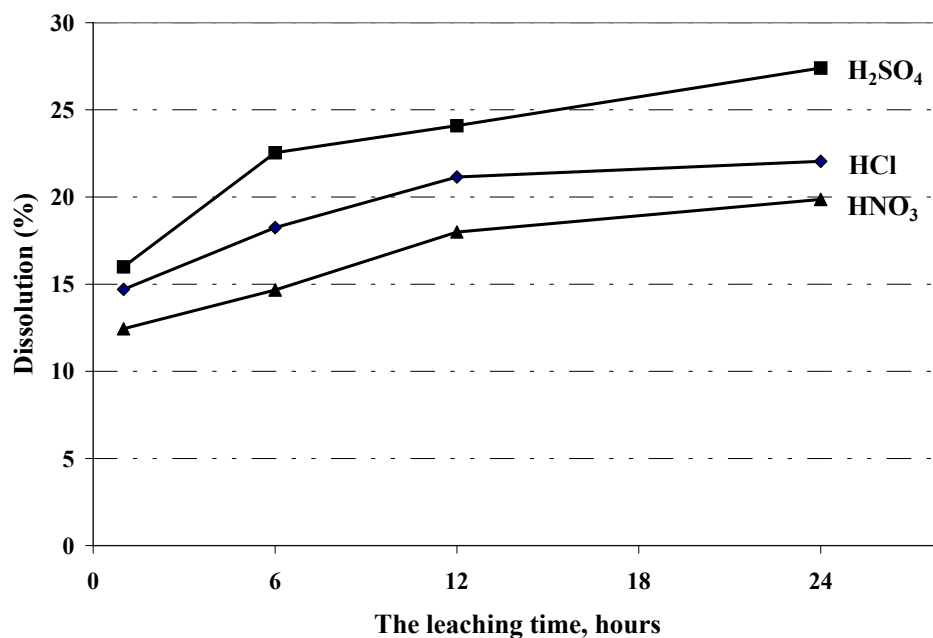


Figure 4.14 The total dissolution percentages of the material in hot acidic

Table 4.6 The chemical compositions and Si/Al ratios of acid activation of diatomite compared to the natural diatomite determined by XRF

Material	Chemical content (% weight)								Si/Al ratio
	SiO ₂	Al ₂ O ₃	Fe ₂ O ₃	K ₂ O	CaO	MgO	MnO	TiO ₂	
Natural diatomite	71.90	14.60	5.78	1.95	0.17	0.69	0.01	0.51	4.35
Cold, 6M H ₂ SO ₄ 120 h	75.83	14.86	4.01	1.97	0.00	0.51	0.00	0.52	4.50
Cold, 6M HCl 120 h	75.57	14.89	3.19	1.97	0.00	0.50	0.00	0.52	4.48
Cold, 6M HNO ₃ 120 h	73.27	14.69	5.44	1.87	0.00	0.51	0.00	0.51	4.40
Hot, 6M H ₂ SO ₄ 24 h	93.56	3.63	0.53	0.80	0.00	0.16	0.00	0.46	22.77
Hot, 6M HCl 24 h	91.14	5.34	0.60	1.12	0.00	0.20	0.00	0.53	15.10
Hot, 6M HNO ₃ 24 h	86.60	8.54	0.85	1.63	0.00	0.32	0.00	0.57	8.96

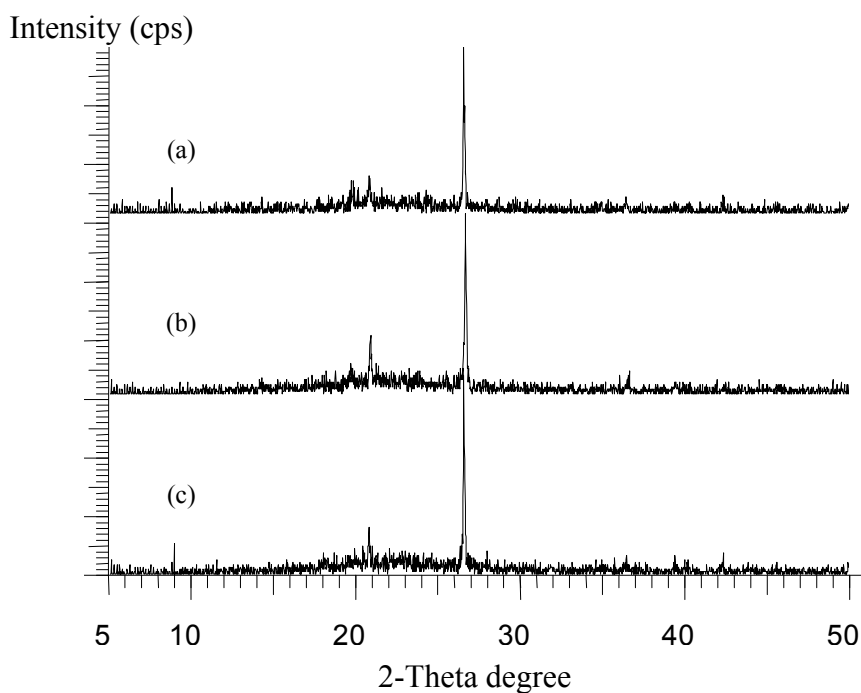


Figure 4.15 XRD patterns of diatomite treated with hot acid (a) 6M HNO₃ (b) 6M HCl and (c) 6M H₂SO₄ for 24 hours

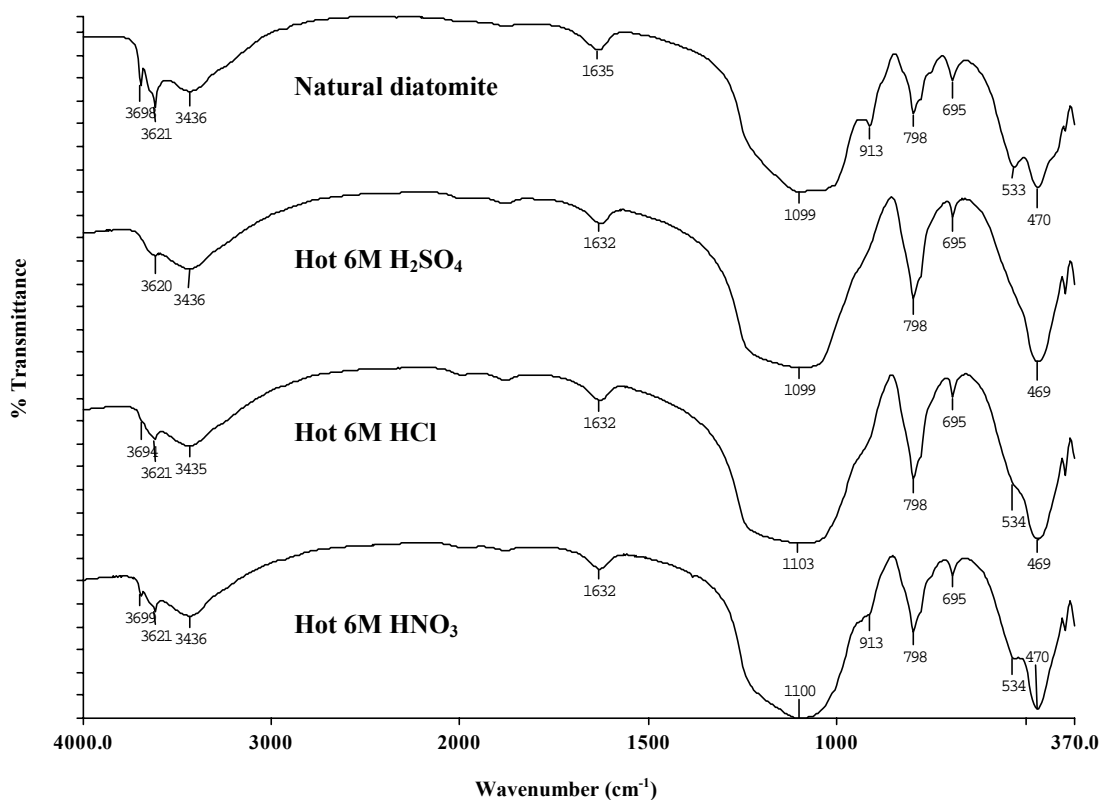


Figure 4.16 IR transmission spectra for diatomite after hot acid activation for 24 hours compared to the natural diatomite sample

Table 4.7 X-ray diffraction analyses of thermal and acid treatment natural diatomite samples

Temperature (°C)	Raw diatomite	Calcined-treated with H ₂ SO ₄	Treated with H ₂ SO ₄ -calcined
900	Amorphous	Amorphous	Amorphous
1000	Amorphous	Amorphous	Amorphous
1100	Cristobalite	Cristobalite	Amorphous

4.5 Starting diatomite materials for synthesis of sodium zeolites

Starting materials for synthesis of sodium zeolites consisted of six samples from different various modified and unmodified diatomite. As mentioned above, all these observations lead us to choose; (No.1) natural diatomite, (No.2) diatomite calcined at 900 °C, (No.3) diatomite calcined at 1000 °C, (No.4) diatomite calcined at 1100 °C, (No.5) diatomite treated with hot 6M H₂SO₄ for 24 hours and (No.6) diatomite first treated with hot 6M H₂SO₄ and then calcined at 1100 °C. The elemental composition weight percentage of the sample No.6 obtained by WDXRF as follows: SiO₂, 94.42; Al₂O₃, 3.68, Fe₂O₃, 0.50; K₂O, 0.68; MgO, 0.14 and TiO₂, 0.43. The Si/Al ratio of this starting material was 22.7. According to Table 4.4 and 4.6 the material of No.1, No.2, No.3 and No.4, the Si/Al ratio is about 4.4 and contains the same type of impurities but different type of phase (from XRD, FT-IR analysis), while the Si/Al ratio of material of No.5 and No.6 is around 22.8. It is also found that the particle size distribution of these materials depends on the treatment conditions. It varies from 9 - 18 μm for all samples (see Table 4.8 and Figure 4.18). They contained with the high purity of silica and low other element impurities. We thought that the different conditions for modification of diatomite would produce the samples with different surface morphology and silica structures which are influential in their reactivity for syntheses of zeolites. Amorphous silica is often highly active for the zeolites synthesis whereas crystalline silica is inactive (Halimatun, Mohd, Salasiah, Endang and Zainab, 1997). The researcher has carried out structural analysis of six starting materials using ²⁹Si magic-angle spinning nuclear magnetic resonance (MAS NMR). The ²⁹Si MAS

NMR spectrum of the natural diatomite and the modified diatomites are given in Figure 4.19.

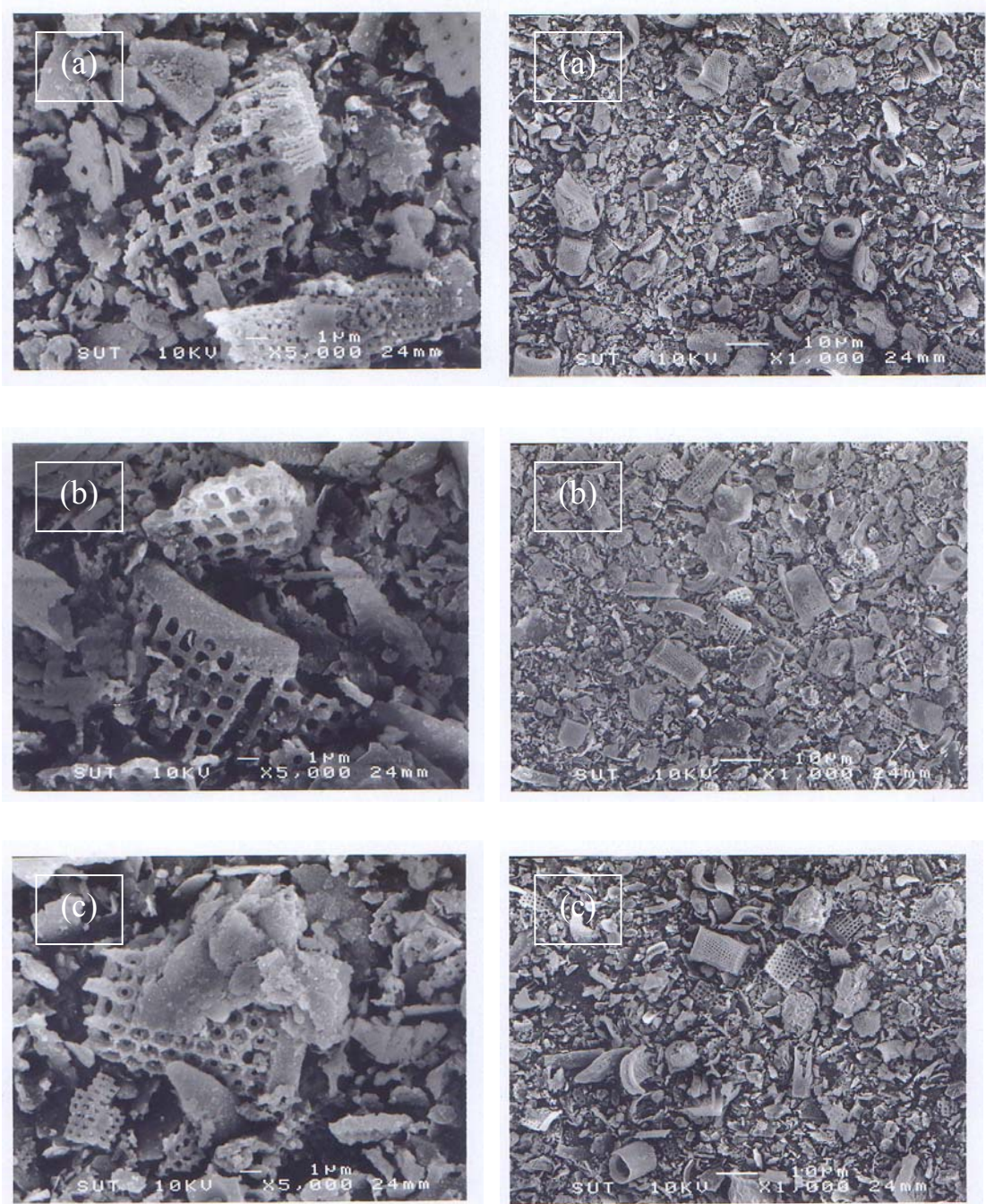


Figure 4.17 SEM micrographs of acid activation (reflux 100 °C 24 hours) for (a) 6M H₂SO₄ (b) 6M HCl (c) 6M HNO₃ with 5000x and 1000x magnification

Table 4.8 The mean particle size of starting diatomite materials

Starting materials	Mean particle size (μm)
Natural raw diatomite	9.88
Diatomite calcined at 900 °C	18.15
Diatomite calcined at 1000 °C	17.16
Diatomite calcined at 1100 °C	16.82
Diatomite treated with hot 6M H_2SO_4	11.48
Diatomite first treated with hot 6M H_2SO_4 and then calcined at 1100 °C	9.17

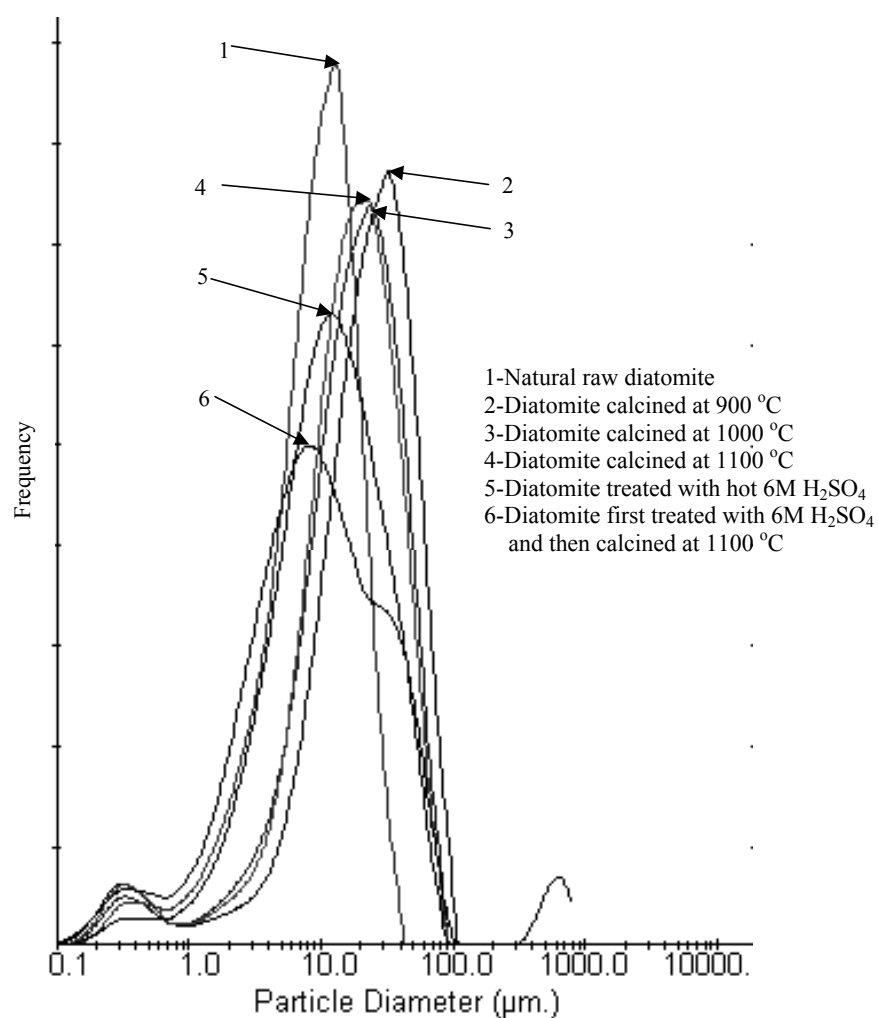


Figure 4.18 Particle size distribution of starting materials for synthesise sodium zeolite

All the spectra were simulated using essentially Gaussian function. As SiO_4 site can be labeled as Q^n , where n designates the number of bridging oxygens (those shared with tetrahedral silicon). The ^{29}Si MAS NMR spectrum of natural diatomite consisted of 6 resonances at -86.1, -92.2, -94.3, -104.8, -108.2 and -112.6 ppm which were characteristic of Q^2 (-86.1, -92.2), Q^3 (-94.3) and Q^4 (-104.8, -108.2, -112.6), respectively. The chemical shifts of ^{29}Si for calcined diatomite at 900 °C, 1000 °C and 1100 °C, and diatomite treated with hot 6M H_2SO_4 and diatomite treated firstly with hot 6M H_2SO_4 then calcined at 1100 °C show two components that appear in the range of -94.1 to -95.8 ppm, corresponding to Q^3 site and -103.2 to -114.1 ppm attributed to Q^4 site (Table 4.9) (Gunter, 1989). In all cases the spectrum was dominated by a large Q^4 ($[\text{Si}(\text{OSi})_4]$) resonance at -103.2 to -114.1 ppm. The low intensity peak corresponding to Q^2 resonance at -86.1 to -92.2 ppm has been assigned on the basis of chemical shift correlations and relaxation data to germinal hydroxyl silanol sites, e.g. to silicon atoms with two siloxane bonds and two hydroxyl groups. The Q^3 resonance at -94.1 to -95.8 was found to be silicon atoms with three siloxane bonds and one hydroxyl group. The sharp intensity peak corresponding to Q^4 resonance at -103.2 to -114.1 ppm was found to be silicon atoms with four siloxane bonds. The compositions of these samples are indicated in Table 4.10 and represented in Figure 4.20. The curves resulting from fitting were obtained with three peaks of Q^4 resonances. The intensities of the Q^4 (in %) about -104, -109.5 and -112.6 ppm are 15.37 to 33.91, 1.15 to 5.56 and 46.29 to 73.15, respectively. The Q^4 about -109.5

ppm being very low intensity when compared with the others, which is expected to be of the crystalline quartz which not influenced by the treatment conditions.

Table 4.9 Chemical shift (ppm) of ^{29}Si MAS NMR in diatomite samples

	Q ²	Q ²	Q ³	Q ⁴	Q ⁴	Q ⁴
Natural diatomite	-86.1	-92.2	-94.3	-104.8	-108.2	-112.6
Diatomite calcined at 900 °C	-	-	-94.5	-104.4	-108.9	-112.4
Diatomite calcined at 1000 °C	-	-	-94.5	-103.2	-109.7	-111.7
Diatomite calcined at 1100 °C	-	-	-94.1	-104.9	-110.5	-113.6
Diatomite treated with hot 6M H ₂ SO ₄	-	-	-94.2	-104.8	-109.5	-113.8
Diatomite treated with hot 6M H ₂ SO ₄ and calcined at 1100 °C	-	-	-95.8	-106.4	-110.4	-114.1

Table 4.10 Percentage of Qⁿ (silicon coordination) in diatomite samples (results from ^{29}Si MAS NMR)

Sample type	Q ⁴			Q ⁴	Q ³	Q ²
	-104.8 ± 1.6 ppm	-109.5 ± 1.3 ppm	-113.0 ± 1.3 ppm	(% total)	(% total)	(% total)
Natural diatomite	15.37	2.23	46.29	63.89	12.78	23.33
Diatomite calcined at 900 °C	21.42	5.56	51.90	78.88	21.12	-
Diatomite calcined at 1000 °C	20.73	3.42	68.82	92.97	7.03	-
Diatomite calcined at 1100 °C	33.91	1.16	55.49	90.56	9.45	-
Diatomite treated with hot 6M H ₂ SO ₄	29.95	1.15	63.85	94.95	5.04	-
Diatomite treated with hot 6M	20.41	3.65	73.15	97.21	2.79	-

H₂SO₄ and calcined at 1100 °C

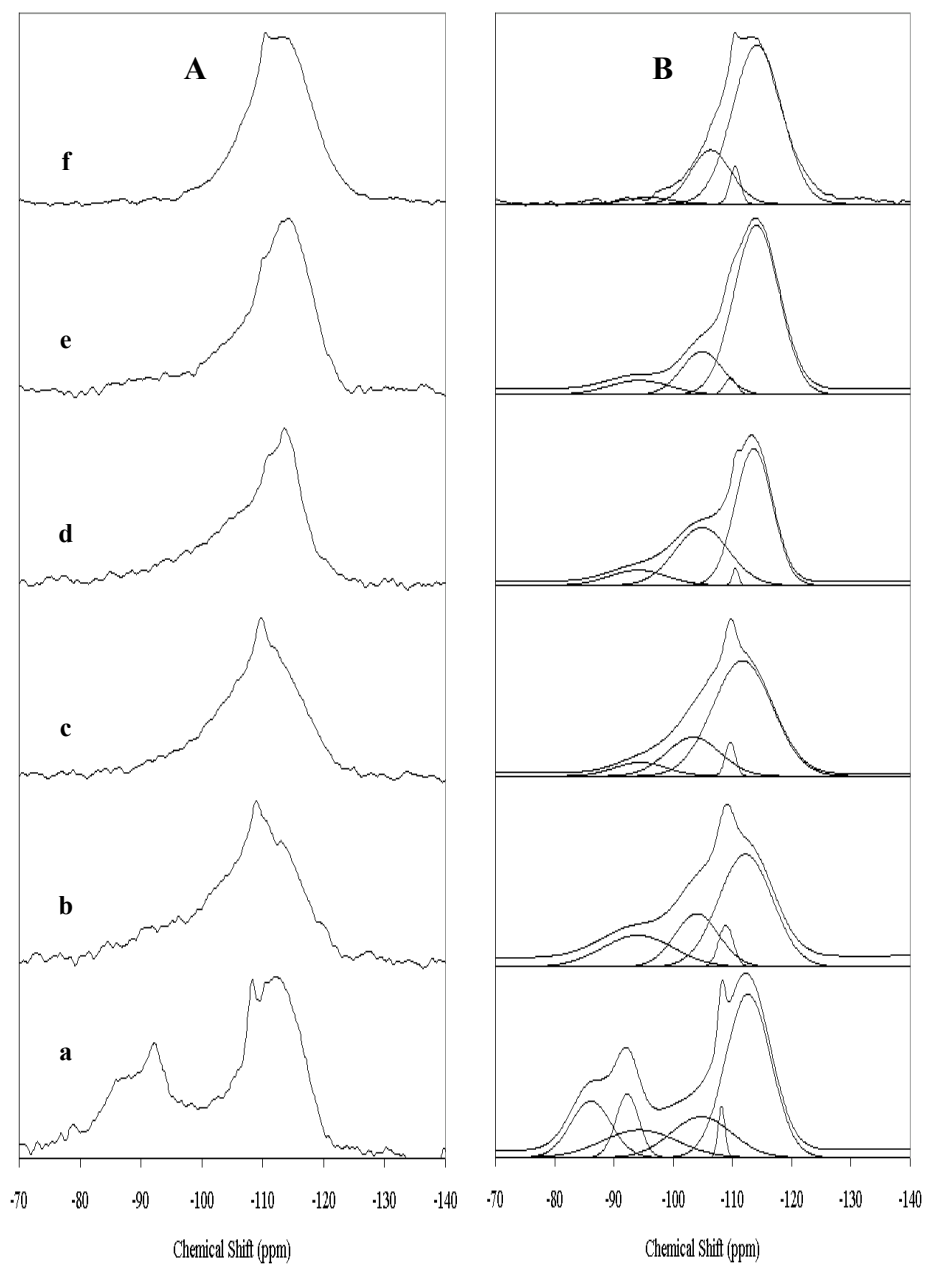


Figure 4.19 Experimental (A) and simulated (B) MAS ²⁹Si-NMR spectra (arbitrary intensity unit) of the various diatomite samples (a) natural diatomite (b) diatomite

calcined at 900 °C, (c) diatomite calcined at 1000 °C, (d) diatomite calcined at 1100 °C, (e) diatomite treated with hot (reflux) 6M H₂SO₄ and (f) diatomite treated with hot (reflux) 6M H₂SO₄ and calcined at 1100 °C

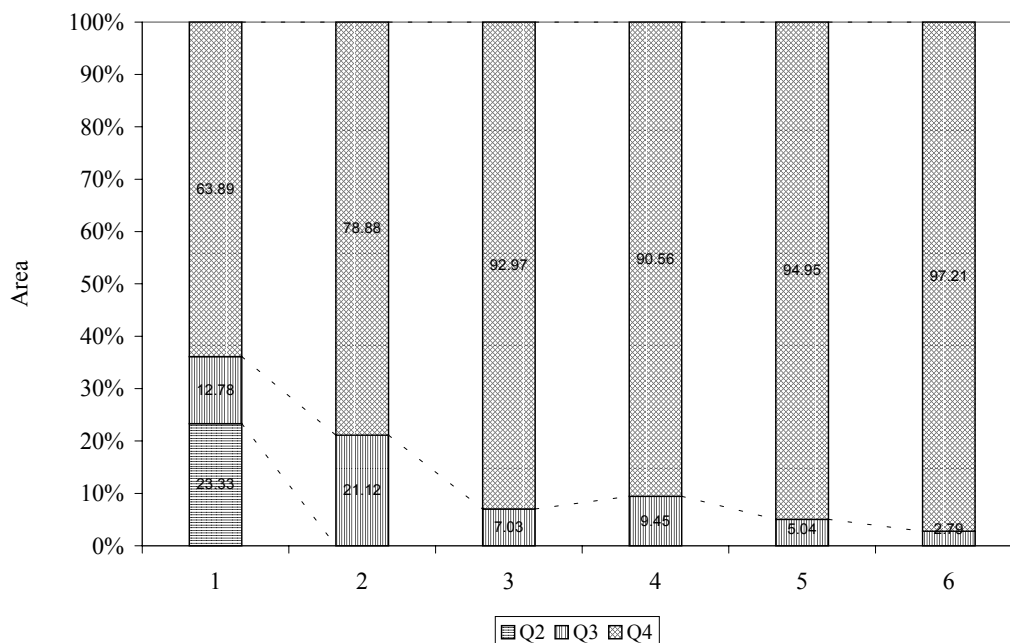


Figure 4.20 The percentage of Q², Q³(total) and Q⁴(total) from simulation of the ²⁹Si MAS NMR spectra of starting diatomite materials (1) natural diatomite (2) diatomite calcined at 900 °C (3) diatomite calcined at 1000 °C (4) diatomite calcined at 1100 °C (5) diatomite treated with hot 6M H₂SO₄ and (6) diatomite first treated with hot 6M H₂SO₄ then calcined at 1100 °C

The Q⁴ (-113) sites are present in pure SiO₂ and the Q⁴(-104.8) sites are unknown. Thus, the peak position for the Q⁴ (-104.8) sites has been allowed to vary in order to obtain the best fit. In addition, the MAS spectra of samples displaying Q⁴ (-104.8) peak are expected to be the chemical shifts of Q⁴ (-113) connected to one or more Q³ nearest neighbors (Sen and Youngman, 2003). The results obtained with ²⁹Si MAS NMR spectra confirmed the expected increase in the relative area of (Q⁴) silicon sites

after the heat and acid treatment. The broadness of these peaks and the pronounced spinning side bands reflect the relatively concentration of Fe present in the samples.



Figure 4.21 diatomite starting material



Figure 4.22 diatomite calcined at 900 °C for starting material



Figure 4.23 diatomite calcined at 1000 °C for starting material



Figure 4.24 diatomite calcined at 1100 °C for starting material



Figure 4.25 diatomite treated with hot 6M H₂SO₄ for starting material



Figure 4.26 diatomite first treated with hot 6M H₂SO₄ then calcined at 1100 °C for starting material

4.6. The synthesis of sodium zeolite

In this work various parameters influencing on the zeolite synthesis such as temperature alkaline concentration, solid/liquid ratio, reaction time and especially different structural silica from starting diatomite materials are investigated. The results show that the zeolites obtained were only analcime (ANA), Na-P1 (GIS), hydroxysodalite (SOD) and cancrinite (CAN). All of zeolitic phases obtained from the different starting diatomite materials under different conditions are reported in Table 4.11.

Table 4.11 Zeolitic phase synthesized from starting diatomite materials using NaOH as activation agents, with the chemical composition reported in collection of simulated XRD patterns for zeolites (Treacy et al., 2001)

Zeolitic product	Chemical composition
analcime	$\text{Na}_{16}(\text{H}_2\text{O})_{16} [\text{Si}_{32}\text{Al}_{16}\text{O}_{96}]$
Na-P1	$\text{Na}_6(\text{H}_2\text{O})_{12} [\text{Si}_{10}\text{Al}_6\text{O}_{32}]$
hydroxysodalite	$\text{Na}_6(\text{H}_2\text{O})_8 [\text{Si}_6\text{Al}_6\text{O}_{24}]$
cancrinite	$\text{Na}_7\text{Ca}_{0.9}(\text{CO}_3)_{1.4}(\text{H}_2\text{O})_{2.1} [\text{Si}_6\text{Al}_6\text{O}_{24}]$

The phase identification is performed by comparing the observed powder patterns with the calculated ones reported in collection of simulated XRD powder patterns for zeolites (Treacy et al., 2001) and their relative intensity yields (int, in counts per second) are reported in Table 4.12. The results of the synthesis condition for all different starting materials for obtaining sodium zeolites are summarized in Table

4.13, 4.14, 4.15, 4.16, 4.17 and 4.18, respectively. The relative intensity yields were given by normalized XRD intensity of the major reflection, see Table 4.12 for each zeolite. Figure 4.27 - 4.32 summarize the different types of zeolite obtained from the experimental condition (temperature, time, concentration of activation solution (NaOH) and solid/liquid ratio). These Figures obtained integration relative intensities (I_{rel}) > 50 for each zeolite phase.

Table 4.12 Reflections (h, k, l), 2θ and [I_{rel}] used in the integration procedure for each zeolite phase

Analcime	Na-P1	Hydroxysodalite	Cancrinite
(211),15.81,[60.2]	(101),12.46,[92.1]	(110),14.16,[61.8]	(110),14.02,[59.5]
(400),25.96,[100]	(200),17.66,[60.6]	(211),24.65,[100]	(101),19.15,[100]
(211),30.54,[51.3]	(112),21.67,[66.1]	(310),31.99,[94.6]	(300),24.40,[55.1]
	(301),28.10,[100]	(222),35.13,[75.7]	(211),27.74,[56.9]

According to XRD patterns of zeolite products, it can be seen that amorphous silica from the starting materials was completely dissolved even though at low temperature and low concentration. However, the zeolite products still contained some impurities from the starting materials, which were hardly dissolved by hydrothermal treatment, thereby remaining in the products. In the synthesis of sodium zeolites, quartz detected a few amounts in the products. It was also not easy to transform quartz into some amorphous at a low concentration of NaOH solution and in a short reaction time, but quartz can be slowly dissolved by the intensive treatment.

Table 4.13 Experimental conditions used for synthesis experiments by natural diatomite material and sodium zeolites obtained

Expt no.	Solution (% w/v)	S:L	T (°C)	Time (h)	Zeolites ^a	Int (cps)
1	10 % NaOH	1:10	100	24	P1	14.5
2	10 % NaOH	1:10	100	72	P1	27.2
3	10 % NaOH	1:10	100	120	P1	39.3
4	10 % NaOH	1:10	100	168	P1	40.7
5	10 % NaOH	1:10	140	24	ANA	69.2
6	10 % NaOH	1:10	140	72	ANA	70.0
7	10 % NaOH	1:10	140	120	ANA	79.4
8	10 % NaOH	1:10	140	168	P1	45.0
9	10 % NaOH	1:10	180	24	ANA	80.0
10	10 % NaOH	1:10	180	72	ANA	80.1
11	10 % NaOH	1:10	180	120	ANA	90.0
12	10 % NaOH	1:10	180	168	ANA	94.5
13	10 % NaOH	1:30	100	24	HS	11.2
14	10 % NaOH	1:30	100	72	HS	27.4
15	10 % NaOH	1:30	100	120	HS	30.8
16	10 % NaOH	1:30	100	168	HS	23.2
17	10 % NaOH	1:30	140	24	HS	19.0
18	10 % NaOH	1:30	140	72	HS	22.6
19	10 % NaOH	1:30	140	120	HS	18.9
20	10 % NaOH	1:30	140	168	HS	20.9
21	10 % NaOH	1:30	180	24	CAN	53.5
22	10 % NaOH	1:30	180	72	CAN	54.2
23	10 % NaOH	1:30	180	120	CAN	67.0
24	10 % NaOH	1:30	180	168	CAN	63.0
25	20 % NaOH	1:10	100	24	HS	28.3
26	20 % NaOH	1:10	100	72	HS	29.8
27	20 % NaOH	1:10	100	120	HS	21.7
28	20 % NaOH	1:10	100	168	HS	26.4
29	20 % NaOH	1:10	140	24	HS	44.1
30	20 % NaOH	1:10	140	72	HS	49.8
31	20 % NaOH	1:10	140	120	HS	54.7
32	20 % NaOH	1:10	140	168	HS	53.8
33	20 % NaOH	1:10	180	24	CAN	62.2
34	20 % NaOH	1:10	180	72	CAN	72.2
35	20 % NaOH	1:10	180	120	CAN	67.7
36	20 % NaOH	1:10	180	168	CAN	74.4
37	20 % NaOH	1:30	100	24	HS	32.0
38	20 % NaOH	1:30	100	72	HS	38.3
39	20 % NaOH	1:30	100	120	HS	40.8
40	20 % NaOH	1:30	100	168	HS	32.2
41	20 % NaOH	1:30	140	24	CAN	47.8
42	20 % NaOH	1:30	140	72	CAN	59.4
43	20 % NaOH	1:30	140	120	CAN	51.6
44	20 % NaOH	1:30	140	168	CAN	52.1
45	20 % NaOH	1:30	180	24	CAN	74.2
46	20 % NaOH	1:30	180	72	CAN	81.2
47	20 % NaOH	1:30	180	120	CAN	79.6
48	20 % NaOH	1:30	180	168	CAN	84.4
49	30 % NaOH	1:10	100	24	HS	42.0

Table 4.13 (Continued)

Expt no.	Solution (% w/v)	S:L	T (°C)	Time (h)	Zeolites ^a	Int (cps)
50	30 % NaOH	1:10	100	72	HS	53.9
51	30 % NaOH	1:10	100	120	HS	39.3
52	30 % NaOH	1:10	100	168	HS	49.1
53	30 % NaOH	1:10	140	24	CAN	47.9
54	30 % NaOH	1:10	140	72	CAN	58.3
55	30 % NaOH	1:10	140	120	CAN	71.4
56	30 % NaOH	1:10	140	168	CAN	71.5
57	30 % NaOH	1:10	180	24	CAN	78.6
58	30 % NaOH	1:10	180	72	CAN	82.9
59	30 % NaOH	1:10	180	120	CAN	81.6
60	30 % NaOH	1:10	180	168	CAN	78.0
61	30 % NaOH	1:30	100	24	HS	38.1
62	30 % NaOH	1:30	100	72	HS	52.9
63	30 % NaOH	1:30	100	120	HS	55.9
64	30 % NaOH	1:30	100	168	HS	64.9
65	30 % NaOH	1:30	140	24	HS; CAN	79.3, 66.2
66	30 % NaOH	1:30	140	72	HS; CAN	70.0, 62.4
67	30 % NaOH	1:30	140	120	HS; CAN	74.3, 67.4
68	30 % NaOH	1:30	140	168	HS; CAN	72.6, 64.1
69	30 % NaOH	1:30	180	24	CAN	73.9
70	30 % NaOH	1:30	180	72	CAN	63.7
71	30 % NaOH	1:30	180	120	CAN	81.2
72	30 % NaOH	1:30	180	168	CAN	76.8

^aP1 = Na-P1; ANA = analcime; HS = hydroxysodalite; CAN = cancrinite

Table 4.14 Experimental conditions used for synthesis experiments by calcined diatomite material at 900 °C and sodium zeolites obtained

Expt no.	Solution (% w/v)	S:L	T (°C)	Time (h)	Zeolites ^a	Int (cps)
1	10 % NaOH	1:10	100	24	P1	35.4
2	10 % NaOH	1:10	100	72	P1	39.0
3	10 % NaOH	1:10	100	120	P1	30.3
4	10 % NaOH	1:10	100	168	P1	56.3
5	10 % NaOH	1:10	140	24	P1	34.0
6	10 % NaOH	1:10	140	72	ANA	74.8
7	10 % NaOH	1:10	140	120	ANA	80.6
8	10 % NaOH	1:10	140	168	ANA	73.0
9	10 % NaOH	1:10	180	24	ANA	87.4
10	10 % NaOH	1:10	180	72	ANA	58.4
11	10 % NaOH	1:10	180	120	ANA	114.4
12	10 % NaOH	1:10	180	168	ANA	70.4
13	10 % NaOH	1:30	100	24	P1	27.0
14	10 % NaOH	1:30	100	72	P1	33.5
15	10 % NaOH	1:30	100	120	P1	46.7
16	10 % NaOH	1:30	100	168	P1	48.3
17	10 % NaOH	1:30	140	24	P1	48.9
18	10 % NaOH	1:30	140	72	P1	43.1
19	10 % NaOH	1:30	140	120	CAN	50.6
20	10 % NaOH	1:30	140	168	ANA; P1	12.0, 19.3
21	10 % NaOH	1:30	180	24	ANA	16.9
22	10 % NaOH	1:30	180	72	CAN	51.4

Table 4.14 (Continued)

Expt no.	Solution (% w/v)	S:L	T (°C)	Time (h)	Zeolites ^a	Int (cps)
23	10 % NaOH	1:30	180	120	ANA	36.0
24	10 % NaOH	1:30	180	168	CAN	59.3
25	20 % NaOH	1:10	100	24	HS	20.7
26	20 % NaOH	1:10	100	72	HS	21.3
27	20 % NaOH	1:10	100	120	HS	31.9
28	20 % NaOH	1:10	100	168	HS	38.9
29	20 % NaOH	1:10	140	24	CAN; HS	26.7, 24.2
30	20 % NaOH	1:10	140	72	CAN; HS	44.8, 28.5
31	20 % NaOH	1:10	140	120	CAN; HS	24.3, 22.8
32	20 % NaOH	1:10	140	168	CAN; HS	54.7, 22.9
33	20 % NaOH	1:10	180	24	CAN	52.5
34	20 % NaOH	1:10	180	72	CAN	65.0
35	20 % NaOH	1:10	180	120	CAN	74.5
36	20 % NaOH	1:10	180	168	CAN	66.1
37	20 % NaOH	1:30	100	24	HS	37.8
38	20 % NaOH	1:30	100	72	HS	41.5
39	20 % NaOH	1:30	100	120	HS	50.0
40	20 % NaOH	1:30	100	168	HS	50.2
41	20 % NaOH	1:30	140	24	HS	102.3
42	20 % NaOH	1:30	140	72	HS	68.2
43	20 % NaOH	1:30	140	120	HS; ANA	58.0, 10.2
44	20 % NaOH	1:30	140	168	HS; ANA	47.5, 17.1
45	20 % NaOH	1:30	180	24	CAN	69.2
46	20 % NaOH	1:30	180	72	CAN	62.9
47	20 % NaOH	1:30	180	120	CAN	70.6
48	20 % NaOH	1:30	180	168	CAN	67.1
49	30 % NaOH	1:10	100	24	HS	34.7
50	30 % NaOH	1:10	100	72	HS	39.0
51	30 % NaOH	1:10	100	120	HS	41.6
52	30 % NaOH	1:10	100	168	HS	49.0
53	30 % NaOH	1:10	140	24	CAN	58.4
54	30 % NaOH	1:10	140	72	CAN	71.1
55	30 % NaOH	1:10	140	120	CAN	62.5
56	30 % NaOH	1:10	140	168	CAN	73.4
57	30 % NaOH	1:10	180	24	CAN	80.2
58	30 % NaOH	1:10	180	72	CAN	68.7
59	30 % NaOH	1:10	180	120	CAN	75.0
60	30 % NaOH	1:10	180	168	CAN	83.3
61	30 % NaOH	1:30	100	24	HS	41.2
62	30 % NaOH	1:30	100	72	HS	49.1
63	30 % NaOH	1:30	100	120	HS	64.5
64	30 % NaOH	1:30	100	168	HS	75.7
65	30 % NaOH	1:30	140	24	HS	72.0
66	30 % NaOH	1:30	140	72	HS	86.8
67	30 % NaOH	1:30	140	120	HS	76.4
68	30 % NaOH	1:30	140	168	HS	87.2
69	30 % NaOH	1:30	180	24	CAN	77.6
70	30 % NaOH	1:30	180	72	CAN	65.0
71	30 % NaOH	1:30	180	120	CAN	58.3
72	30 % NaOH	1:30	180	168	CAN	54.2

^aP1 = Na-P1; ANA = analcime; HS = hydroxysodalite; CAN = cancrinite

Table 4.15 Experimental conditions used for synthesis experiments by calcined diatomite material at 1000 °C and sodium zeolites obtained

Expt no.	Solution (% w/v)	S:L	T (°C)	Time (h)	Zeolites ^a	Int (cps)
1	10 % NaOH	1:10	100	24	P1	34.7
2	10 % NaOH	1:10	100	72	P1	43.0
3	10 % NaOH	1:10	100	120	P1	47.2
4	10 % NaOH	1:10	100	168	P1	35.0
5	10 % NaOH	1:10	140	24	ANA	67.1
6	10 % NaOH	1:10	140	72	ANA	74.6
7	10 % NaOH	1:10	140	120	ANA	87.2
8	10 % NaOH	1:10	140	168	ANA	105.1
9	10 % NaOH	1:10	180	24	ANA	104.3
10	10 % NaOH	1:10	180	72	ANA	123.6
11	10 % NaOH	1:10	180	120	ANA	113.7
12	10 % NaOH	1:10	180	168	ANA	119.3
13	10 % NaOH	1:30	100	24	-	-
14	10 % NaOH	1:30	100	72	P1	57.5
15	10 % NaOH	1:30	100	120	P1	46.7
16	10 % NaOH	1:30	100	168	P1	54.8
17	10 % NaOH	1:30	140	24	P1	31.8
18	10 % NaOH	1:30	140	72	P1	47.8
19	10 % NaOH	1:30	140	120	P1	28.6
20	10 % NaOH	1:30	140	168	P1	29.1
21	10 % NaOH	1:30	180	24	CAN	52.3
22	10 % NaOH	1:30	180	72	CAN	50.4
23	10 % NaOH	1:30	180	120	CAN; ANA	22.9, 44.2
24	10 % NaOH	1:30	180	168	CAN; ANA	67.6, 10.8
25	20 % NaOH	1:10	100	24	HS	29.0
26	20 % NaOH	1:10	100	72	HS; P1	11.5, 42.9
27	20 % NaOH	1:10	100	120	P1	58.3
28	20 % NaOH	1:10	100	168	HS; P1	25.2, 22.5
29	20 % NaOH	1:10	140	24	CAN	45.0
30	20 % NaOH	1:10	140	72	CAN	55.6
31	20 % NaOH	1:10	140	120	CAN	55.4
32	20 % NaOH	1:10	140	168	CAN	68.2
33	20 % NaOH	1:10	180	24	CAN	54.2
34	20 % NaOH	1:10	180	72	CAN	77.9
35	20 % NaOH	1:10	180	120	CAN	73.8
36	20 % NaOH	1:10	180	168	CAN	70.3
37	20 % NaOH	1:30	100	24	HS	40.0
38	20 % NaOH	1:30	100	72	HS	33.0
39	20 % NaOH	1:30	100	120	HS	44.5
40	20 % NaOH	1:30	100	168	P1	56.4
41	20 % NaOH	1:30	140	24	HS	49.3
42	20 % NaOH	1:30	140	72	HS	47.5
43	20 % NaOH	1:30	140	120	HS; ANA	43.4, 13.1
44	20 % NaOH	1:30	140	168	HS; ANA	35.2, 33.3
45	20 % NaOH	1:30	180	24	CAN	68.6
46	20 % NaOH	1:30	180	72	CAN	70.2
47	20 % NaOH	1:30	180	120	CAN	83.6
48	20 % NaOH	1:30	180	168	CAN	78.3
49	30 % NaOH	1:10	100	24	HS	46.1
50	30 % NaOH	1:10	100	72	HS	58.7

Table 4.15 (Continued)

Expt no.	Solution (% w/v)	S:L	T (°C)	Time (h)	Zeolites ^a	Int (cps)
51	30 % NaOH	1:10	100	120	HS	42.6
52	30 % NaOH	1:10	100	168	HS	16.7
53	30 % NaOH	1:10	140	24	HS	42.7
54	30 % NaOH	1:10	140	72	HS; CAN	51.8, 54.3
55	30 % NaOH	1:10	140	120	HS; CAN	64.1, 56.7
56	30 % NaOH	1:10	140	168	HS; CAN	31.4, 61.7
57	30 % NaOH	1:10	180	24	CAN; HS	50.2, 28.2
58	30 % NaOH	1:10	180	72	CAN; HS	70.5, 40.4
59	30 % NaOH	1:10	180	120	CAN; HS	72.6, 44.7
60	30 % NaOH	1:10	180	168	CAN; HS	77.2, 46.9
61	30 % NaOH	1:30	100	24	HS	47.9
62	30 % NaOH	1:30	100	72	HS	25.8
63	30 % NaOH	1:30	100	120	HS	38.0
64	30 % NaOH	1:30	100	168	HS	39.5
65	30 % NaOH	1:30	140	24	HS	59.0
66	30 % NaOH	1:30	140	72	HS	69.3
67	30 % NaOH	1:30	140	120	HS	68.1
68	30 % NaOH	1:30	140	168	HS	60.3
69	30 % NaOH	1:30	180	24	CAN; HS	46.0, 13.6
70	30 % NaOH	1:30	180	72	CAN; HS	36.8, 22.1
71	30 % NaOH	1:30	180	120	CAN; HS	53.7, 12.3
72	30 % NaOH	1:30	180	168	CAN; HS	40.3, 14.8

^aP1 = Na-P1; ANA = analcime; HS = hydroxysodalite; CAN = cancrinite

Table 4.16 Experimental conditions used for synthesis experiments by calcined diatomite material at 1100 °C and sodium zeolites obtained

Expt no.	Solution (% w/v)	S:L	T (°C)	Time (h)	Zeolites ^a	Int (cps)
1	10 % NaOH	1:10	100	24	P1	36.8
2	10 % NaOH	1:10	100	72	P1	41.9
3	10 % NaOH	1:10	100	120	P1	50.0
4	10 % NaOH	1:10	100	168	P1	46.3
5	10 % NaOH	1:10	140	24	P1; ANA	44.6, 33.5
6	10 % NaOH	1:10	140	72	ANA	93.0
7	10 % NaOH	1:10	140	120	ANA	114.3
8	10 % NaOH	1:10	140	168	ANA	107.1
9	10 % NaOH	1:10	180	24	HS	56.7
10	10 % NaOH	1:10	180	72	HS	33.0
11	10 % NaOH	1:10	180	120	ANA	100.9
12	10 % NaOH	1:10	180	168	ANA	119.6
13	10 % NaOH	1:30	100	24	P1	19.8
14	10 % NaOH	1:30	100	72	P1	44.5
15	10 % NaOH	1:30	100	120	P1	66.1
16	10 % NaOH	1:30	100	168	P1	67.2
17	10 % NaOH	1:30	140	24	P1	108.2
18	10 % NaOH	1:30	140	72	P1	94.1
19	10 % NaOH	1:30	140	120	P1	107.2
20	10 % NaOH	1:30	140	168	P1	78.9
21	10 % NaOH	1:30	180	24	ANA	116.7

Table 4.16 (Continued)

Expt no.	Solution (% w/v)	S:L	T (°C)	Time (h)	Zeolites ^a	Int (cps)
22	10 % NaOH	1:30	180	72	ANA	89.7
23	10 % NaOH	1:30	180	120	ANA	44.3
24	10 % NaOH	1:30	180	168	ANA; CAN	22.1, 43.5
25	20 % NaOH	1:10	100	24	HS	26.5
26	20 % NaOH	1:10	100	72	HS	33.5
27	20 % NaOH	1:10	100	120	HS	48.6
28	20 % NaOH	1:10	100	168	HS	43.6
29	20 % NaOH	1:10	140	24	HS	44.3
30	20 % NaOH	1:10	140	72	CAN	71.5
31	20 % NaOH	1:10	140	120	CAN	72.9
32	20 % NaOH	1:10	140	168	CAN	81.3
33	20 % NaOH	1:10	180	24	CAN	61.9
34	20 % NaOH	1:10	180	72	CAN	71.0
35	20 % NaOH	1:10	180	120	CAN	74.0
36	20 % NaOH	1:10	180	168	CAN	82.2
37	20 % NaOH	1:30	100	24	-	-
38	20 % NaOH	1:30	100	72	HS	20.7
39	20 % NaOH	1:30	100	120	HS	21.2
40	20 % NaOH	1:30	100	168	ANA	25.5
41	20 % NaOH	1:30	140	24	ANA	35.1
42	20 % NaOH	1:30	140	72	ANA; HS	36.2, 16.2
43	20 % NaOH	1:30	140	120	ANA; HS	5.7, 8.2
44	20 % NaOH	1:30	140	168	ANA; CAN	29.7, 27.9
45	20 % NaOH	1:30	180	24	CAN	72.7
46	20 % NaOH	1:30	180	72	CAN	64.6
47	20 % NaOH	1:30	180	120	CAN	71.4
48	20 % NaOH	1:30	180	168	CAN	34.1
49	30 % NaOH	1:10	100	24	HS	35.7
50	30 % NaOH	1:10	100	72	HS; ANA	51.1, 16.4
51	30 % NaOH	1:10	100	120	HS; ANA	53.7, 18.8
52	30 % NaOH	1:10	100	168	HS; ANA	68.0, 24.6
53	30 % NaOH	1:10	140	24	HS	67.2
54	30 % NaOH	1:10	140	72	HS	20.0
55	30 % NaOH	1:10	140	120	HS; CAN	70.3, 96.9
56	30 % NaOH	1:10	140	168	HS; CAN	82.6, 88.8
57	30 % NaOH	1:10	180	24	CAN	87.1
58	30 % NaOH	1:10	180	72	CAN	76.6
59	30 % NaOH	1:10	180	120	CAN	63.7
60	30 % NaOH	1:10	180	168	CAN	95.1
61	30 % NaOH	1:30	100	24	-	-
62	30 % NaOH	1:30	100	72	HS; ANA	15.6, 22.5
63	30 % NaOH	1:30	100	120	HS; ANA	33.8, 26.3
64	30 % NaOH	1:30	100	168	HS; ANA	37.0, 17.4
65	30 % NaOH	1:30	140	24	HS	44.3
66	30 % NaOH	1:30	140	72	HS	54.8
67	30 % NaOH	1:30	140	120	HS	77.1
68	30 % NaOH	1:30	140	168	HS	79.1
69	30 % NaOH	1:30	180	24	CAN	32.0
70	30 % NaOH	1:30	180	72	CAN	72.4
71	30 % NaOH	1:30	180	120	CAN	74.3
72	30 % NaOH	1:30	180	168	CAN	67.9

^aP1 = Na-P1; ANA = analcime; HS = hydroxysodalite; CAN = cancrinite

Table 4.17 Experimental conditions used for synthesis experiments by diatomite material treated with 6M H₂SO₄ and sodium zeolites obtained

Expt no.	Solution (% w/v)	S:L	T (°C)	Time (h)	Zeolites ^a	Int (cps)
1	10 % NaOH	1:10	100	24	P1	161.4
2	10 % NaOH	1:10	100	72	P1; ANA	127.7, 61.1
3	10 % NaOH	1:10	100	120	P1; ANA	25.1, 120.0
4	10 % NaOH	1:10	100	168	P1; ANA	162.1, 49.9
5	10 % NaOH	1:10	140	24	ANA	193.8
6	10 % NaOH	1:10	140	72	ANA	160.8
7	10 % NaOH	1:10	140	120	ANA	190.6
8	10 % NaOH	1:10	140	168	ANA	187.9
9	10 % NaOH	1:10	180	24	ANA	185.6
10	10 % NaOH	1:10	180	72	ANA	180.8
11	10 % NaOH	1:10	180	120	ANA	166.9
12	10 % NaOH	1:10	180	168	ANA	180.5
13	10 % NaOH	1:30	100	24	P1	69.5
14	10 % NaOH	1:30	100	72	P1	15.6
15	10 % NaOH	1:30	100	120	P1	16.7
16	10 % NaOH	1:30	100	168	P1	108.3
17	10 % NaOH	1:30	140	24	HS	53.1
18	10 % NaOH	1:30	140	72	HS	34.4
19	10 % NaOH	1:30	140	120	HS	40.6
20	10 % NaOH	1:30	140	168	HS	51.9
21	10 % NaOH	1:30	180	24	CAN	118.9
22	10 % NaOH	1:30	180	72	CAN	118.0
23	10 % NaOH	1:30	180	120	CAN	116.5
24	10 % NaOH	1:30	180	168	CAN	113.7
25	20 % NaOH	1:10	100	24	HS	45.3
26	20 % NaOH	1:10	100	72	HS	103.6
27	20 % NaOH	1:10	100	120	HS	124.0
28	20 % NaOH	1:10	100	168	HS	51.2
29	20 % NaOH	1:10	140	24	CAN	73.7
30	20 % NaOH	1:10	140	72	CAN	120.1
31	20 % NaOH	1:10	140	120	CAN	111.8
32	20 % NaOH	1:10	140	168	CAN	113.5
33	20 % NaOH	1:10	180	24	CAN	137.5
34	20 % NaOH	1:10	180	72	CAN	131.9
35	20 % NaOH	1:10	180	120	CAN	136.9
36	20 % NaOH	1:10	180	168	CAN	120.9
37	20 % NaOH	1:30	100	24	HS	80.2
38	20 % NaOH	1:30	100	72	HS	140.4
39	20 % NaOH	1:30	100	120	HS	161.4
40	20 % NaOH	1:30	100	168	HS	148.2
41	20 % NaOH	1:30	140	24	HS	119.6
42	20 % NaOH	1:30	140	72	HS	133.1
43	20 % NaOH	1:30	140	120	HS	110.2
44	20 % NaOH	1:30	140	168	HS	116.5
45	20 % NaOH	1:30	180	24	CAN	137.0
46	20 % NaOH	1:30	180	72	CAN	125.9
47	20 % NaOH	1:30	180	120	CAN	129.2
48	20 % NaOH	1:30	180	168	CAN	142.7
49	30 % NaOH	1:10	100	24	HS	107.5
50	30 % NaOH	1:10	100	72	HS	140.2

Table 4.17 (Continued)

Expt no.	Solution (% w/v)	S:L	T (°C)	Time (h)	Zeolites ^a	Int (cps)
51	30 % NaOH	1:10	100	120	HS	135.2
52	30 % NaOH	1:10	100	168	HS	138.2
53	30 % NaOH	1:10	140	24	CAN	127.1
54	30 % NaOH	1:10	140	72	CAN	142.8
55	30 % NaOH	1:10	140	120	CAN	138.2
56	30 % NaOH	1:10	140	168	CAN	117.7
57	30 % NaOH	1:10	180	24	CAN	162.2
58	30 % NaOH	1:10	180	72	CAN	141.4
59	30 % NaOH	1:10	180	120	CAN	145.6
60	30 % NaOH	1:10	180	168	CAN	127.6
61	30 % NaOH	1:30	100	24	HS	94.0
62	30 % NaOH	1:30	100	72	HS	133.6
63	30 % NaOH	1:30	100	120	HS	150.6
64	30 % NaOH	1:30	100	168	HS	162.4
65	30 % NaOH	1:30	140	24	HS	158.1
66	30 % NaOH	1:30	140	72	HS	176.3
67	30 % NaOH	1:30	140	120	HS	169.2
68	30 % NaOH	1:30	140	168	HS	165.6
69	30 % NaOH	1:30	180	24	HS	166.0
70	30 % NaOH	1:30	180	72	HS	150.3
71	30 % NaOH	1:30	180	120	HS	174.0
72	30 % NaOH	1:30	180	168	HS	117.3

^aP1 = Na-P1; ANA = analcime; HS = hydroxysodalite; CAN = cancrinite

Table 4.18 Experimental conditions used for synthesis experiments by diatomite material first treated with 6M H₂SO₄ then calcined at 1100 °C and sodium zeolites obtained

Expt no.	Solution (% w/v)	S:L	T (°C)	Time (h)	Zeolites ^a	Int (cps)
1	10 % NaOH	1:10	100	24	P1	118.9
2	10 % NaOH	1:10	100	72	P1	170.4
3	10 % NaOH	1:10	100	120	P1	176.8
4	10 % NaOH	1:10	100	168	P1; ANA	156.9, 39.6
5	10 % NaOH	1:10	140	24	ANA	189.6
6	10 % NaOH	1:10	140	72	ANA	200.5
7	10 % NaOH	1:10	140	120	ANA	203.3
8	10 % NaOH	1:10	140	168	ANA	189.4
9	10 % NaOH	1:10	180	24	ANA	157.2
10	10 % NaOH	1:10	180	72	ANA	119.0
11	10 % NaOH	1:10	180	120	ANA	193.9
12	10 % NaOH	1:10	180	168	CAN	100.3
13	10 % NaOH	1:30	100	24	P1	134.5
14	10 % NaOH	1:30	100	72	P1	143.7
15	10 % NaOH	1:30	100	120	P1	116.6
16	10 % NaOH	1:30	100	168	P1	202.3
17	10 % NaOH	1:30	140	24	HS; P1	47.5, 76.2
18	10 % NaOH	1:30	140	72	HS; P1	36.7, 74.1

Table 4.18 (Continued)

Expt no.	Solution (% w/v)	S:L	T (°C)	Time (h)	Zeolites ^a	Int (cps)
19	10 % NaOH	1:30	140	120	HS; P1	36.1, 93.7
20	10 % NaOH	1:30	140	168	HS; P1	47.7, 56.1
21	10 % NaOH	1:30	180	24	CAN; ANA	100.2, 29.6
22	10 % NaOH	1:30	180	72	CAN	115.4
23	10 % NaOH	1:30	180	120	CAN; ANA	118.8, 16.1
24	10 % NaOH	1:30	180	168	ANA	100.2
25	20 % NaOH	1:10	100	24	HS	13.1
26	20 % NaOH	1:10	100	72	HS	96.2
27	20 % NaOH	1:10	100	120	HS	121.0
28	20 % NaOH	1:10	100	168	HS	106.1
29	20 % NaOH	1:10	140	24	CAN	100.1
30	20 % NaOH	1:10	140	72	CAN	125.4
31	20 % NaOH	1:10	140	120	CAN	141.0
32	20 % NaOH	1:10	140	168	CAN	124.2
33	20 % NaOH	1:10	180	24	CAN	136.0
34	20 % NaOH	1:10	180	72	CAN	135.3
35	20 % NaOH	1:10	180	120	CAN	139.4
36	20 % NaOH	1:10	180	168	CAN	139.4
37	20 % NaOH	1:30	100	24	HS	67.3
38	20 % NaOH	1:30	100	72	HS	124.2
39	20 % NaOH	1:30	100	120	HS	165.7
40	20 % NaOH	1:30	100	168	HS	94.8
41	20 % NaOH	1:30	140	24	HS; CAN	33.1, 68.2
42	20 % NaOH	1:30	140	72	CAN	116.6
43	20 % NaOH	1:30	140	120	CAN	124.4
44	20 % NaOH	1:30	140	168	CAN	126.5
45	20 % NaOH	1:30	180	24	CAN	138.1
46	20 % NaOH	1:30	180	72	CAN	145.5
47	20 % NaOH	1:30	180	120	CAN	134.0
48	20 % NaOH	1:30	180	168	CAN	135.0
49	30 % NaOH	1:10	100	24	HS	104.3
50	30 % NaOH	1:10	100	72	HS	133.5
51	30 % NaOH	1:10	100	120	HS	153.3
52	30 % NaOH	1:10	100	168	HS	101.9
53	30 % NaOH	1:10	140	24	CAN	135.7
54	30 % NaOH	1:10	140	72	CAN	132.4
55	30 % NaOH	1:10	140	120	CAN	131.2
56	30 % NaOH	1:10	140	168	CAN	143.2
57	30 % NaOH	1:10	180	24	CAN	141.2
58	30 % NaOH	1:10	180	72	CAN	138.4
59	30 % NaOH	1:10	180	120	CAN	138.4
60	30 % NaOH	1:10	180	168	CAN	118.6
61	30 % NaOH	1:30	100	24	HS	95.4
62	30 % NaOH	1:30	100	72	HS	133.0
63	30 % NaOH	1:30	100	120	HS	168.0
64	30 % NaOH	1:30	100	168	HS	160.2
65	30 % NaOH	1:30	140	24	CAN	86.0
66	30 % NaOH	1:30	140	72	HS	160.6
67	30 % NaOH	1:30	140	120	CAN	103.4
68	30 % NaOH	1:30	140	168	CAN	86.3

Table 4.18 (Continued)

Expt no.	Solution (% w/v)	S:L	T (°C)	Time (h)	Zeolites ^a	Int (cps)
69	30 % NaOH	1:30	180	24	CAN	151.2
70	30 % NaOH	1:30	180	72	CAN	131.4
71	30 % NaOH	1:30	180	120	CAN	93.2
72	30 % NaOH	1:30	180	168	CAN	143.0

^aP1 = Na-P1; ANA = analcime; HS = hydroxysodalite; CAN = cancrinite

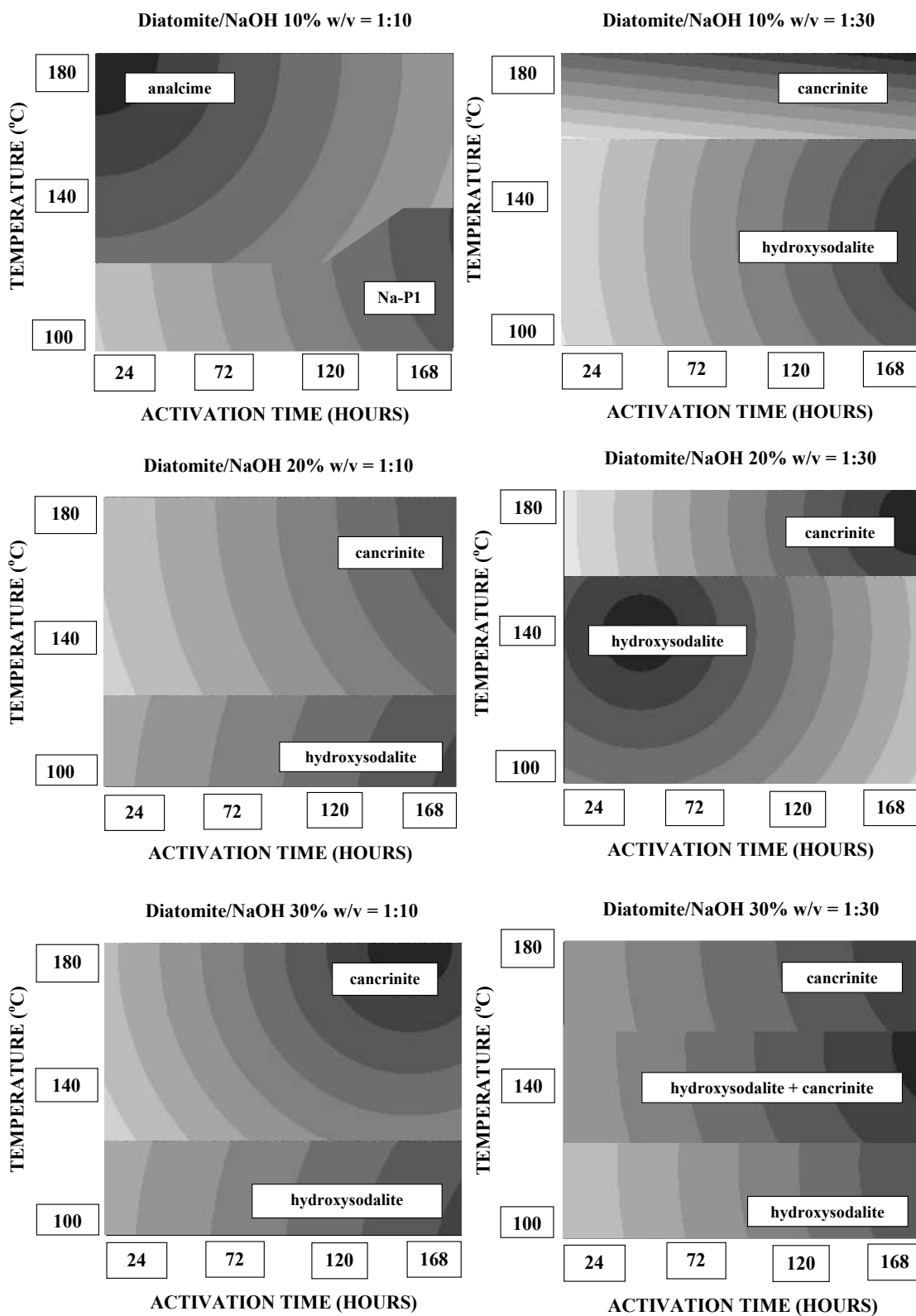


Figure 4.27 Zeolite products obtained from natural diatomite starting material

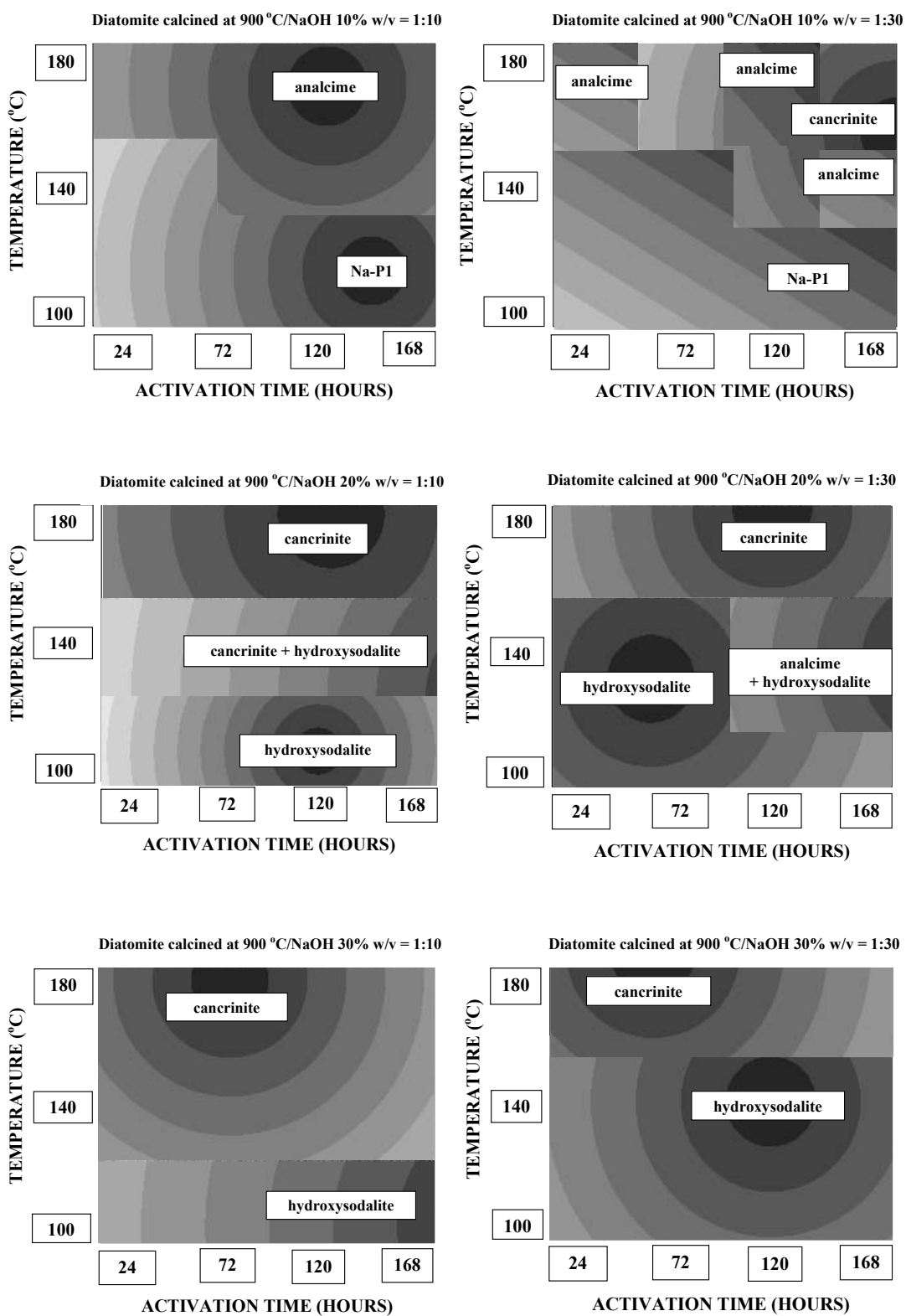


Figure 4.28 Zeolite products obtained from diatomite calcined at 900 °C

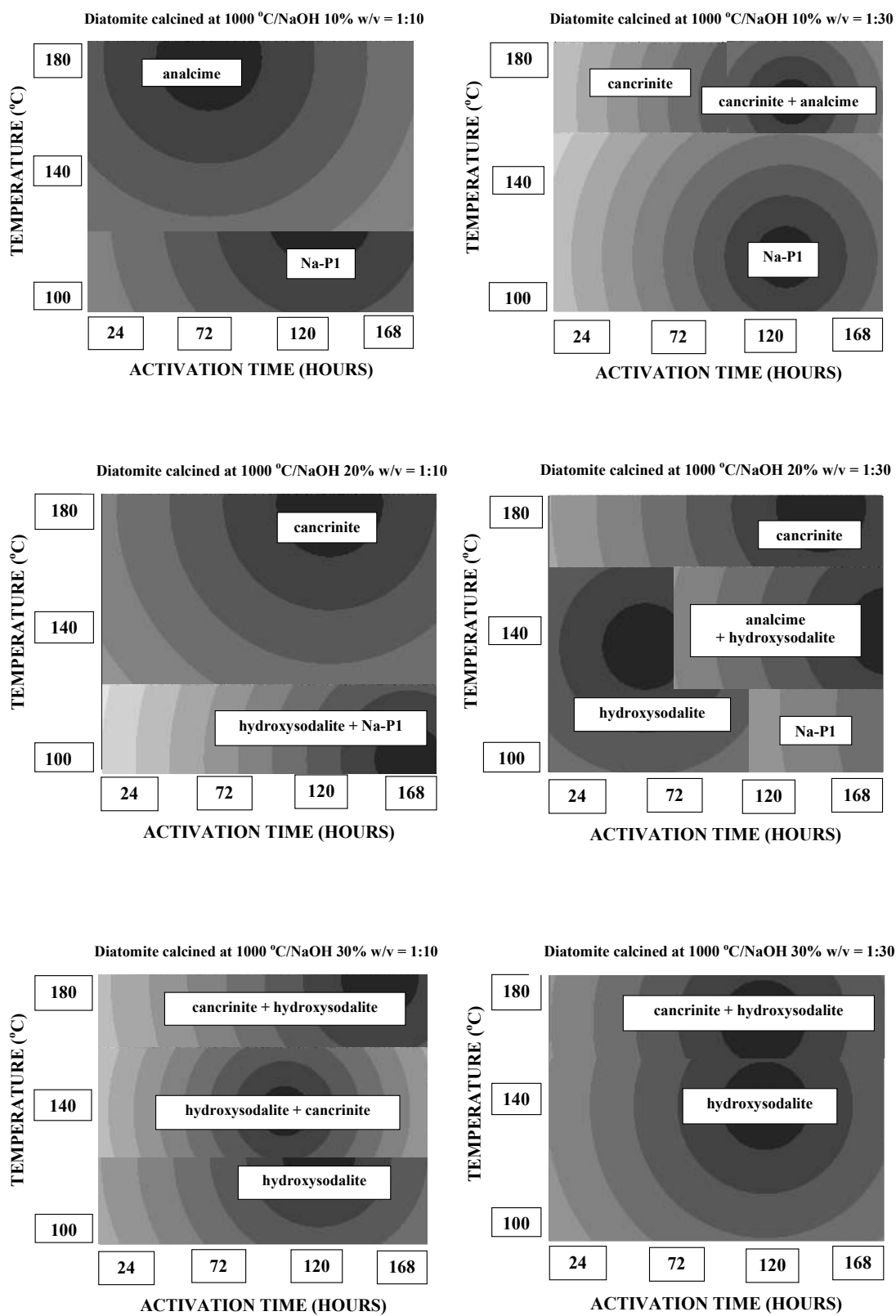


Figure 4.29 Zeolite products obtained from diatomite calcined at 1000 °C

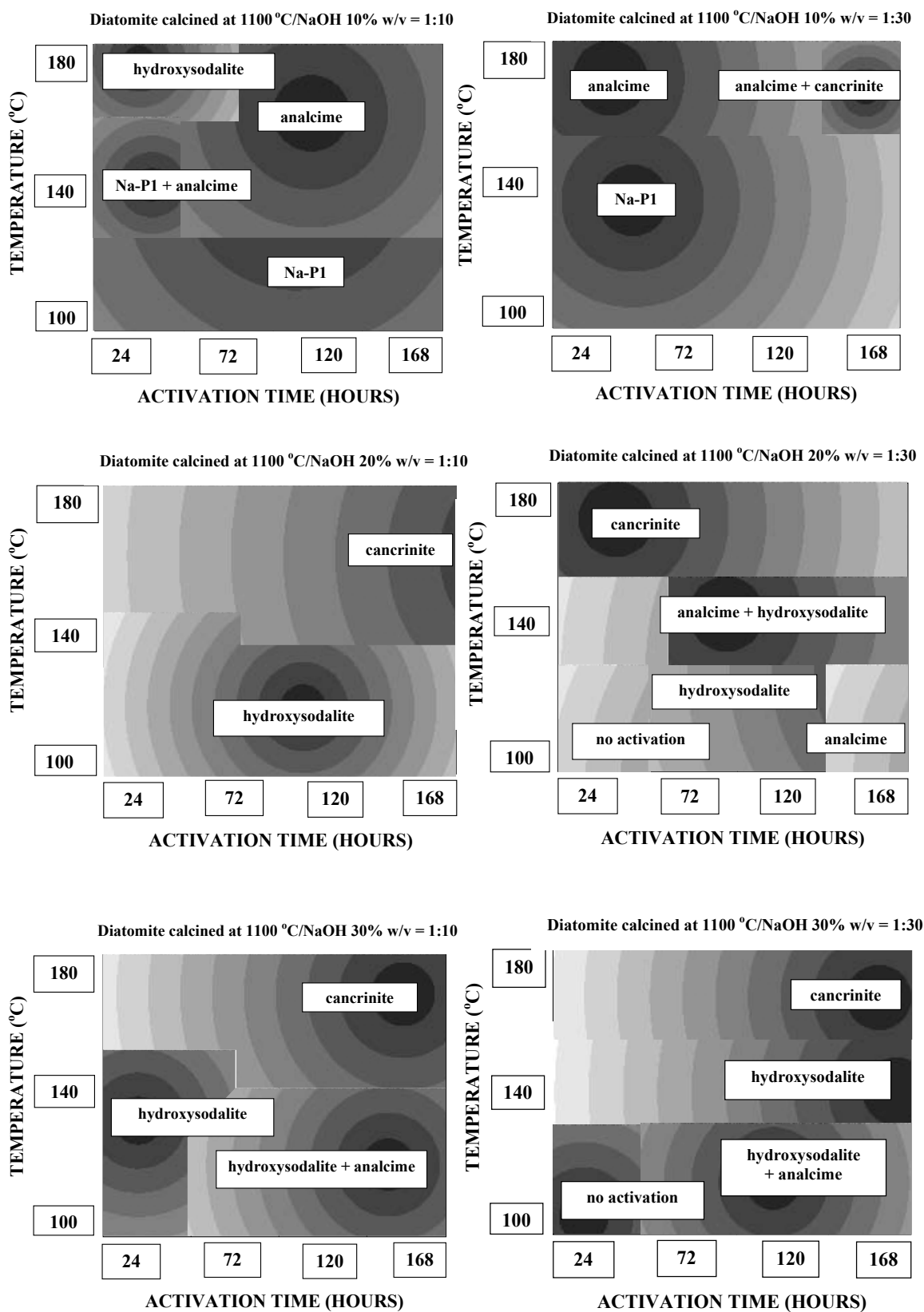


Figure 4.30 Zeolite products obtained from diatomite calcined at 1100 °C

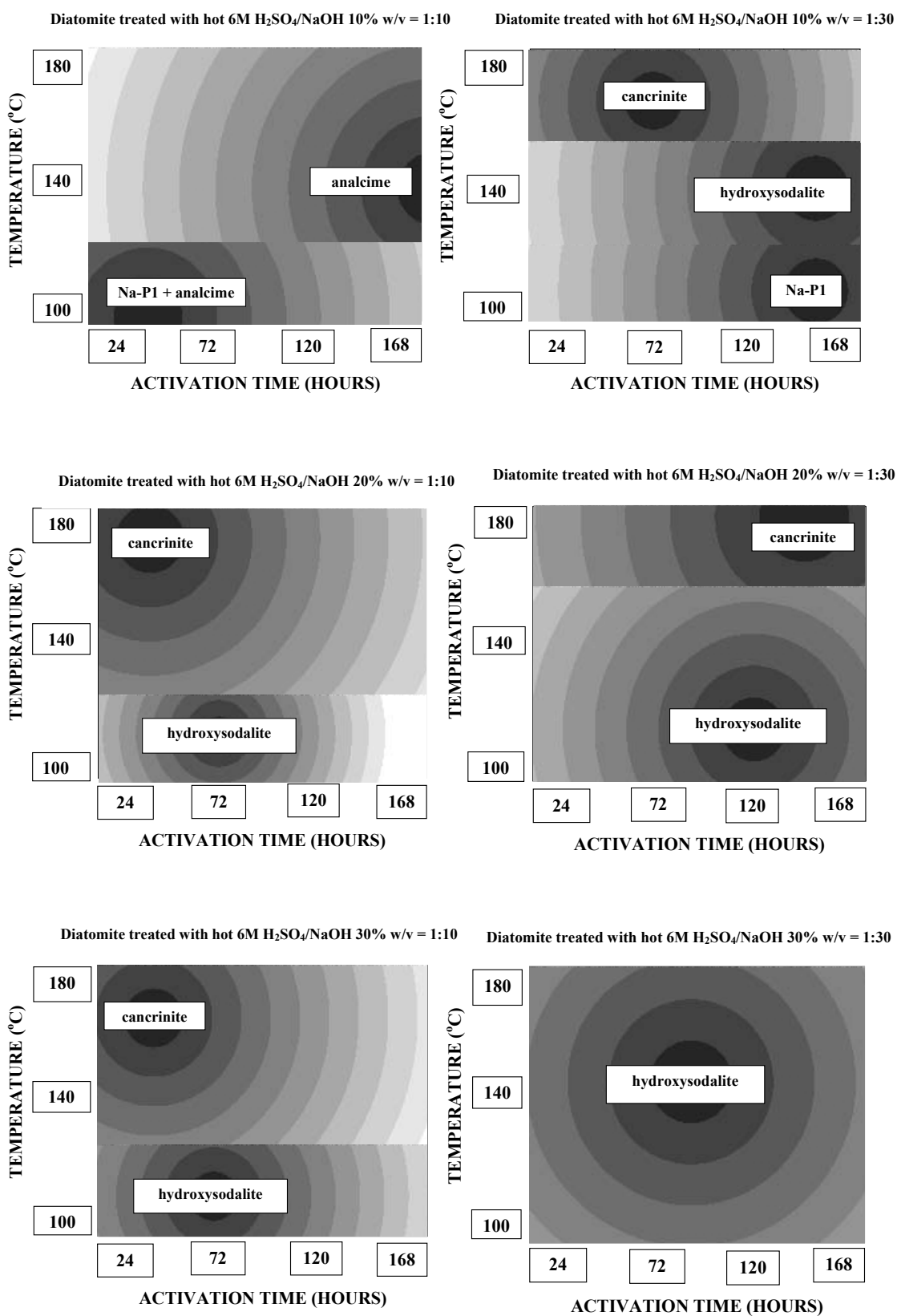


Figure 4.31 Zeolite products obtained from diatomite treated with hot 6M H₂SO₄

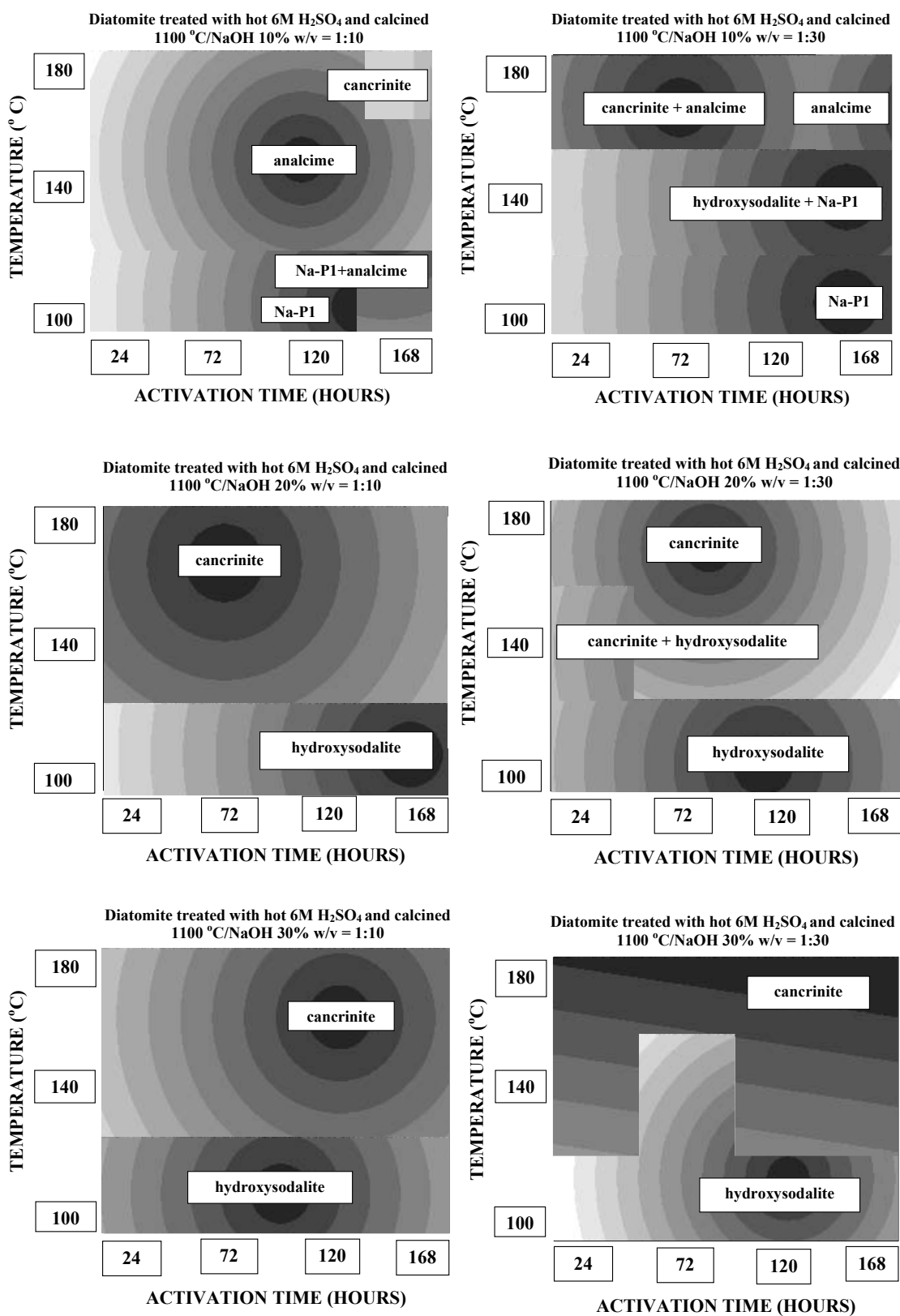


Figure 4.32 Zeolite products obtained from diatomite treated with acid and thermal

4.6.1 Effect of the starting materials

To study the effect of the starting materials in the synthesis of sodium zeolite, the natural diatomite and modified diatomite (calcined at 900 °C, calcined at 1000 °C, calcined at 1100 °C, treated with hot 6M H₂SO₄ and first treated with hot 6M H₂SO₄ then calcined at 1100 °C) were selected. In this section, the optimum condition to synthesize sodium zeolites from this starting material, which was treated with hot 6M H₂SO₄ then calcined at 1100 °C, was first considered. The condition synthesis of Na-P1 was 10 % w/v NaOH concentration, solid/liquid ratio equal to 1/10, the reaction temperature of 100 °C and reaction time 120 hours and for analcime was 10 % w/v of NaOH concentration, solid/liquid ratio equal to 1/10, the reaction temperature of 140 °C and the reaction time 120 hours. The obtained cancrinite zeolite condition was 20 % w/v of NaOH concentration, solid/liquid ratio is equal to 1/30, the reaction temperature at 180 °C and the reaction time 72 hours and the formation of hydroxysodalite zeolite condition was 30 % w/v of NaOH concentration, solid/liquid ratio equal to 1/30, the reaction temperature of 100 °C and the reaction time 120 hours. The XRD patterns of four series of sodium zeolites are compared to the pattern of the each starting materials, as shown in Figure 4.33 - 4.36. The starting materials are designed as follows: Di - H₂SO₄ - C(T), Di denotes the natural diatomite, H₂SO₄ denotes the acid treatment with hot 6M H₂SO₄ and C(T) denotes calcined temperature when T being the calcination temperature. From the XRD patterns, each of sodium zeolite peaks started to appear gradually. Similar results were obtained for all starting materials. From the XRD results, natural diatomite material gave the lowest sodium zeolites yield because of the high concentration of impurity phase and the presence of high SiOH groups.

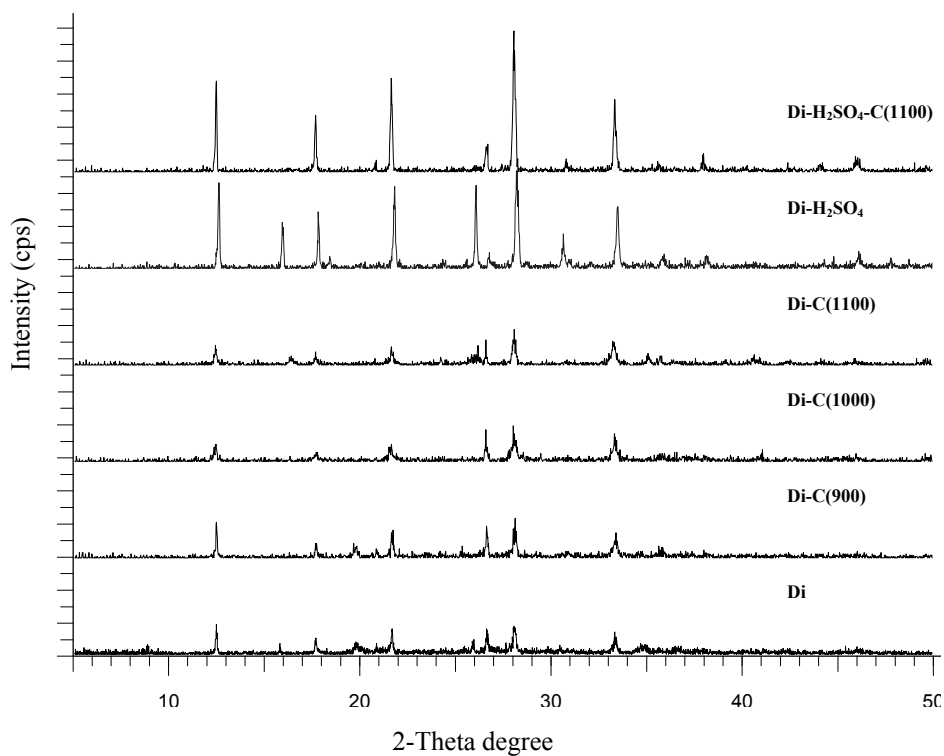


Figure 4.33 Na-P1 XRD peaks obtained from the reaction of each diatomite materials activated at 100 °C with 10 % NaOH concentration, S/L=1/10 for 120 hours

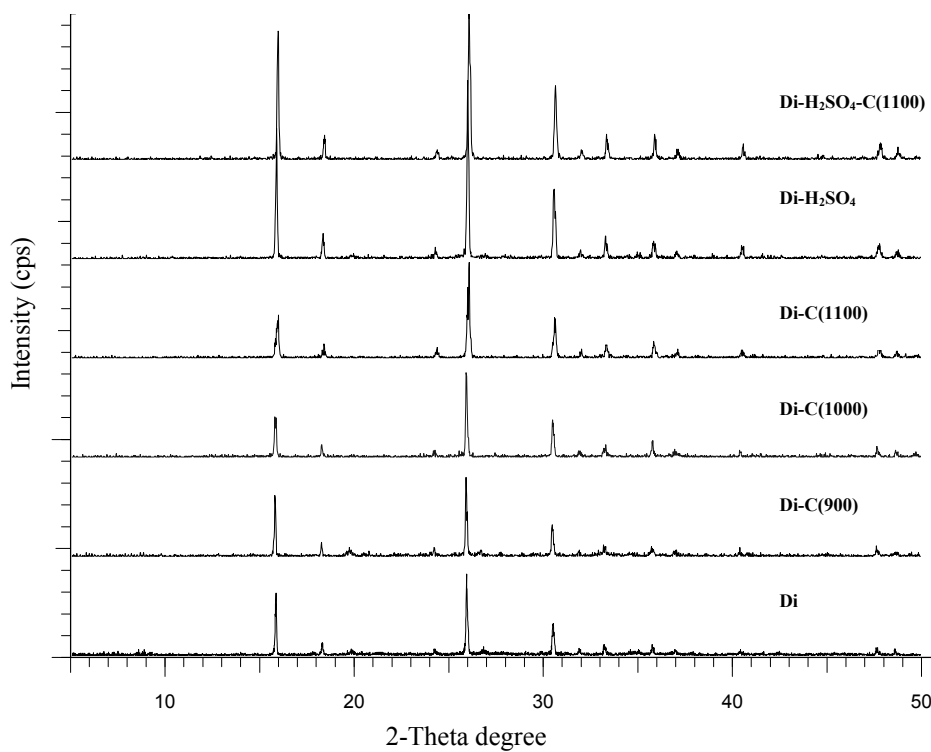


Figure 4.34 Analcime XRD peaks obtained from the reaction of each diatomite materials activated at 140 °C with 10 % NaOH concentration, S/L =1/10 for 120 hours

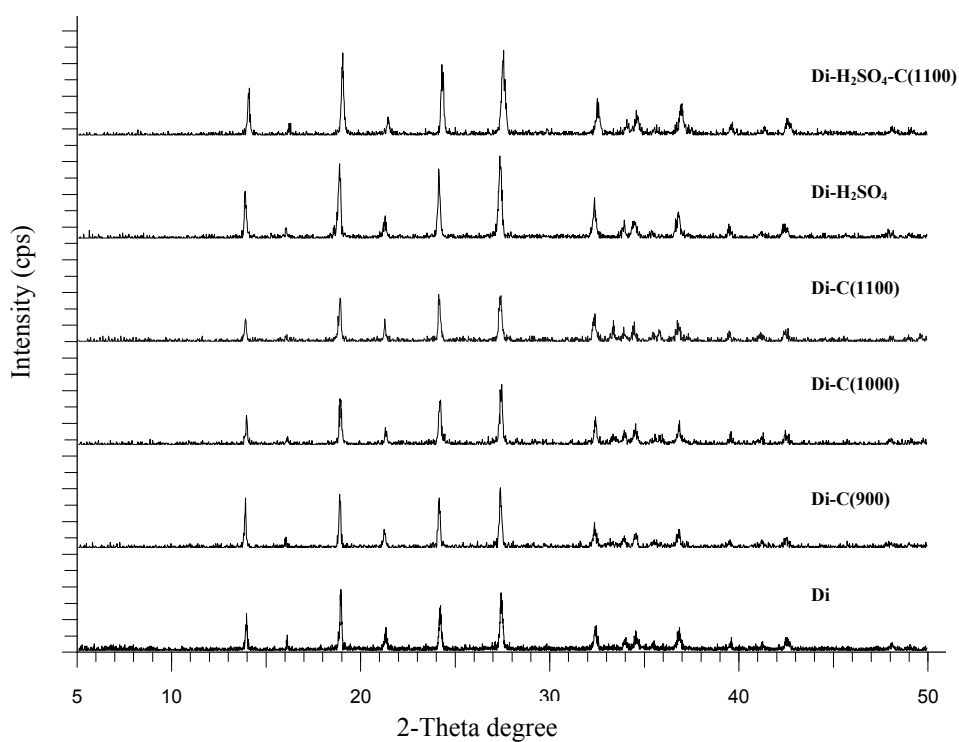


Figure 4.35 Cancrinite XRD peaks obtained from the reaction of each diatomite materials activated at 180 °C with 20 % NaOH concentration, S/L=1/30 for 72 hours

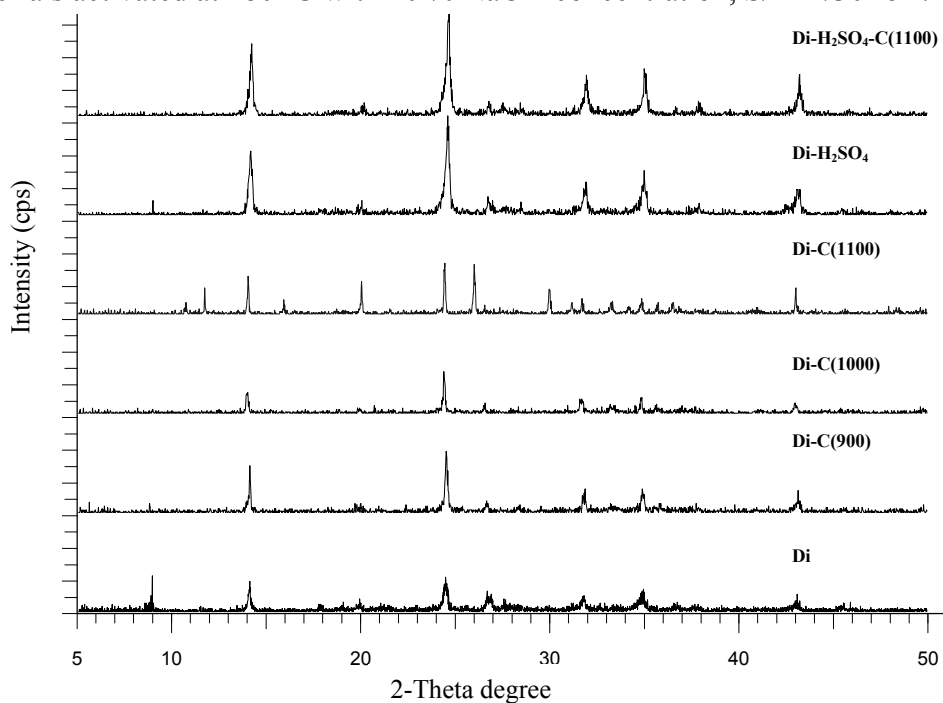


Figure 4.36 Hydroxysodalite XRD peaks obtained from the reaction of each diatomite materials activated at 100 °C with 30 % NaOH concentration, S/L=1/30 for 120 hours

The SiOH groups make it less active towards sodium zeolites synthesis. The zeolites obtained from calcined diatomite samples at various temperature are higher than sodium zeolites obtained from natural diatomite material. Because of the high calcination temperature, the SiOH groups are almost eliminate in the dehydroxylation process (Halimatou et al., 1997) and the smaller particle size (higher surface area) favours contact between the reactants and decreases diffusion time (Antonucci, Crisafulli, Giordano and Burriesci, 1985). Considering the sodium zeolites products started to appear gradually from natural diatomite material, calcined at 900 °C, calcined at 1000 °C, calcined at 1100 °C, treated with hot 6M H₂SO₄, first treated with hot 6M H₂SO₄ then calcined at 1100 °C. It is cleared from the ²⁹Si MAS NMR spectra that the starting materials contain different amount of Q², Q³(total), Q⁴(total) species. The starting materials with higher Q⁴ ([Si(OSi)₄]) content achieve a higher conversion in the zeolitization process. In addition, not only the Q⁴ contents of starting material but also the particle size, the impurity phase and Al(OH)₃ can affect the zeolite synthesis.

4.6.2 Effect of alkalinity concentration, the solid/liquid ratio and the reaction temperature

In this section, the effect of NaOH concentration, the solid/liquid ratio and temperature on the synthesis of sodium zeolites (Na-P1, analcime, cancrinite and hydroxysodalite) were investigated. The results showed that Na-P1 zeolite is obtained at higher yields with low temperatures (100 °C and 140 °C) and low reagent concentrations (10 % NaOH and 20 % NaOH) (see Table 4.19). Under the extreme conditions (140 °C, 180 °C and 20 % NaOH, 30 % NaOH), hydroxysodalite zeolite and cancrinite zeolite were obtained instead of former zeolite. Hydroxysodalite zeolite and cancrinite zeolite were obtained in high proportions with 20 % - 30 % NaOH solution at 140 °C and 180 °C. At the higher reagent concentration (30 %) and higher temperature (180 °C) cancrinite zeolite and hydroxysodalite with lower proportions were obtained, whereas analcime zeolite was synthesized with lower temperature. Temperature was also an important factor affecting the formation of sodium zeolites. It was found that cancrinite zeolite was the stable zeolite phase under high NaOH concentration and high temperature. The transformations of all starting materials result mainly from a change of the NaOH concentration and temperature whereas the solid/liquid (S/L) ratio seems to be less important. Other important parameters for the zeolitization of starting materials is the activation time. Figure 4.37 - 4.40 show XRD pattern of the sodium zeolite products under the optimum condition at various reaction times. The Maximum efficiency for Na-P1 zeolite was attained after 144 hours of reaction at 100 °C with 10 % NaOH and S/L = 1/10 ratio and for analcime was 10 % NaOH (S/L = 1/10) at 140 °C after 132 hours of activations. The experiment condition to obtained the shorter activation periods and maximum

efficiency of cancrinite zeolite was 20 % NaOH, S/L = 1/10, at 180 °C after 72 hours. For maximum hydroxysodalite zeolite, the synthesis was obtained at 100 °C, 30 % NaOH, S/L = 1/30 and 96 hours.

Table 4.19 Zeolitic material synthesized as a function of reaction parameters.

NaOH concentration (%)	S/L	Temperature (°C)	Zeolitic product ^a
10 % NaOH	1/10	100	P1
		140-180	ANA
	1/30	100-140	HS, P1
		180	ANA, CAN
20 % NaOH	1/10	100	HS, P1
		140-180	CAN, HS
	1/30	100	HS, P1
		140-180	CAN, HS, ANA
30 % NaOH	1/10	100	HS, ANA
		140-180	CAN, HS
	1/30	100	HS, ANA
		140-180	CAN, HS

^aP1 = Na-P1; ANA = analcime; HS = hydroxysodalite; CAN = cancrinite

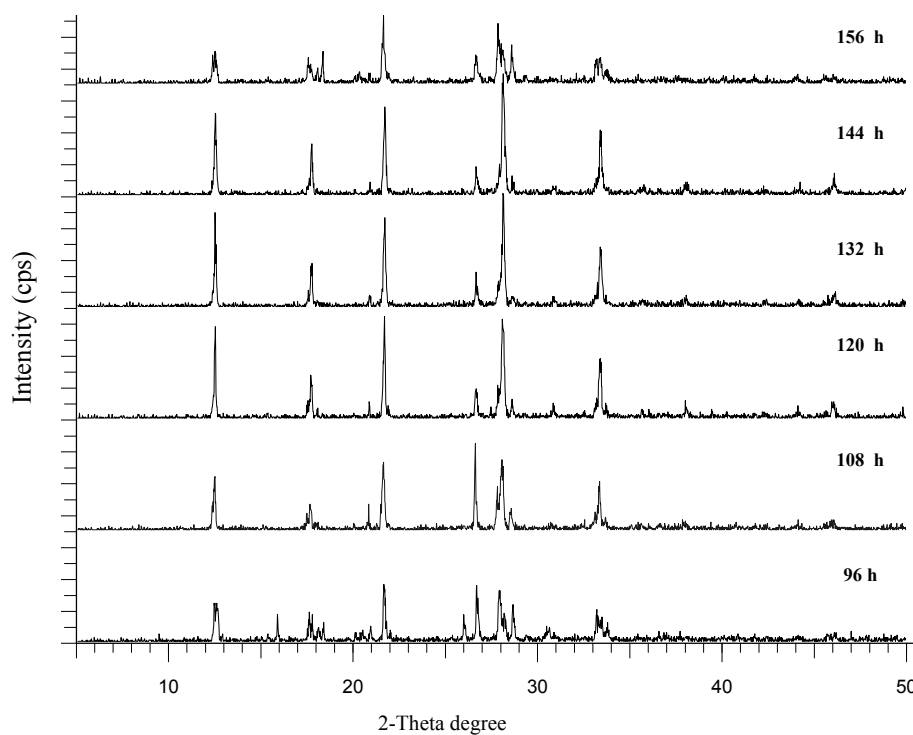


Figure 4.37 XRD patterns of Na-P1 zeolite obtained in activated with 10 % NaOH concentration, S/L = 1/10 and reaction temperature 100 °C for various times

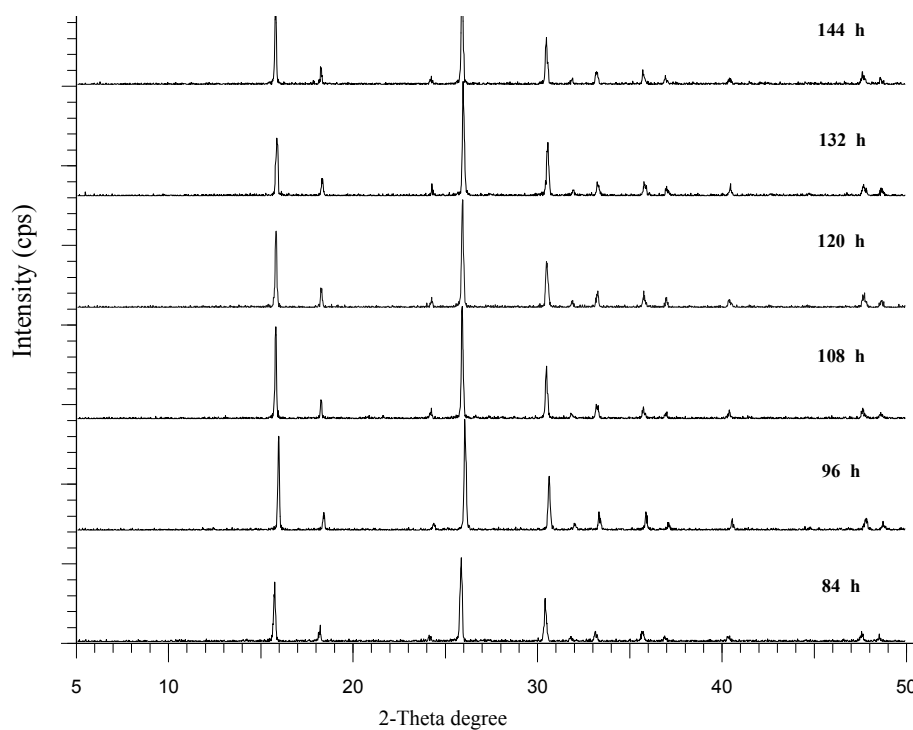


Figure 4.38 XRD patterns of analcime zeolite obtained in activated with 10 % NaOH concentration, S/L = 1/10 and reaction temperature 140 °C for various times

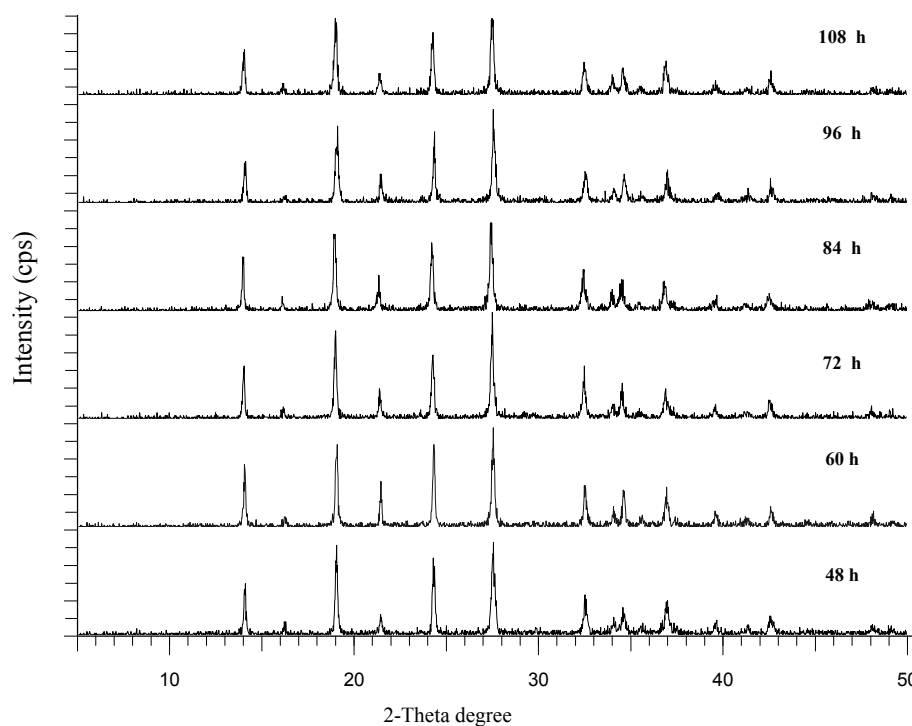


Figure 4.39 XRD patterns of cancrinite zeolite obtained in activated with 20 % NaOH concentration, S/L = 1/30 and reaction temperature 180 °C for various times

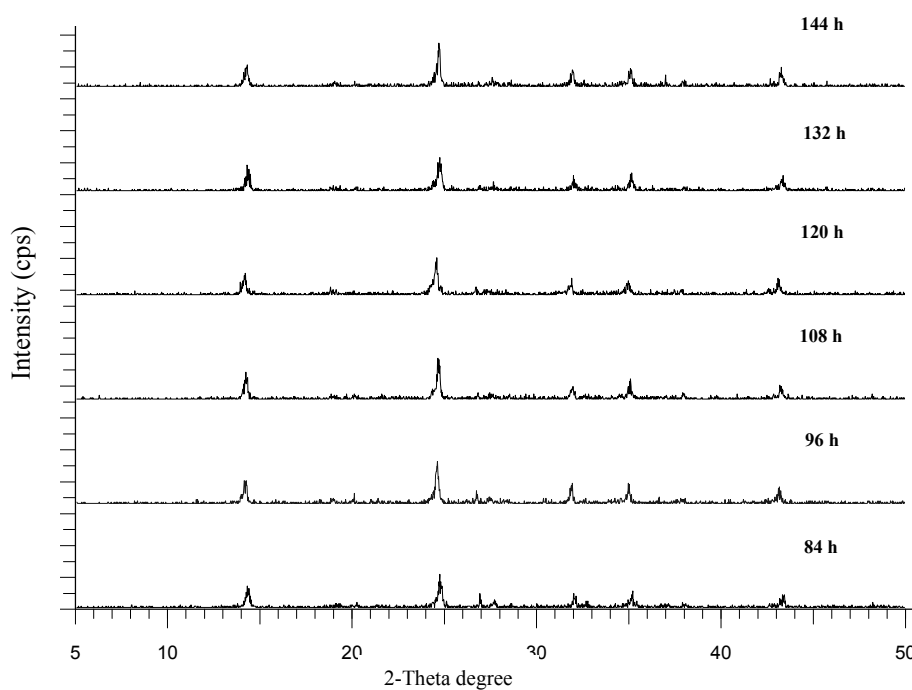


Figure 4.40 XRD patterns of hydroxysodalite zeolite obtained in activated with 30 % NaOH concentration, S/L = 1/30 and reaction temperature 100 °C for various times

The growth rate tends to increase by increasing reaction time. The cancrinite zeolite produced from 20 % NaOH condition and activated at 180 °C grew at the fastest rate till 72 hours. After 72 hours, all yields decrease within the range of observing. The plots of XRD intensity (counts/second) of each sodium zeolite products with reaction time from various experiment conditions are shown in Figure 4.41-4.44. In a similar manner to the XRD measurement, the IR spectra of the highest yield of each sodium zeolite are shown in Figure 4.45. The IR bands assignment of the Na-P1, analcime, cancrinite and hydroxysodalite compared with the references are demonstrated in Table 4.20.

In the IR spectra, the 800 and 780 cm^{-1} bands of quartz almost did not appear in all spectra indicated that a few of quartz in the final products. The absorption spectra of all obtained zeolites were in total accordance with the different absorption peaks given by Flanigen, Khatami and Szymanski, 1971; Breck, 1974. Na-P1 zeolite showed absorption bands at 1111, 1003, 774, 739, 675, 603 and 435 cm^{-1} and at 1000, 740, 687, 622 and 450 cm^{-1} for the analcime as well as 1108, 1038, 1006, 961, 757, 682, 624, 567, 503, 459, 428 and 387 cm^{-1} for cancrinite. Bands at 1113, 985, 736, 708, 666, 567, 463 and 435 cm^{-1} were belong to hydroxysodalite zeolite. The band position of zeolite Na-P1 at 603 cm^{-1} was attributed to single four rings (S4R) related to a phillipsite structure.

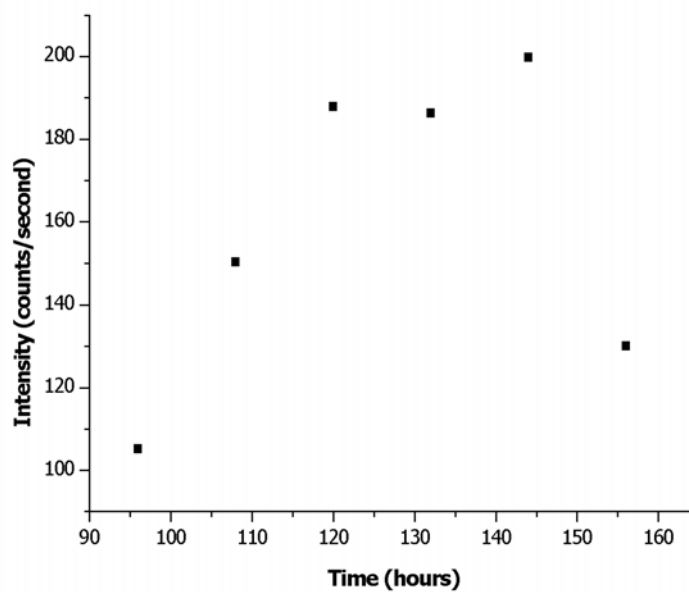


Figure 4.41 The XRD intensity of Na-P1 zeolite obtained from the activated with 10 % NaOH concentration, S/L = 1/10 and reaction temperature 100 °C for 96, 108, 120, 132, 144 and 156 hours

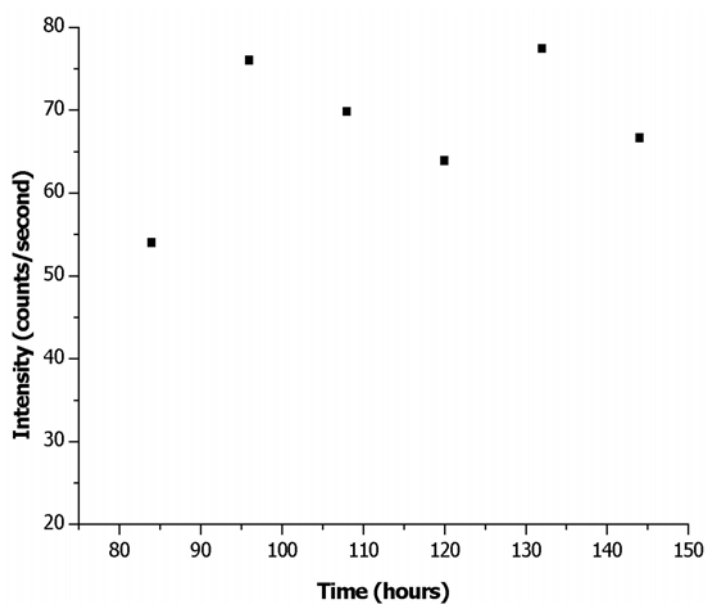


Figure 4.42 The XRD intensity of analcime zeolite obtained from the activated with 10 % NaOH concentration, S/L = 1/10 and reaction temperature 140 °C for 84, 96, 108, 120, 132 and 144 hours

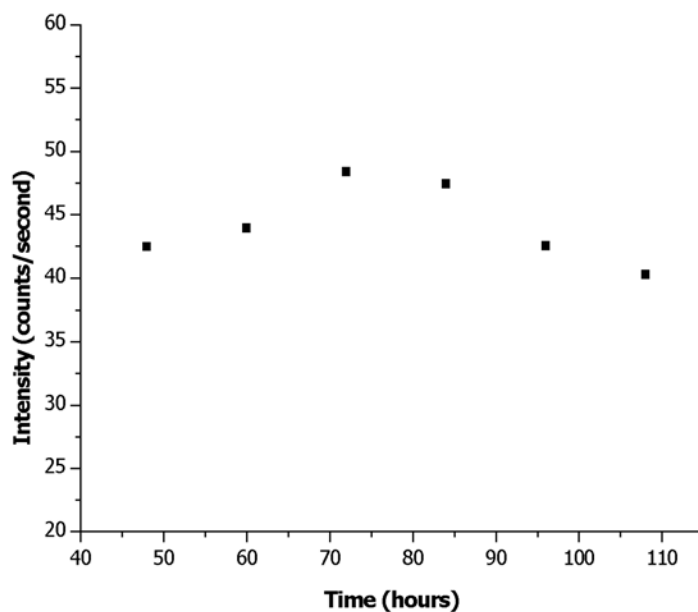


Figure 4.43 The XRD intensity of cancrinite zeolite obtained from the activated with 20 % NaOH concentration, S/L = 1/30 and reaction temperature 180 °C for 48, 60, 72, 84, 96 and 108 hours

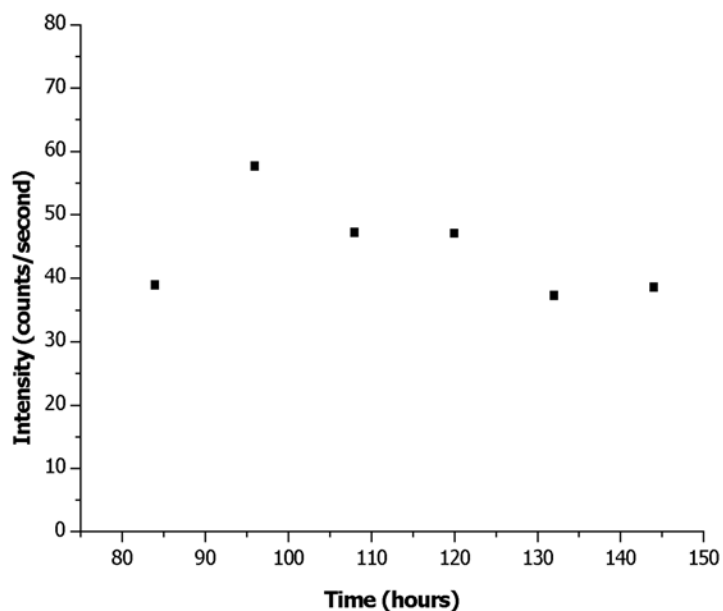


Figure 4.44 The XRD intensity of hydroxysodalite zeolite obtained from the activated with 30 % NaOH concentration, S/L = 1/30 and reaction temperature 100 °C for 84, 96, 108, 120, 132 and 144 hours

However, the bands at 1111, 1003, 774, 739, 675 and 435 cm^{-1} were at higher wavenumber than those from more than Flanigen's work. A very weak band at 622 cm^{-1} of analcime zeolite was assigned to the single 4- or 6- membered rings and related to analcime structure type. The spectrum of the 622 cm^{-1} was quite similar to the spectrum of the Flanigen's work (615 cm^{-1}). The cancrinite zeolite bands (in this work) at 624 and 567 cm^{-1} , assigned to the single 4- or 6- membered rings, that related to cancrinite structure type, were similar to the references (Flanigen et al., 1971) and the bands of hydroxysodalite zeolite (in this work) at 567 cm^{-1} , assigned to the 6- membered rings, that related to sodalite structure type, was close to the value of the Dusica's work (560 cm^{-1}) (Dusica, Igor, Aleksandra and Predrag, 2003).

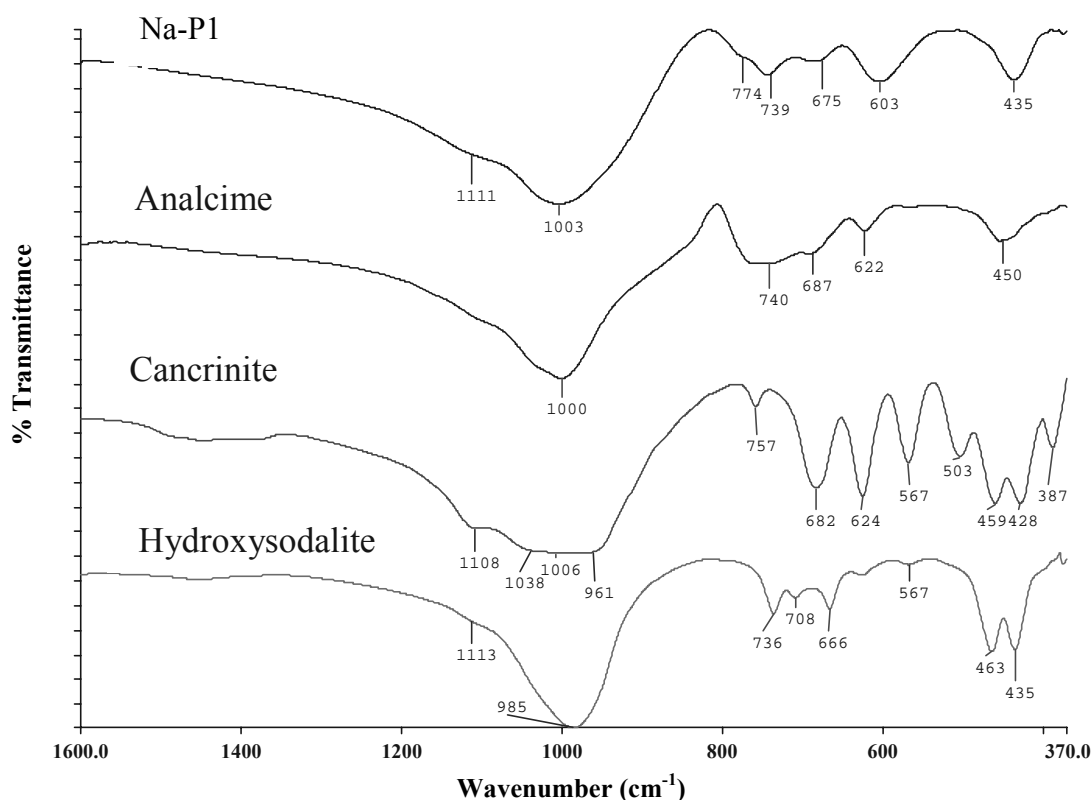


Figure 4.45 IR spectra of each sodium zeolite obtained from diatomite starting material treated with maximum efficiency of synthesis

Table 4.20 Infrared absorption bands (cm^{-1}) for each sodium zeolites from references and the experiments

Zeolite	Asym. Stretch	Sym. Stretch	Dbl. ring	T-O Bend
Na-P1	1105mwsh	772mwsh	600m	435ms
(Flanigen et al., 1971)	995-1000s	738mw 670mw		
Analcime	1162vwsh	740m	615vw	442ms
(Flanigen et al., 1971)	1012s 952s	686wb		410msh
Cancrinite	1095mw	755w	624m	498mw
(Flanigen et al., 1971)	1035msh 1000s 965msh	680m	567m	458ms 429ms
Hydroxysodalite	1096vwsh	729m	560wb*	461ms
(Flanigen et al., 1971)	986s	701mw 660m		432ms
Na-P1 (Experiment)	1111, 1003	774, 739 675	603	435
Analcime (Experiment)	1000	740, 687	622	450
Cancrinite	1108, 1038	757, 682	624, 567, 503	459, 428
(Experiment)	1006, 961			387
Hydroxysodalite	1113, 985	736, 708	567	463, 435
(Experiment)		666		

*(Dusica et al., 2003)

s = strong; ms = medium strong; m = medium; mw = medium weak;

w = weak; vw = very weak; sh = shoulder; b = broad

In order to examine the morphology of obtained sodium zeolites, the sample that had the XRD pattern obviously dominated by one type of detected zeolite and this zeolite is viewed by the SEM in Figure 4.46 - 4.49. It was found that the Na-P1 appeared in fairly equant, but somewhat irregular shapes and the analcime had icosahedral shape. The cancrinite appeared in fractal shape comprised of extended bars and the hydroxysodalite had prismatic particle shape. The means particle sizes of Na-P1, analcime, cancrinite and hydroxysodalite were 14, 116, 17 and 10 μm , respectively. The result of the particle sizes is illustrated in Figure 4.50.

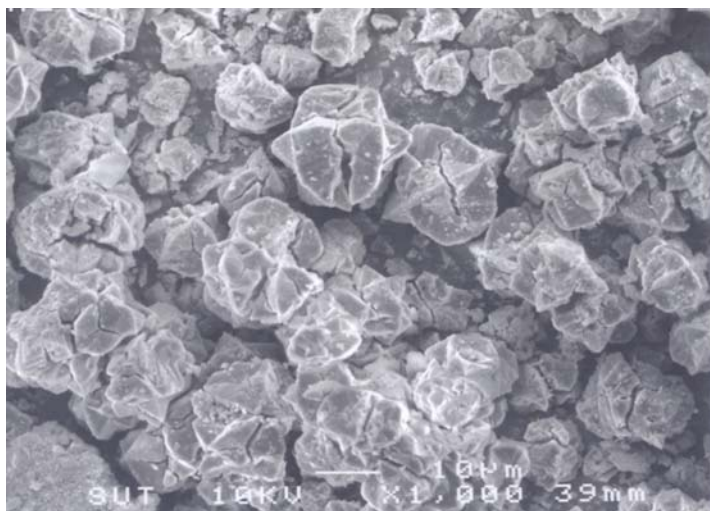


Figure 4.46 SEM micrograph of Na-P1 zeolite

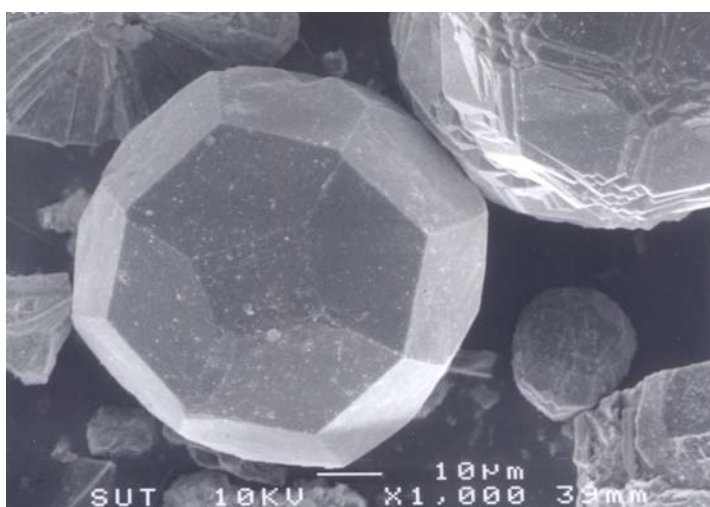


Figure 4.47 SEM micrograph of analcime zeolite

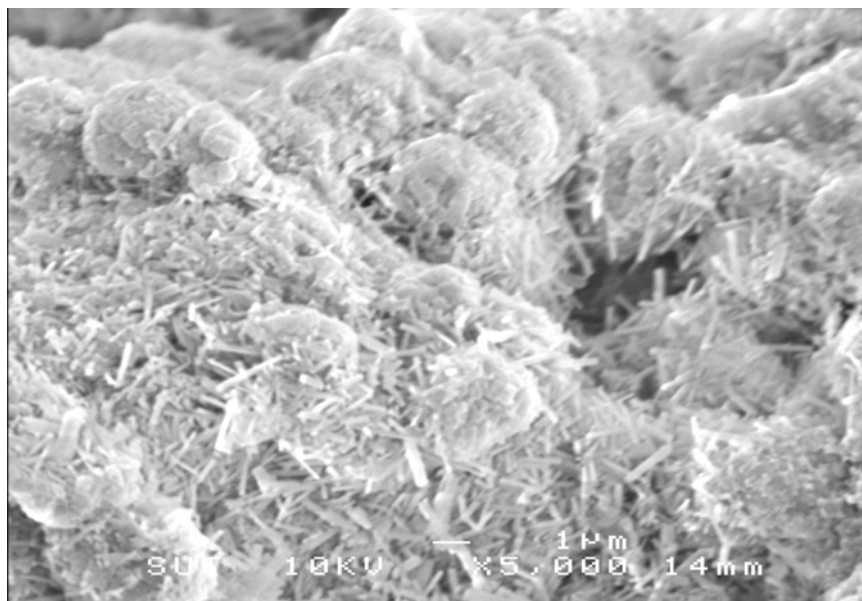


Figure 4.48 SEM micrograph of cancrinite zeolite

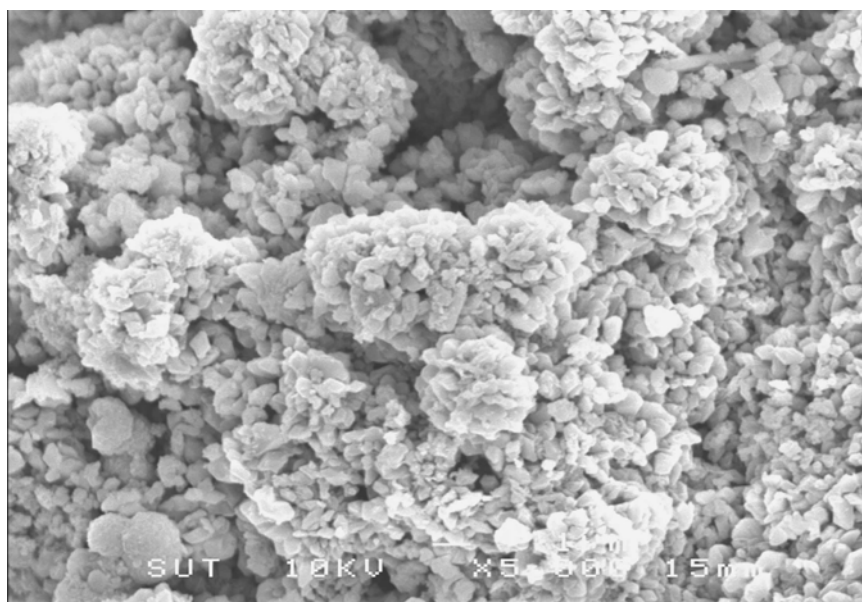


Figure 4.49 SEM micrograph of hydroxysodalite zeolite

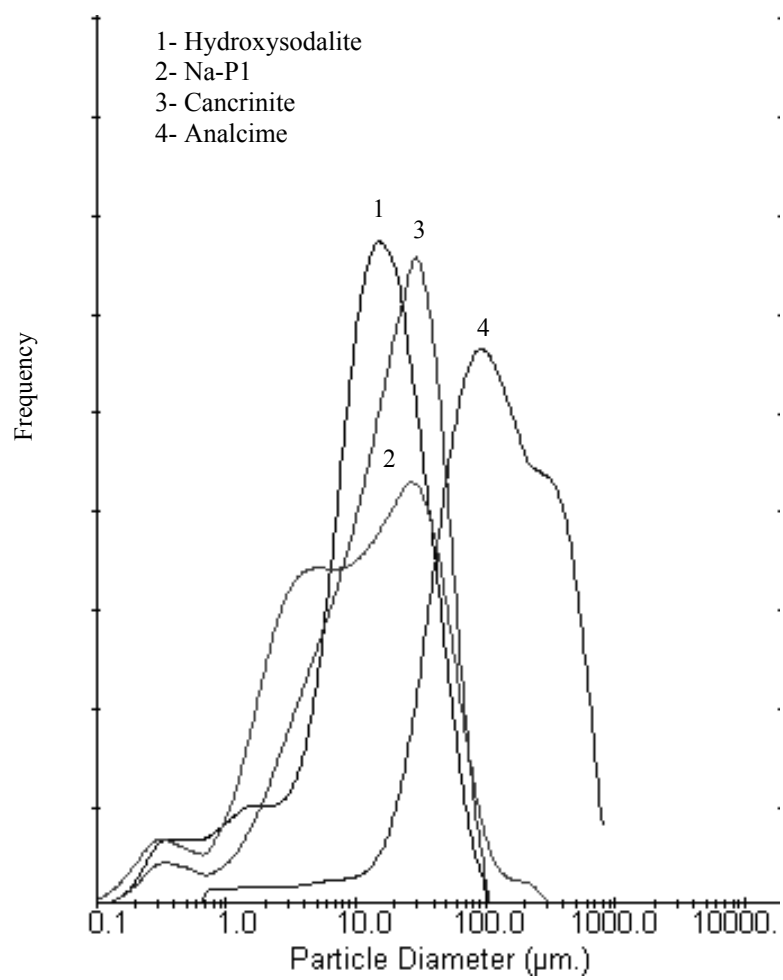


Figure 4.50 The particle size distributions of sodium zeolites obtained

4.7 Ammonium removal from aqueous solution by sodium zeolite

obtained

In the aqueous solution, ammonia can exist in either un-ionized form (NH_3) and/or ionized form (NH_4^+) depending on the pH and temperature. Of these two forms of ammonium, only the ionized form can be removed by the ion exchange operation, the pH of the aqueous solution must be at or below 7. During all ammonium removal experiment work, the pH was maintained at a value of 6.5 and it was assumed that ammonia existed in the ionic form and was used for ion exchange. Ion exchange is an endothermic process. Hence, an increase in temperature tends to increase the exchange capacity of this process (Sheng and Chang, 1996). The calibration curve was carried out from the series nessler standard solution are presented in Figure 4.51.

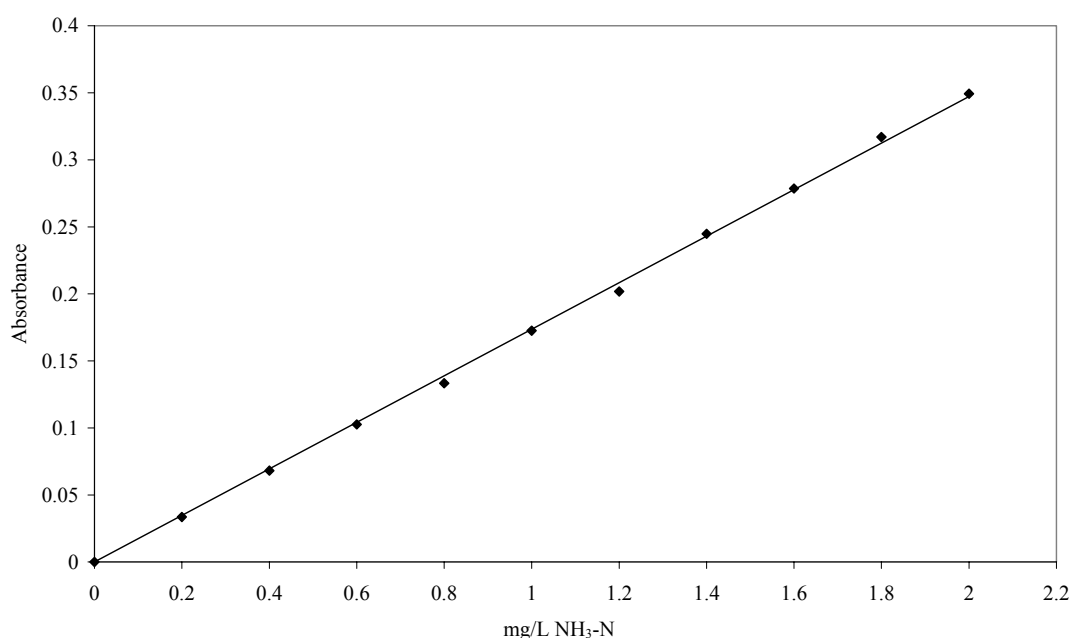


Figure 4.51 Calibration curve of standard nessler reagent

The Langmuir and Freundlich parameters were determined by the following procedures. The amount of ammonium accumulated on the solid sample was calculated by the following expressions as the difference between the amount present in the initial ammonium concentration and that remaining in solution after equilibrium with the solid sample.

$$Q = \frac{(C_0 - C_e)V}{M} \quad (1)$$

where:

Q (mg/g) is the amount of ammonium adsorbed;

C₀ (mg/L) represents initial ammonium concentration;

C_e (mg/L) represents equilibrium ammonium concentration;

V (L) is the volume of solution;

M (g) is the mass of solid sample.

The results determined by using Eq. (1) are plotted vs. time as shown in Figure 4.52 - 4.55. The initial ammonium concentration provides the necessary driving force to overcome all mass-transfer resistances of ammonium between the aqueous and solid phases. The removal of ammonium is high in the initial about 5 hours, but thereafter the rate significantly levels off and eventually approaches zero, i.e. when equilibrium is obtained. These changes in the rate of removal might be due to the fact that, initially, all adsorbent sites were vacant and the solute concentration gradient was high. Afterwards, the ammonium uptake rate by the solid sample decreased significantly, due to decrease in adsorption sites.

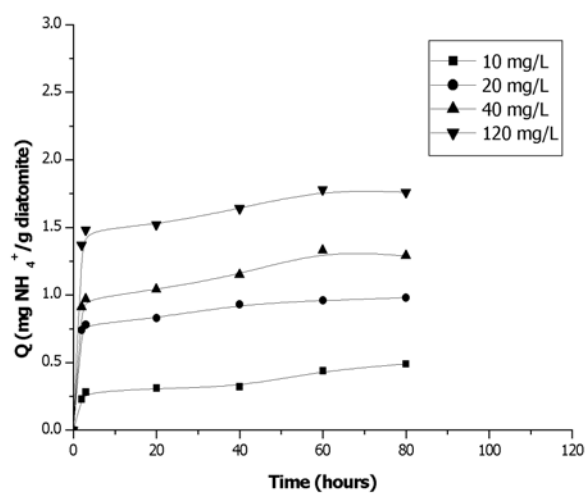


Figure 4.52 Plot of initial ammonium concentration in the aqueous solution on the exchange capacity of diatomite at 25 °C and pH 6.5

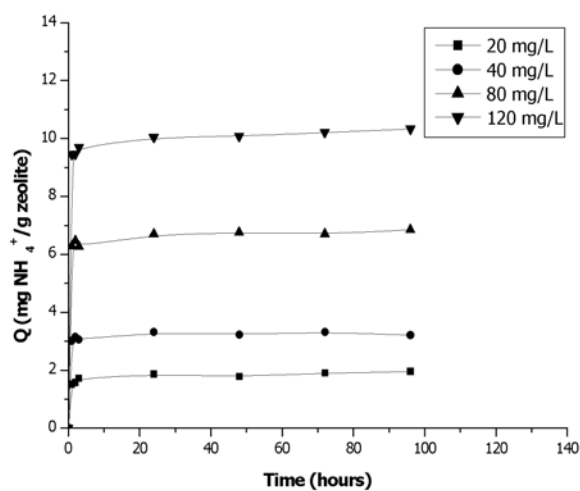


Figure 4.53 Plot of initial ammonium concentration in the aqueous solution on the exchange capacity of Na-P1 zeolite at 25 °C and pH 6.5

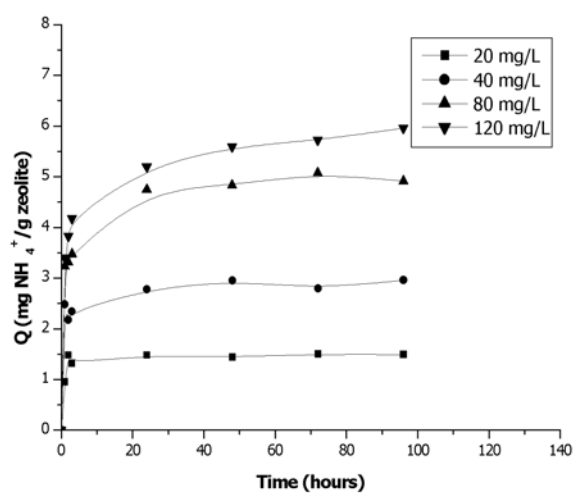


Figure 4.54 Plot of initial ammonium concentration in the aqueous solution on the exchange capacity of analcime zeolite at 25 °C and pH 6.5

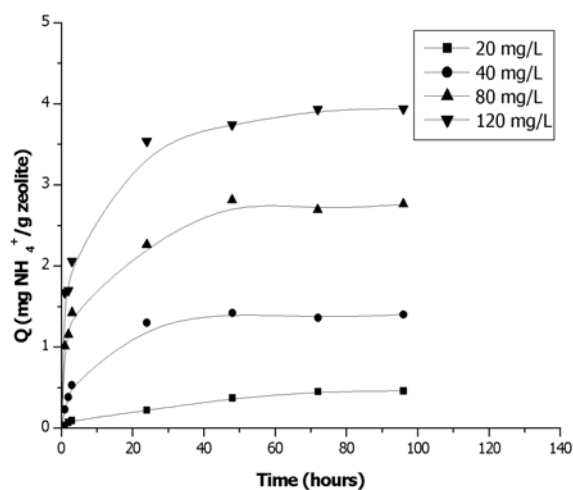


Figure 4.55 Plot of initial ammonium concentration in the aqueous solution on the exchange capacity of cancrinite zeolite at 25 °C and pH 6.5

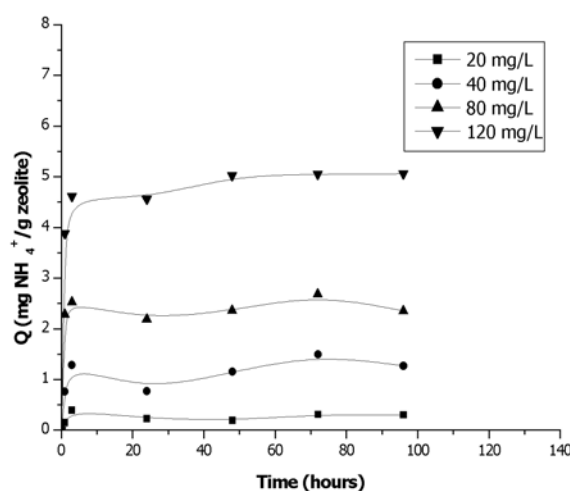


Figure 4.56 Plot of initial ammonium concentration in the aqueous solution on the exchange capacity of hydroxysodalite zeolite at 25 °C and pH 6.5

A decreasing removal amount, particularly towards the end of the experiment, indicated a possible monolayer of ammonium ion on the outer surface and pores of the solid sample and pore diffusion onto the inner surface of solid particles through the film due to continuous agitation maintained during the experiment. The adsorption of ammonium by natural diatomite and each sodium zeolite was initially fast, during the first 1 to 5 hours, depending on the initial ammonium concentration, and then gradually decreased with increase in contact time. With the increase of ammonium concentration in solution, the adsorption capacity of the ammonium ion also increases. Singh and Prasad (1997) observed that with high concentrations of ammonium (98.76 mg NH₄⁺/100 mL) adsorption by 13X molecular sieve synthetic zeolites becomes constant, possibly because of complete removal of Na⁺ by NH₄⁺ cations.

The equilibrium removal of the ammonium ion considered can be mathematically expressed in terms of adsorption isotherms. Adsorption isotherms are essential for the description of how ammonium ion concentration will interact with natural diatomite and zeolites, and are useful to optimize the use of these materials as an adsorbent. Therefore, empirical equation (Freundlich or Langmuir isotherm model) are important for adsorption data interpretation and predictions. Both Freundlich and Langmuir models were used for the evaluation of experimental results. The Freundlich and Langmuir models are as follows:

$$Q = K_f C_e^{1/n} \quad (2)$$

$$Q = \frac{abC_e}{1 + bC_e} \quad (3)$$

These models are rearranged to the linear form.

$$\text{Log}Q = \text{log}K_f + \frac{1}{n} \text{log}C_e \quad (4)$$

$$\frac{1}{Q} = \frac{1}{abC_e} + \frac{1}{b} \quad (5)$$

Plotting the experimental data using Eqs. (4) and (5) are shown in Figure 4.57 - 4.61. The values of a , b , K_f and $1/n$ that best fitted the data as well as the corresponding correlation coefficients (R^2 values) are presented in Table 4.21. From the regression coefficient value of natural diatomite and analcime zeolite fitted to the Langmuir equation are shown in Figure 4.57 (b) and 4.59 (b), respectively. The Langmuir isotherm of Na-P1, cancrinite and hydroxysodalite zeolites were non-conclusive; that is, it contained negative values and with small the regression coefficients suggesting that they are not indicative of anything interpretable. The results from analysis gave Langmuir constants; $a = 0.049$, $b = 2.57$ of natural diatomite and $a = 0.048$, $b = 8.12$

of analcime zeolite. The results indicate that the Langmuir isotherm had a better fit than the Freundlich for these materials. To investigate the sodium zeolite characteristics of adsorption, the Freundlich equation was fitted to the arithmetic isotherm are shown in Figure 4.58 (a), 4.60 (a) and 4.61(a). Values for K_f and $1/n$ were determined from the y-intercept and the slope, respectively (see Table 4.21), by applying the best line to the data using a linear regression analysis. The intercept is an indicator of adsorption capacity and the slope of adsorption intensity.

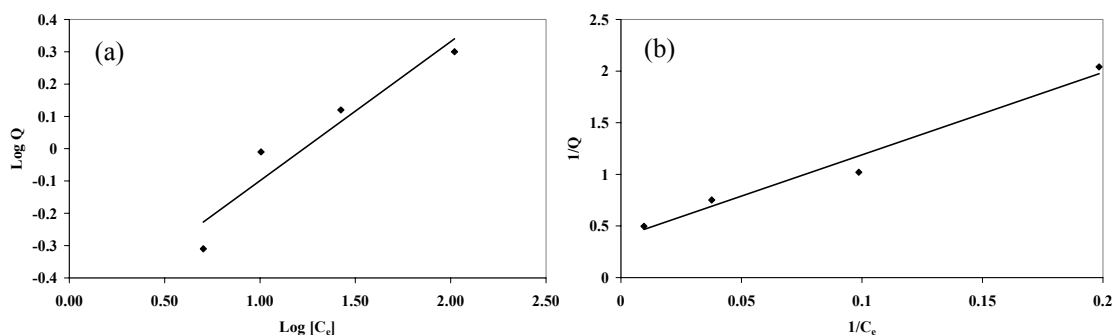


Figure 4.57 Linearised Freundlich isotherm (a) and linearised Langmuir isotherm (b) for ammonium removal by natural raw diatomite

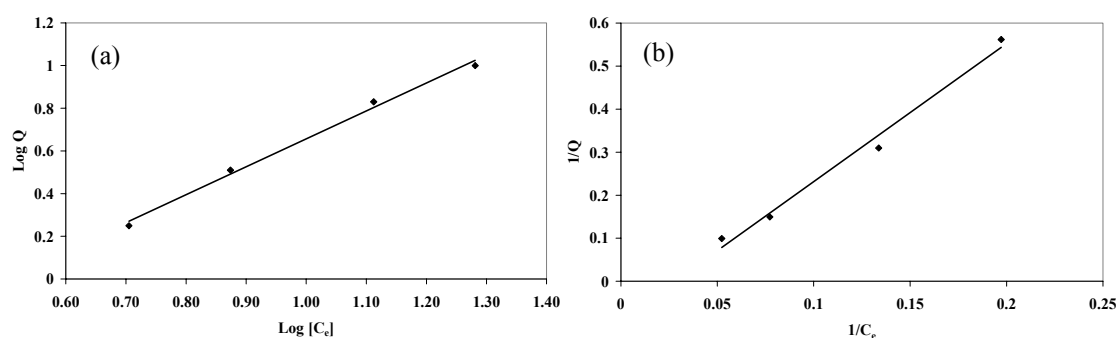


Figure 4.58 Linearised Freundlich isotherm (a) and Linearised Langmuir isotherm (b) for ammonium removal by Na-P1 zeolite

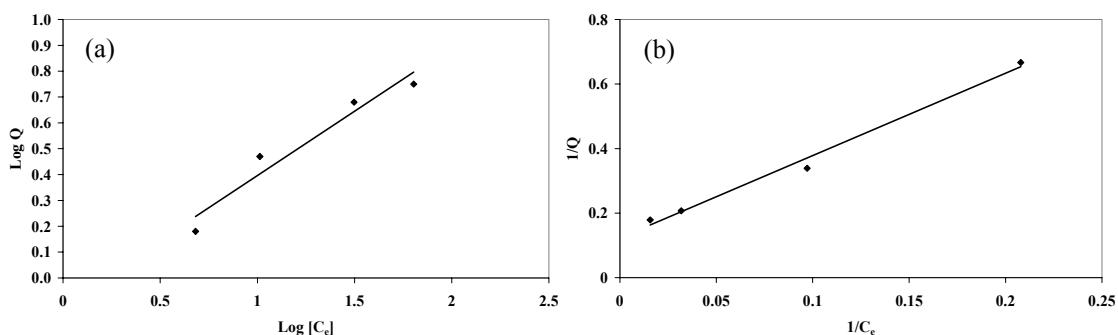


Figure 4.59 Linearised Freundlich isotherm (a) and Linearised Langmuir isotherm (b) for ammonium removal by analcime zeolite

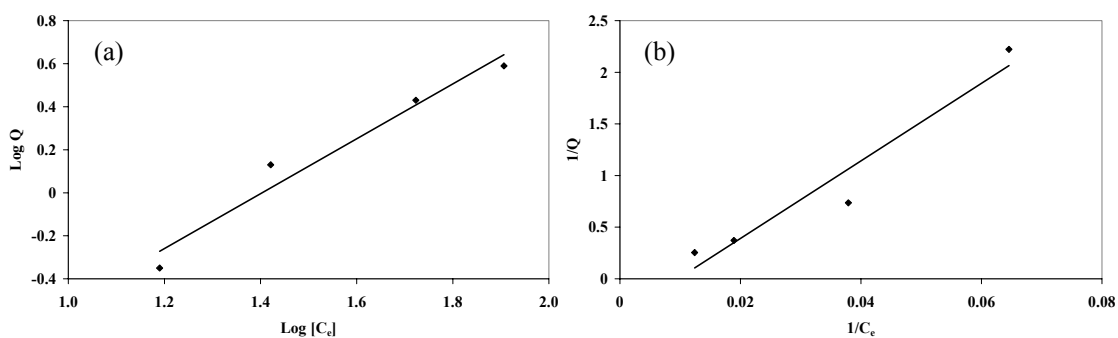


Figure 4.60 Linearised Freundlich isotherm (a) and Linearised Langmuir isotherm (b) for ammonium removal by cancrinite zeolite

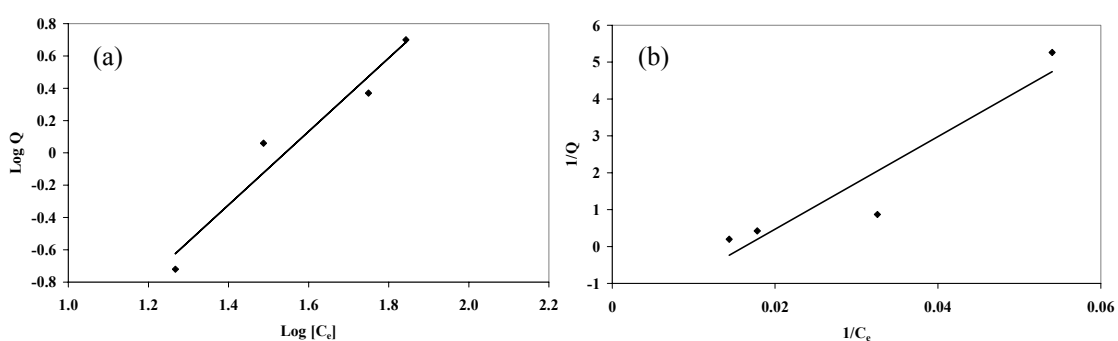


Figure 4.61 Linearised Freundlich isotherm (a) and Linearised Langmuir isotherm (b) for ammonium removal by hydroxysodalite zeolite

Table 4.21 Langmuir and Freundlich models parameters for best fit and corresponding correlation coefficients

	Natural diatomite	Na-P1 zeolite	Analcime zeolite	Cancrinite zeolite	Hydroxysodalite zeolite
Freundlich model					
K_f	0.296	0.223	0.790	0.016	0.0003
$1/n$	0.430	1.308	0.498	1.274	2.272
n	2.324	0.765	2.008	0.785	0.440
r^2	0.912	0.994	0.942	0.960	0.952
Langmuir model					
a	0.049	-0.028	0.048	-0.010	-0.016
b	2.566	-11.211	8.123	-2.775	-0.492
r^2	0.975	0.987	0.990	0.937	0.890

It can be concluded that the adsorption of diatomite and analcime zeolite exhibits Langmuir behaviour which indicates a monolayer adsorption but the adsorption of Na-P1, hydroxysodalite and cancrinite zeolite was best represented by the Freundlich model, which indicates a heterogeneous surface binding (Al-Ghouti et al., 2003). A high value of n for diatomite and analcime zeolite indicated that adsorption was good over the entire range of concentrations studied, while a steep slope of Na-P1, cancrinite and hydroxysodalite zeolite meant that adsorption was good at higher concentrations but poor at lower concentration. A value for $1/n$ below one for natural diatomite material and analcime zeolite indicates a normal Langmuir isotherm while $1/n$ above one for Na-P1, cancrinite and hydroxysodalite zeolite is indicative for a

cooperative sorption. A value of the intercept (K_f) in the range of 0.0003 - 0.790 indicated a low capacity for adsorption. In fact, a greater value K_f indicates a higher capacity for adsorption.

As a consequence, the best models fitting the data for ammonium removal seem to be the Langmuir isotherms for the natural diatomite and analcime. It can be represented by the following empirical formula:

$$Q = \frac{0.125C_e}{1 + 2.566C_e} \quad (6)$$

$$Q = \frac{0.391C_e}{1 + 8.123C_e} \quad (7)$$

On the other hand the Freundlich model was best fitted with the data of Na-P1, cancrinite and hydroxysodalite and the Freundlich isotherms are obtained as follows:

$$Q = 0.223C_e^{1.308} \quad (8)$$

$$Q = 0.016C_e^{1.274} \quad (9)$$

$$Q = 0.0003C_e^{2.272} \quad (10)$$

The experimental uptake equilibrium data for natural diatomite material and each sodium zeolite are shown in Figure 4.62. The aqueous phase concentrations are expressed in mg/L NH_4^+ and those of the exchanger phase in percentage of removed ammonium. The results show that the percentage of ammonium ion removal more efficiently in Na-P1, cancrinite and hydroxysodalite zeolite at high initial concentrations whereas the natural diatomite and analcime zeolite at low concentrations.

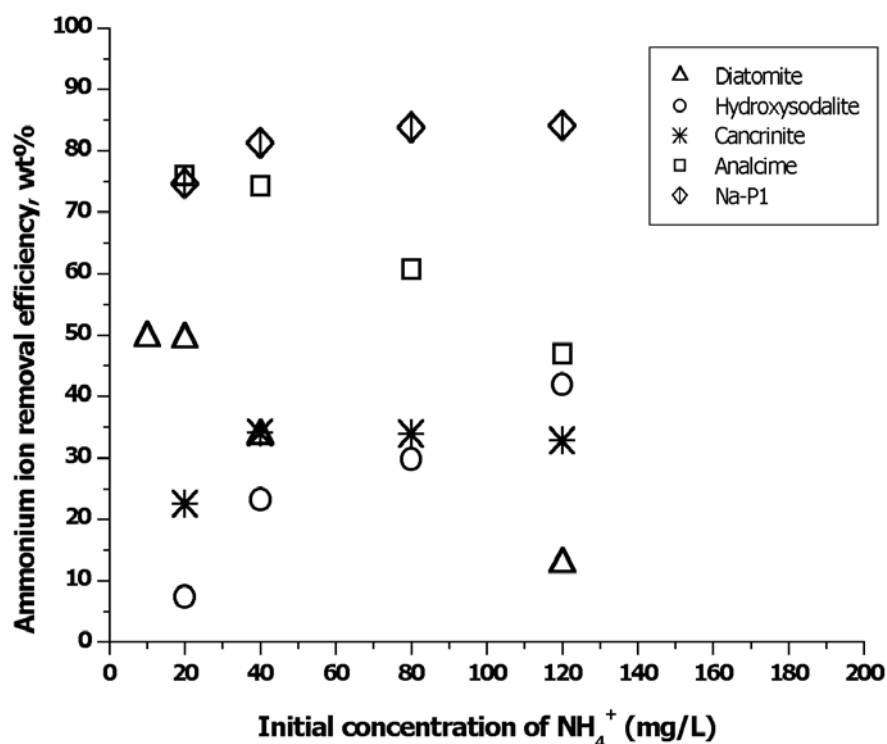


Figure 4.62 The ammonium ion removal efficiency of natural diatomite material and each sodium zeolite material

4.8 Cation exchange capacity

The cation exchange capacity (CEC) was determined on the natural diatomite material by ammonium acetate method and found to be 26 meq/100 g. The CEC of zeolitic products was determined by ammonium acetate modified method and found to be 173 meq/100 g for Na-P1, 36 meq/100 g for analcime, 87 meq/100 g for hydroxysodalite and 67 meq/100 g for cancrinite.

The analcime zeolite behaved as Langmuir isotherm as did natural diatomite material. It may be because the CEC value of analcime zeolite (36 meq/100 g) was close to natural diatomite material (26 meq/100 g). However, the CEC value of analcime zeolite was very low when compared to Na-P1, hydroxysodalite and

cancrinite zeolite. This may result from the mean particle size of analcime zeolite being very large (116 μm) compared to Na-P1 (14 μm), hydroxysodalite (10 μm) and cancrinite (17 μm). So, it can be concluded that the adsorption of analcime zeolite may behave as monolayer like the natural diatomite. Moreover, it was observed that the efficiency of both materials in NH_4^+ removal decreased with increasing NH_4^+ concentration. It may be because all active sites of both materials were already occupied by NH_4^+ at low concentration when NH_4^+ concentration increased, so it did not effect the NH_4^+ removal. On the other hand, Na-P1, cancrinite and hydroxysodalite zeolite behaved according to Freundlich adsorption isotherm and was observed that with high concentrations of NH_4^+ , the efficiency of these zeolites in NH_4^+ removal increased. It might be due to the removal of NH_4^+ by these zeolites involving not only the adsorption process but also an ion exchange process.

Chapter V

Conclusions

The experimental investigations on the formation of sodium zeolites from diatomite and modified diatomite materials proved that these materials are a low cost silica-alumina material suitable for zeolite synthesis. The synthesis of sodium zeolites was carried out by using natural diatomite, diatomite calcined at 900 °C, diatomite calcined at 1000 °C, diatomite calcined at 1100 °C, diatomite treated with hot 6M H₂SO₄, and diatomite first treated with hot 6M H₂SO₄ then calcined at 1100 °C, activated with 10 % - 30 % w/v of NaOH solution in the temperature of 100 - 180 °C and the reaction time from 24 - 168 hours under an autogenous pressure. The sodium zeolites had been successfully converted from all starting materials. The zeolitic products synthesized were Na-P1, analcime, cancrinite and hydroxysodalite. The hydrothermal transformation of starting diatomite material into sodium zeolites depends on how the natural diatomite was treated, the calcination temperature, the particle size, the NaOH concentration, the reaction temperature and the solid/liquid ratio. Solid/liquid ratio seems to have less influence on the kind of sodium zeolites obtained and zeolites formation. The higher amorphous silica (SiO₄) containing in the different starting material are active silica sources in the synthesis of sodium zeolites whereas the presence of SiOH groups reduce the reactivity of the silica. Also, the smaller particle size of starting diatomite materials made amorphous silica (SiO₄) more active towards sodium zeolites synthesis due to higher surface area. It was found

that the starting material obtained from natural diatomite treated with hot 6M H₂SO₄ then calcined at 1100 °C was the most reactive to synthesize zeolites. The highest crystallinity of Na-P1 zeolite was obtained from this starting material at low temperature and at low reagent concentrations but under the extreme condition, cancrinite and hydroxysodalite zeolites were obtained. The analcime zeolite was obtained with both of lower concentration for lower temperature and higher concentration for higher temperature. The maximum crystallinity of each sodium zeolite was obtained when the reaction time increased. The best condition to get the pure Na-P1 zeolite with high crystallinity had been found to be at 144 hours of reaction at 100 °C with 10 % NaOH and S/L = 1/10 ratio and the best obtained analcime zeolite crystallinity condition was 10 % NaOH, S/L = 1/10, the reaction temperature of 140 °C and the reaction time 132 hours. The optimum condition for cancrinite synthesized was 20 % NaOH, S/L = 1/30, the reaction temperature of 180 °C and the reaction time 72 hours and the best formation of high hydroxysodalite zeolite crystallinity was 30 % NaOH, S/L = 1/30, the reaction temperature of 100 °C and the reaction time 96 hours.

These zeolite products obtained are very interesting because of their applications as sorbents of ammonium ion from wastewater, which arise from the farming activities. The removal of ammonium ion from synthetic solution was demonstrated successfully on a laboratory scale with a selective ion exchange process. The data obtained from batch studies were applied to Langmuir and Freundlich isotherms. The Langmuir isotherm gave an adequate correlation coefficient value for natural diatomite and analcime zeolite. While the correlation coefficient value from the Freundlich isotherm were adequate for Na-P1, cancrinite and hydroxysodalite zeolite.

Natural raw diatomite material and the analcime zeolite removed ammonium ion successfully in dilute initial ammonium ion concentration while Na-P1, cancrinite and hydroxysodalite zeolites can remove ammonium ion efficiently in higher initial ammonium ion concentration. Na-P1 zeolite can remove efficiently ammonium ion more than natural diatomite and the other sodium zeolites due to its maximum CEC (173 meq/100g). Finally, this study emphasizes that natural diatomite material from Lampang Province can be used in the synthesis of sodium zeolites, and zeolite Na-P1 obtained is most likely more effective for removal of ammonium ion in water.

Suggestions for future work

There are some topics that may be interesting to be investigated such as synthesis of potassium zeolites or other zeolites by diatomite material and especially interesting topics are the effect of $\text{SiO}_2/\text{Al}_2\text{O}_3$ ratio on the zeolitization, and investigation of obtained zeolitic product properties. In addition, a study of utilization of NH_4^+ -zeolite as soil conditioner is also interesting.

References

References

- Aicha, G-B., Thibaud, C., Jocelyne, M., Francois, F. and Jacques, L. (2003). Spectroscopic characterization of biogenic silica. **Journal of Non-Crystalline Solids**. 316 : 331-337.
- Al-Degs, Y., Khraisheh, M. A. M. and Tutunji, M. F. (2001). Sorption of lead ions on diatomite and manganese oxides modified diatomite. **Water Research**. 35 [15]: 3724-3728.
- Al-Ghouti, M. A., Khraisheh, M. A. M., Allen, S. J. and Ahmad, M. N. (2003). The removal of dyes from textile wastewater: a study of the physical characteristics and adsorption mechanisms of diatomaceous earth. **Journal of Environmental Management**. 69: 229-238.
- Anand, S. and Michael, W. G. (1999). The adsorption of SO₂ by zeolites synthesized from fly ash. **Environmental Science & Technology**. 33: 1464-1469.
- Antonucci, P. L., Crisafulli, M. L., Giordano, N. and Burriesci, N. (1985). Zeolitization of perlite. **Materials Letters**. 3[7,8]: 302-307.
- APHA. (1992). **Standard methods for the examination of water and wastewater**. 18th ed. American public health association, American water works association and water environment federation, Washington, DC.
- Baccouche, A., Srasra, E. and Maaoui, M .El.. (1998). Preparation of Na-P1 and sodalite octahydrate zeolites from interstratified illite-smectite. **Applied Clay Science**. 13 [4]: 255-273.

- Bekkum, H. V., Mflanigen, E. and Cjansen, J. (1991). **Introduction to zeolite science and practice, zeolite and molecular sieves**. 58: 13-33.
- Belver, C., Munoz, M. A. B. and Vicente, M. A. (2002). Chemical activation of kaolinite under acid and alkaline condition. **Chemistry of Materials**. 14: 2033-2043.
- Bibliothek, D. D. (1998). **Industrial inorganic chemicals and products vol.5: phosphate fertilizers to sodium carbonates**. 4059.
- Biswajit, G., Dinesh, C. and Subhash, B. (1994). Synthesis of zeolite A from calcined diatomaceous clay: optimization studies. **Industrial & Engineering Chemistry Research**. 33: 2107-2110.
- Boukadir, D., Bettahar, N. and Derriche, Z. (2002). Synthesis of zeolite 4A and HS from natural materials. **Analytical Chimica - Science Materials**. 27 [4]: 1-13.
- Breck, D.W. (1974). **Zeolite molecular sieve: structure chemistry and use**. John Wiley and Sons. New York.
- Cheetham, A. K. and Peter, D. (1992). **Solid state chemistry compounds**. Clarendon Press.
- Chistidis, G. E., Paspaliaris, I. and Kontopoulos, A. (1999). Zeolitization of perlite fines: Mineralogical characteristic at the end products and mobilization of chemical elements. **Applied Clay Science**. 15: 305-221.
- Christopher, A., Gholam, H., Tai, S. M., Paul, A. M., Ryan, C. G., Tedros, A. and Laura, D. L. T. (1996). Synthesis and properties of zeolites from coal fly ash. **Environmental Science & Technology**. 30: 735-742.

- Dusica, V., Igor, M., Aleksandra, R. and Predrag, L. (2003). Effect of Na₂O/SiO₂ mol ratio on the crystal type of zeolite synthesized from coal fly ash. **Journal of Serbian Chemical Society**. 68[6]: 471-478.
- Dyer, A. (1998). **An introduction to zeolite molecular sieve**. New York: John Wiley and Sons Ltd.
- Feijen, E. J. P., Martens J. A. and Jacobs, P. A. (1994). Zeolites and related microporous materials: State of the art 1994 studies in surface science and catalysis. **Zeolites and their mechanism of synthesis**. Elsevier Science.
- Flanigen, E. M., Khatami, H. and Szymanski, H. A. (1971). **Molecular sieve zeolite I**. Adv. Chem. Ser. 101. (American Chemical Society, Washington D.C): 201-229.
- Goren, R., Baykara, T. and Marsoglu, M. (2002). A study on the purification of diatomite in hydrochloric acid. **Scandinavian Journal of Metallurgy**. 31: 115-119.
- Gualtieri, A.F. (2001). Synthesis of sodium zeolites from a natural halloysite. **Physics and Chemistry Minerals**. 28: 719-728.
- Gunter, E. (1989). Multinuclear solid-state NMR in silicate and zeolite chemistry. **Trends in analytical chemistry**. 8 [9]: 343-347.
- Halimatun, H., Mohd, N. M. M., Salasiah, E., Endang, L. and Zainab, R. (1997). ²⁹Si MAS NMR, XRD and FESEM studies of rice husk silica for the synthesis of zeolites. **Journal of Non-Crystalline Solids**. 211: 126-131.
- Hassan, M. S., Ibrahim, I. A. and Ismael, I. S. (1999). Diatomaceous deposits of Fayium, Egypt; characterization and evaluation for industrial application. **Chinese Journal of Geochemistry**. 18 [3]: 233-240.

- Hollman, G. G., Steenbruggen, G. and Janssen-Jurkovicova, M. (1999). A two-step process for the synthesis of zeolites from coal fly ash. **Fuel**. 78: 1225-1230.
- Hotta, M., Torii, K. and Asaka, M. (1975). Synthesis of zeolite X from diatomite by treatment with sodium hydroxide-sodium chloride solution. **Tohoku Kogyo Gijutsu Shikensho Hokoku**. 6: 632-639.
- Inglethorpe, S. D. J. and Morgan, D. J. (1992). National conference on “Geologic resources of Thailand: potential for future development”. **The laboratory assessment of diatomite**. 210-221.
- Inglethorpe, S. D. J., Utha-aroon, C. and Chanyavanich, C. (1997). The international conference on stratigraphy and tectonic evolution of Southeast Asia and South Pacific Bangkok, Thailand. **An inventory of diatomite deposits of the Lampang Basin, northern Thailand**. 669-685.
- Juan, R., Hernandez, S., Querol, X., Andres, JM. and Moreno, N. (2002). Zeolite material synthesised from fly ash: use as cationic exchanger. **Journal of Chemical Technology and Biotechnology**. 77: 299-304.
- Khodabandeh, S. and Davis, M. E. (1997). Alteration of perlite to calcium zeolites. **Microporous Materials**. 9: 161-172.
- Maria, C. (1997). **Environmental sampling and analysis lab manual**. Lewis publishers. New York. P.313.
- Michaelw, G. and Darryl, D. (1997). Zeolites synthesized from class F fly ash and sodium aluminate slurry. **Journal of the American Ceramic Society**. 80 [9]: 2449-2453.

- Michihiro, M., Chikashi, T. and Motohide, M. (2002). Resource recovery of waste incineration fly ash: synthesis of zeolites A and P. **Journal of the American Ceramic Society.** 85 [7]: 1873-1875.
- Midivnishvili, O. M. and Uridiya, L. Ya. (1976). Production of synthetic zeolites based on diatomite and sodium aluminate. **Seriya Khimicheskaya.** 2 [2]: 176-180.
- Miyamoto, M. (1984). Synthesis of zeolite from the Noto diatomaceous earth. **Ishikawa-ken Kogyo Shikenjo Kenkyu Hokoku.** 32: 49-54.
- Molina, A. and Poole, C. (2004). A comparative study using two methods to produce zeolites from fly ash. **Minerals Engineering.** 17: 167-173.
- Nishido, H., Sakamoto, T., Doi, A. and Akagi, Y. (1982). Artificial transformation of diatomaceous earth into zeolites. Part 2. Studies of the effective industrial usage of the diatomaceous earth from Hiruzen district, Okayama prefecture. **Okayama Rika Daigaku.** 7: 33-44.
- Ojima, J. (2003). Determining of crystalline silica in respirable dust samples by infrared spectrophotometry in the presence of interferences. **Journal of Occupational Health.** 45: 94-103.
- Otal, E., Arenas, L. F. V., Moreno, N., Querol, X., Parapar, J. V. and Pereira, C. F. (2003). Application of zeolitized coal fly ashes to the depuration of liquid wastes. **International Ash Utilization Symposium, Center for Applied Energy Research, University of Kentucky.** Paper # 59.
- Owen, R. B. and Utha-aroon, C. (1999). Diatomaceous sedimentation in the Tertiary Lampang Basin, Northern Thailand. **Journal of Paleolimnology.** 22: 81-95.

- Payan, A. V. (1999). Arsenic and lead removal from water using tailored zeolites. **M. Sc. Thesis. University of Puerto Rico.**
- Pfenninger, A. (1999). Molecular sieves, Vol. 2. **Manufacture and used of zeolites for adsorption processes.** (pp 164-197). Springer-Verlag.
- Poole, C., Prijatama, H. and Rice, N. M, (2000). Preparation and utilisation of synthetic zeolite from PFA waste. **Ion exchange at the millennium Churchill College, Cambridge, 16-21 July 2000, proceeding of IEX 2000.** 150-157.
- Querol, X., Alastuey, A., Lopez-soler, A. and Plana, F. (1997). A fast method for recycling fly ash: microwave-assisted zeolite synthesis. **Environmental Science & Technology.** 31 [9]: 2527-2533.
- Querol, X., Moreno, N., Umana, J. C., Alastuey, A., Hernandez, E., Lopez-soler and A., Plana, F. (2002). Synthesis of zeolites from coal fly ash: an overview. **International Journal of Coal Geology.** 50: 413-423.
- Roland, E. and Kleinschmit, P. (1998). **Industrial inorganic chemical and products.** 6: 5169-5214.
- Ruiz, R., Blanco, C., Pesquera, C., Gonzalez, F., Benito, I. and Lopez, J.L. (1997). Zeolitization of a bentonite and its application to removal of ammonium ion from wastewater. **Applied Clay Science.** 12 [1-2]: 73-83.
- Sakamoto, T., Nishido, H. and Doi, A. (1981). Artificial transformation of diatomaceous earth into zeolites. Part 1. Studies of the effective industrial usage of the diatomaceous earth from Hiruzen district, Okayama prefecture. **Okayama Rika Daigaku.** 6: 39-49.

- Sen, S. and Youngman, R. E. (2003). NMR study of Q-speciation and connectivity in K_2O-SiO_2 glasses with high silica content. **Journal of Non-Crystalline Solids**. 331: 100-107.
- Shawabkeh, R. A. and Tutunji, M. F. (2003). Experimental study and modeling of basic dye sorption by diatomaceous clay. **Applied Clay Science**. 24: 111-120.
- Sheng, H. L. and Chang, L. W. (1996). Ammonium removal from aqueous solution by ion exchange. **Industrial & Engineering Chemistry Research**. 35: 553-558.
- Shiuh, (1997). U. S. Pat. 5, 565, 568.
- Sidheswaran, P. and Bhat, A. N. (1997). Synthesis of sodalitehydrate from clays. **Indian Journal of Chemistry Section A-Inorganic Bio-Inorganic Physical Theoretical & Analytical Chemistry**. 36 [8]: 672-676.
- Singh, G. and Prasad, B. (1997). Removal of ammonia from coke-plant wastewater by using synthetic zeolite. **Water Environment Research**. 69 [2]: 157-161
- Thai ceramic directory. (2001-2003). 130-131.
- Tomlinson, A. A. G. (1998). **Modern zeolites, materials science foundations**. 3: 11-64.
- Treacy, M. M. A. and Higgins, J. B. (2001). **Collection of simulated XRD powder patterns for zeolites**. International zeolite Association. Elsevier.
- Tsanov, Ts., Pavlova, Yu. and Karamisheva, P. (1979). Studies on the possibilities of producing zeolite products from diatomites. **Sofiya**. 26 [1]: 19-27.
- Vilma, S., Ursula, K. and Ruby, C. (2003). Synthesis of mordenite from diatomite: a case of zeolite synthesis from natural material. **Journal of Chemical Technology and Biotechnology**. 78: 485-488.

- Yuan, P., Wu, D. Q., Lin, Z. Y., Diao, G. Y., Peng, J. L. and Wei, J. F. (2001). Study on the hydroxyl species of diatomite using DRIFT spectroscopy. **Spectroscopy and Spectral Analysis**. 21 [6]: 783-786.
- Yuan, P., Wu, D. Q., He, H. P. and Lin, Z. Y. (2004). The hydroxyl species and acid sites on diatomite surface: a combined IR and Raman study. **Applied Surface Science**. 227: 30-39.
- Van der marel, H. W. and Beutelspacher, H. (1976). **Atlas of Infrared Spectroscopy of Clay Minerals and their Admixtures**. Elsevier. 275-279.
- Weng, H., Shen, Z., Yuan, M., Guo, D. and Chen, J. (1999). Stability of diatomaceous silica and its geochemical implication. **Chinese Science Bulletin**. 44 [23]: 2205-2208.

Appendices

Appendix A

Simulated XRD powder patterns for zeolites

ANA

Analcime

CHEMICAL COMPOSITION: $[\text{Na}_{16}(\text{H}_2\text{O})_{16}] [\text{Si}_{32}\text{Al}_{16}\text{O}_{96}]$
Cyclopean Islands, Greece

REFINED COMPOSITION: $[\text{Na}_{16}(\text{H}_2\text{O})_{16}] [\text{Si}_{32}\text{Al}_{16}\text{O}_{96}]$

CRYSTAL DATA: $Ia\bar{3}d$ (No. 230)

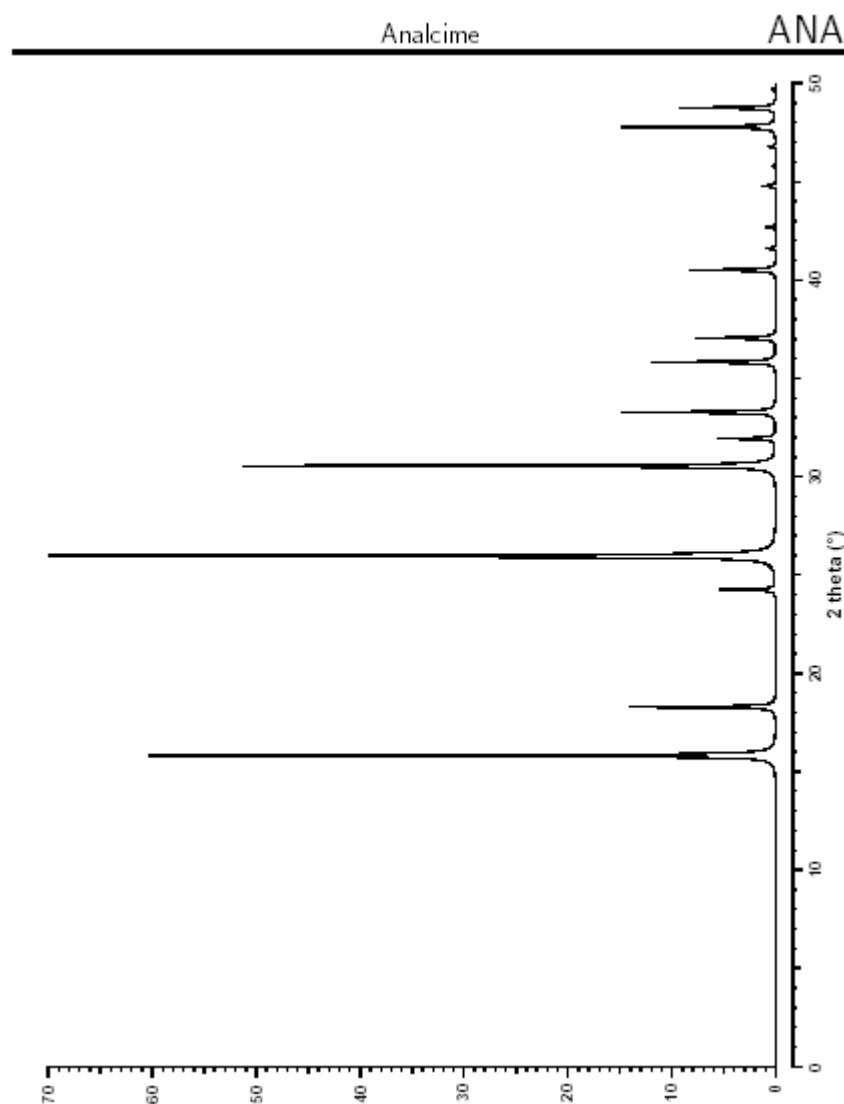
$a = 13.73 \text{ \AA}$ $b = 13.73 \text{ \AA}$ $c = 13.73 \text{ \AA}$

$\alpha = 90^\circ$ $\beta = 90^\circ$ $\gamma = 90^\circ$

X-ray single crystal refinement, $R = 0.04$

REFERENCE: G. Ferraris, D. W. Jones and J. Yerkess,
Z. Kristallogr. **135** 240-252 (1972).

<i>h</i>	<i>k</i>	<i>l</i>	2θ	<i>d</i>	<i>M</i>	<i>I</i> _{rel}	<i>h</i>	<i>k</i>	<i>l</i>	2θ	<i>d</i>	<i>M</i>	<i>I</i> _{rel}	<i>h</i>	<i>k</i>	<i>l</i>	2θ	<i>d</i>	<i>M</i>	<i>I</i> _{rel}
2	1	1	15.81	5.605	24	60.2	5	2	1	35.82	2.507	48	11.9	4	4	4	45.78	1.982	8	0.4
2	2	0	18.28	4.854	12	14.1	4	4	0	37.04	2.427	12	7.7	5	4	3	46.78	1.942	48	0.7
3	2	1	24.25	3.669	48	5.4	6	1	1	40.50	2.227	24	2.8	6	4	0	47.77	1.904	24	14.9
4	0	0	25.96	3.433	6	100.0	5	3	2	40.50	2.227	48	5.5	5	5	2	48.74	1.868	24	0.2
3	3	2	30.54	2.927	24	51.3	6	2	0	41.60	2.171	24	1.0	6	3	3	48.74	1.868	24	6.9
4	2	2	31.93	2.803	24	5.5	5	4	1	42.68	2.119	48	0.9	7	2	1	48.74	1.868	48	2.3
4	3	1	33.27	2.693	48	14.8	6	3	1	44.77	2.024	48	1.3	6	4	2	49.69	1.835	48	0.4



CAN

Cancrinite

CHEMICAL COMPOSITION: $[\text{Na}_7\text{Ca}_{0.9}(\text{CO}_3)_{1.4}(\text{H}_2\text{O})_{2.1}] [\text{Si}_6\text{Al}_6\text{O}_{24}]$
Synthetic crystal.

REFINED COMPOSITION: $[\text{Na}_8(\text{CO}_3)_{1.2}(\text{H}_2\text{O})_2] [\text{Si}_6\text{Al}_6\text{O}_{24}]$

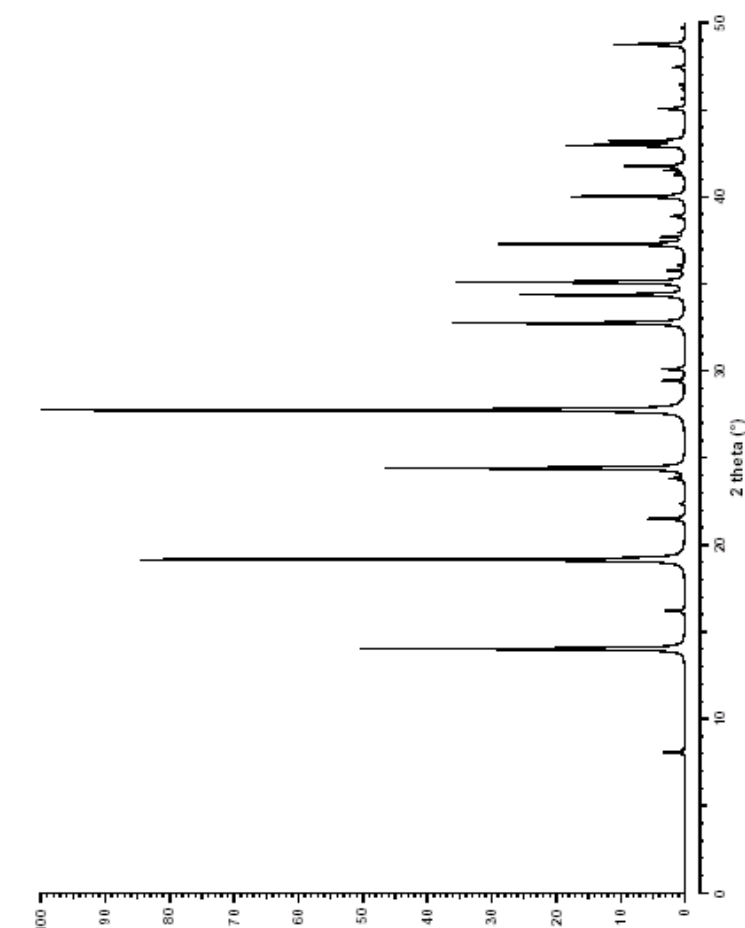
CRYSTAL DATA: $P6_3$ (No. 173)
 $a = 12.635 \text{ \AA}$ $b = 12.635 \text{ \AA}$ $c = 5.115 \text{ \AA}$
 $\alpha = 90^\circ$ $\beta = 90^\circ$ $\gamma = 120^\circ$
X-ray single crystal refinement, $R = 0.04$

REFERENCE: Y. I. Smolin, Y. F. Shepelev, I. K. Butikova and I. B. Kobayakov,
Kristallografiya 26 63-66 (1981).

<i>h</i>	<i>k</i>	<i>l</i>	2θ	<i>d</i>	<i>M</i>	<i>I</i> _{rel}	<i>h</i>	<i>k</i>	<i>l</i>	2θ	<i>d</i>	<i>M</i>	<i>I</i> _{rel}	<i>h</i>	<i>k</i>	<i>l</i>	2θ	<i>d</i>	<i>M</i>	<i>I</i> _{rel}
1	0	0	8.08	10.942	6	3.9	2	2	1	33.34	2.688	12	0.1	2	1	2	41.51	2.175	12	1.9
1	1	0	14.02	6.317	6	59.5	3	1	1	34.36	2.610	12	10.2	1	4	1	41.75	2.164	12	6.7
2	0	0	16.20	5.471	6	3.7	1	3	1	34.36	2.610	12	19.8	4	1	1	41.75	2.164	12	4.4
1	0	1	19.15	4.634	12	100.0	0	0	2	35.09	2.557	2	42.0	3	3	0	42.95	2.106	6	21.6
1	2	0	21.49	4.136	6	0.6	3	2	0	35.77	2.510	6	1.3	3	0	2	43.20	2.094	12	13.6
2	1	0	21.49	4.136	6	6.1	2	3	0	35.77	2.510	6	1.7	2	4	0	43.78	2.068	6	0.2
1	1	1	22.36	3.975	12	1.0	1	0	2	36.06	2.490	12	1.2	5	0	1	45.06	2.012	12	4.9
2	0	1	23.81	3.736	12	2.7	4	0	1	37.27	2.412	12	34.0	2	2	2	45.64	1.988	12	0.5
3	0	0	24.40	3.647	6	55.1	1	4	0	37.67	2.388	6	3.4	5	1	0	46.19	1.965	6	0.5
1	2	1	27.74	3.216	12	56.9	4	1	0	37.67	2.388	6	0.7	3	1	2	46.43	1.956	12	0.4
2	1	1	27.74	3.216	12	61.4	1	1	2	37.95	2.371	12	1.1	1	3	2	46.43	1.956	12	0.5
2	2	0	28.25	3.159	6	0.3	2	0	2	38.87	2.317	12	2.6	2	4	1	47.42	1.917	12	1.3
3	1	0	29.43	3.035	6	0.9	2	3	1	40.01	2.254	12	10.4	4	2	1	47.42	1.917	12	1.1
1	3	0	29.43	3.035	6	3.2	3	2	1	40.01	2.254	12	10.4	4	0	2	48.74	1.868	12	13.1
3	0	1	30.09	2.970	12	4.3	5	0	0	41.25	2.188	6	1.7	1	5	1	49.70	1.835	12	0.5
4	0	0	32.74	2.736	6	42.6	1	2	2	41.51	2.175	12	1.5	5	1	1	49.70	1.835	12	0.3

Cancrinite

CAN



GIS

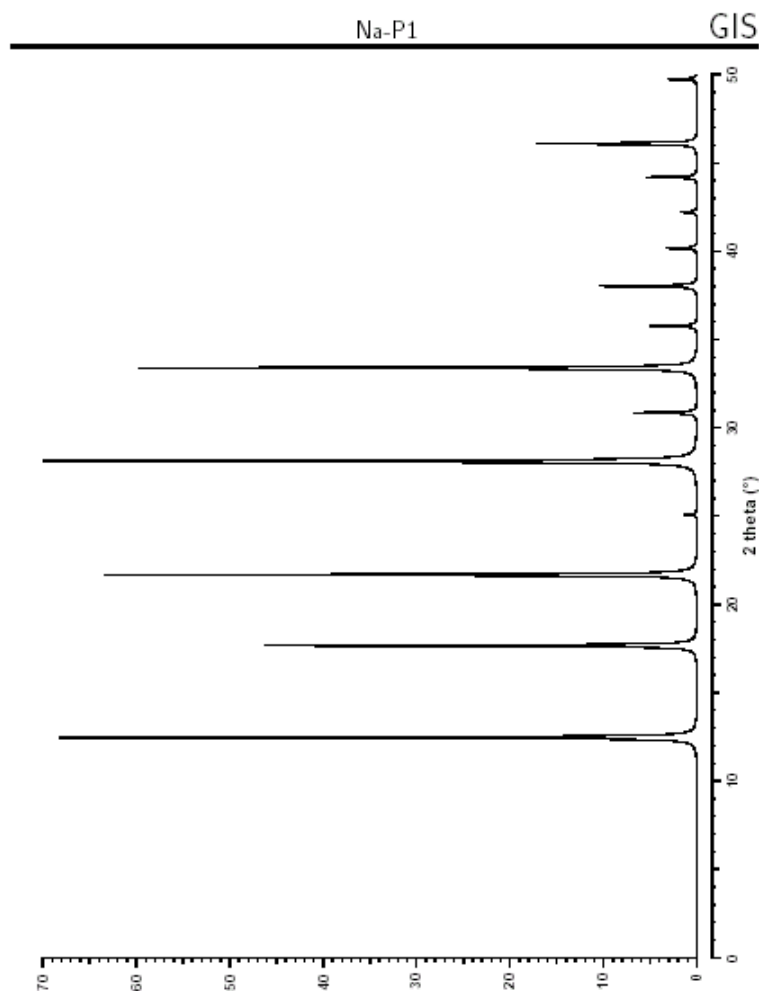
Na-P1

CHEMICAL COMPOSITION: $[\text{Na}_6(\text{H}_2\text{O})_{12}] [\text{Si}_{10}\text{Al}_6\text{O}_{32}]$ REFINED COMPOSITION: $[\text{Na}_{5.92}(\text{H}_2\text{O})_{11.28}] [\text{Si}_{9.92}\text{Al}_{6.08}\text{O}_{32}]$

CRYSTAL DATA: $\bar{1}\bar{1}$ (No. 82)
 $a = 10.043 \text{ \AA}$ $b = 10.043 \text{ \AA}$ $c = 10.043 \text{ \AA}$
 $\alpha = 90^\circ$ $\beta = 90^\circ$ $\gamma = 90^\circ$
 X-ray twinned crystal refinement, $R = 0.05$

REFERENCE: Ch. Baerlocher and W. M. Meier,
Z. Kristallogr. 135 339–354 (1972).

<i>h</i>	<i>k</i>	<i>l</i>	2θ	<i>d</i>	<i>M</i>	I_{rel}	<i>h</i>	<i>k</i>	<i>l</i>	2θ	<i>d</i>	<i>M</i>	I_{rel}	<i>h</i>	<i>k</i>	<i>l</i>	2θ	<i>d</i>	<i>M</i>	I_{rel}	
1	0	1	12.46	7.101	8	92.1	2	3	1	33.38	2.684	8	11.5	2	4	2	44.18	2.050	8	0.5	
1	1	0	12.46	7.101	4	1.0	1	3	2	33.38	2.684	8	12.7	2	2	4	44.18	2.050	8	0.4	
2	0	0	17.66	5.022	4	60.6	1	2	3	33.38	2.684	8	7.5	1	4	3	46.08	1.970	8	0.2	
0	0	2	17.66	5.022	2	2.7	0	0	4	35.76	2.511	2	6.8	3	1	4	46.08	1.970	8	0.1	
2	1	1	21.67	4.100	8	13.3	3	0	3	38.01	2.367	8	0.4	5	0	1	46.08	1.970	8	3.3	
1	1	2	21.67	4.100	8	66.1	4	1	1	38.01	2.367	8	0.6	5	1	0	46.08	1.970	4	2.2	
1	2	1	21.67	4.100	8	7.0	1	1	4	38.01	2.367	8	1.0	1	3	4	46.08	1.970	8	11.1	
2	0	2	25.08	3.551	8	0.8	3	3	0	38.01	2.367	4	0.3	4	3	1	46.08	1.970	8	0.9	
2	2	0	25.08	3.551	4	1.1	1	4	1	38.01	2.367	8	12.0	1	0	5	46.08	1.970	8	1.6	
3	1	0	28.10	3.176	4	1.6	4	0	2	40.15	2.246	8	1.4	4	1	3	46.08	1.970	8	2.0	
3	0	1	28.10	3.176	8	100.0	2	0	4	40.15	2.246	8	0.9	3	4	1	46.08	1.970	8	1.8	
1	0	3	28.10	3.176	8	34.9	4	2	0	40.15	2.246	4	2.3	2	5	1	49.72	1.834	8	0.2	
2	2	2	30.84	2.899	8	9.0	3	2	3	42.20	2.141	8	1.0	5	1	2	49.72	1.834	8	2.9	
2	1	3	33.38	2.684	8	3.5	2	3	3	42.20	2.141	8	0.3	2	1	5	49.72	1.834	8	0.7	
3	1	2	33.38	2.684	8	45.0	3	3	2	42.20	2.141	8	1.0	1	5	2	49.72	1.834	8	0.3	
3	2	1	33.38	2.684	8	1.2	4	2	2	44.18	2.050	8	6.5								

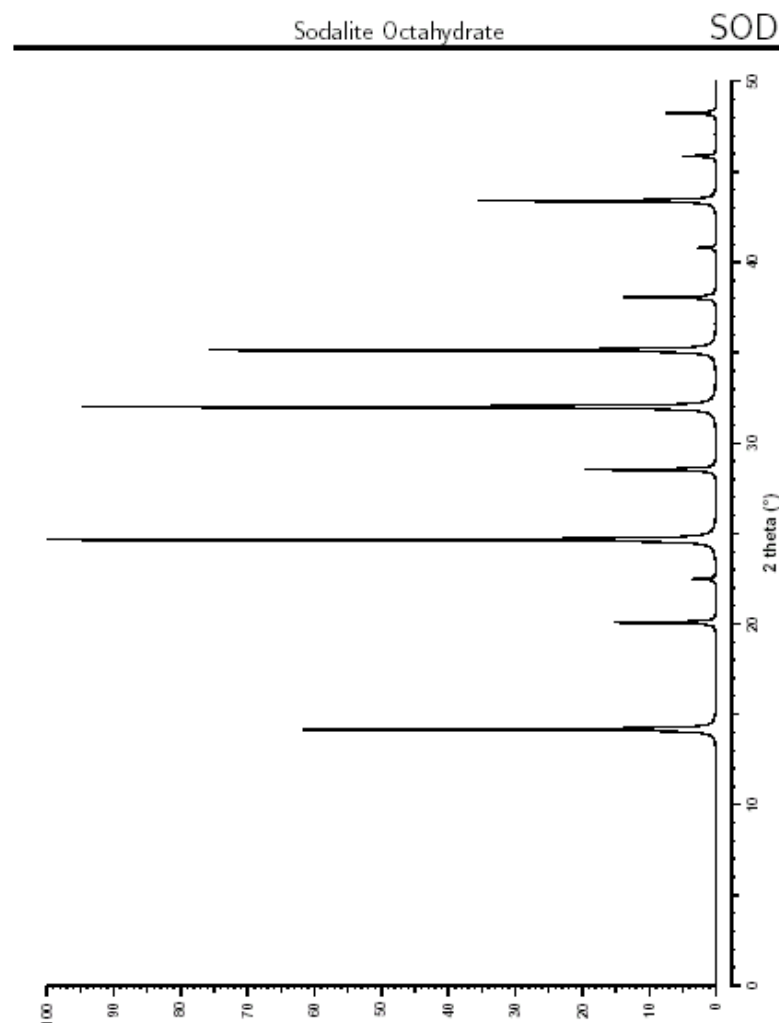


SOD

Sodalite Octahydrate

CHEMICAL COMPOSITION: $[\text{Na}_6(\text{H}_2\text{O})_8][\text{Si}_6\text{Al}_6\text{O}_{24}]$ REFINED COMPOSITION: $[\text{Na}_6(\text{H}_2\text{O})_8][\text{Si}_6\text{Al}_6\text{O}_{24}]$ CRYSTAL DATA: $P\bar{4}3m$ (No. 218) $a = 8.848 \text{ \AA}$ $b = 8.848 \text{ \AA}$ $c = 8.848 \text{ \AA}$ $\alpha = 90^\circ$ $\beta = 90^\circ$ $\gamma = 90^\circ$ X-ray Rietveld refinement, $R_{\text{wp}} = 0.091$, $R_{\text{p}} = 0.047$ REFERENCE: J. Felsche, S. Luger and Ch. Baerlocher,
Zeolites 6 367-372 (1986).

<i>h</i>	<i>k</i>	<i>l</i>	2θ	<i>d</i>	<i>M</i>	I_{rel}	<i>h</i>	<i>k</i>	<i>l</i>	2θ	<i>d</i>	<i>M</i>	I_{rel}	<i>h</i>	<i>k</i>	<i>l</i>	2θ	<i>d</i>	<i>M</i>	I_{rel}	
1	1	0	14.16	6.256	12	61.8	3	1	0	31.99	2.798	24	94.6	4	1	1	43.39	2.085	24	19.6	
2	0	0	20.07	4.424	6	15.1	2	2	2	35.13	2.554	8	75.7	4	2	0	45.86	1.978	24	4.9	
2	1	0	22.47	3.957	24	3.6	3	2	1	38.06	2.365	48	13.9	4	2	1	47.06	1.931	48	0.1	
2	1	1	24.65	3.612	24	100.0	4	0	0	40.79	2.212	6	2.7	3	3	2	48.24	1.886	24	7.5	
2	2	0	28.53	3.128	12	19.6	3	3	0	43.39	2.085	12	15.8								

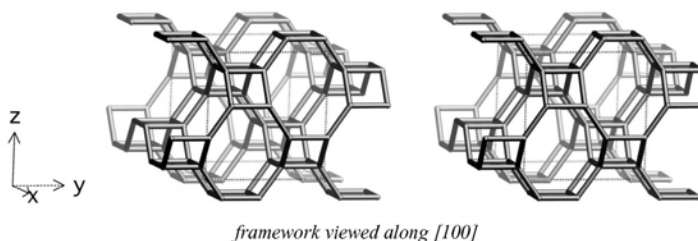


Appendix B

Atlas of zeolite structure types

GIS

Framework Type

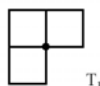
I4₁/amd

Idealized cell constants: tetragonal, I4₁/amd (origin choice 2), a = 9.8Å, c = 10.2Å

Coordination sequences and vertex symbols: T₁ (16, 2) 4 9 18 32 48 67 92 120 150 185 4-4-4-8₂-8-8

Secondary building units: 8 or 4

Loop configuration of T-Atoms:



Isotypic framework structures:

*Gismondine⁽¹⁾
 [Al-Co-P-O]-GIS⁽²⁾
 [Co-Al-P-O]-GIS⁽³⁾
 [Co-Ga-P-O]-GIS⁽⁴⁾
 [Co-P-O]-GIS⁽⁵⁾
 [Ga-Si-O]-GIS⁽⁶⁾
 [Mg-Al-P-O]-GIS⁽³⁾
 [Zn-Ga-P-O]-GIS⁽⁷⁾
 [(NH₄)₄][Zn₄B₄P₈O₃₂]-GIS⁽⁸⁾
 [Cs₄][Zn₄B₄P₈O₃₂]-GIS⁽⁸⁾
 [Rb₄][Zn₄B₄P₈O₃₂]-GIS⁽⁸⁾
 Amicite⁽⁹⁾
 Garronite^(10,11)

Gobbinsite⁽¹²⁾
 High-silica Na-P⁽¹³⁾
 Low-silica Na-P (MAP)⁽¹⁴⁾
 MAPO-43⁽¹⁵⁾
 MAPSO-43^(16,17)
 Na-P1⁽¹⁸⁾
 Na-P2⁽¹⁹⁾
 SAPO-43⁽²⁰⁾
 Synthetic Ca-garronite⁽²¹⁾
 Synthetic amicite⁽²²⁾
 Synthetic garronite⁽²²⁾
 Synthetic gobbinsite⁽²²⁾
 TMA-gismondine⁽²³⁾

Alternate designation: Gismondite (discredited)
 synthetic zeolite B (disused)

References:

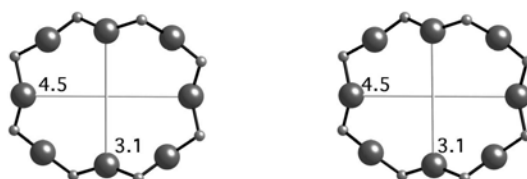
- (1) Fischer, K. and Schramm, V. *Adv. Chem. Ser.*, **101**, 250-258 (1971)
- (2) Feng, P.Y., Bu, X.H. and Stucky, G.D. *Nature*, **388**, 735-741 (1997)
- (3) Feng, P., Bu, X., Gier, T.E. and Stucky, G.D. *Microporous and Mesoporous Materials*, **23**, 221-229 (1998)
- (4) Cowley, A.R. and Chippindale, A.M. *Chem. Commun.*, 673-674 (1996)
- (5) Yuan, H.M., Chen, J.S., Zhu, G.S., Li, J.Y., Yu, J.H., Yang, G.D. and Xu, R. *Inorg. Chem.*, **39**, 1476-1479 (2000)

Gismondine

Type Material

GIS

Crystal chemical data:	[Ca ²⁺ ₄ (H ₂ O) ₁₆] [Al ₈ Si ₈ O ₃₂]-GIS monoclinic, P112 ₁ /a a = 9.843Å, b = 10.023Å, c = 10.616Å, γ = 92.417° ⁽¹⁾ (Relationship to unit cell of Framework Type: a' = a, b' = b, c' = c)
Framework density:	15.3 T/1000Å ³
Channels:	{[100] 8 3.1 x 4.5 ↔ [010] 8 2.8 x 4.8}*** (variable due to considerable flexibility of the framework)



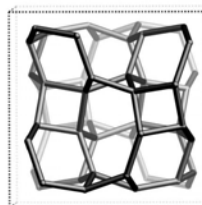
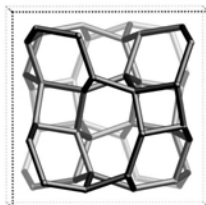
8-ring viewed along [100]

References (cont.):

- (6) Cho, H.H., Kim, S.H., Kim, Y.G., Kim, Y.C., Koller, H., Cambor, M.A. and Hong, S.B. *Chem. Mater.*, **12**, 2292-2300 (2000)
- (7) Chippindale, A.M., Cowley, A.R. and Peacock, K.J. *Microporous and Mesoporous Materials*, **24**, 133-141 (1998)
- (8) Kniep, R., Schäfer, G., Engelhardt, H. and Boy, I. *Angew. Chem. Int. Ed.*, **38**, 3642-3644 (1999)
- (9) Alberti, A. and Vezzalini, G. *Acta Crystallogr.*, **B35**, 2866-2869 (1979)
- (10) Artioli, G. *Am. Mineral.*, **77**, 189-196 (1992)
- (11) Artioli, G. and Marchi, M. *Powder Diffraction*, **14**, 190-194 (1999)
- (12) McCusker, L.B., Baerlocher, Ch. and Nawaz, R. *Z. Kristallogr.*, **171**, 281-289 (1985)
- (13) Håkansson, U., Fälvh, L. and Hansen, S. *Acta Crystallogr.*, **C46**, 1363-1364 (1990)
- (14) Albert, B.R., Cheetham, A.K., Stuart, J.A. and Adams, C.J. *Microporous and Mesoporous Materials*, **21**, 133-142 (1998)
- (15) Pluth, J.J., Smith, J.V. and Bennett, J.M. *J. Am. Chem. Soc.*, **111**, 1692-1698 (1989)
- (16) Flanigen, E.M., Lok, B.M., Patton, R.L. and Wilson, S.T. *Pure Appl. Chem.*, **58**, 1351-1358 (1986)
- (17) Flanigen, E.M., Lok, B.M., Patton, R.L. and Wilson, S.T. In *Proc. 7th Int. Zeolite Conf.*, (eds. Y. Murakami, A. Iijima and J.W. Ward), pp. 103-112 (1986), Kodansha, Tokyo
- (18) Baerlocher, Ch. and Meier, W.M. *Z. Kristallogr.*, **135**, 339-354 (1972)
- (19) Hansen, S., Håkansson, U. and Fälvh, L. *Acta Crystallogr.*, **C46**, 1361-1362 (1990)
- (20) Helliwell, M., Kaucic, V., Cheetham, G.M.T., Harding, M.M., Kariuki, B.M. and Rizkallah, P.J. *Acta Crystallogr.*, **B49**, 413-420 (1993)
- (21) Schropfer, L. and Joswig, W. *Eur. J. Mineral.*, **9**, 53-65 (1997)
- (22) Ghobarkar, H. and Schaefer, O. *Mater. Res. Bull.*, **34**, 517-525 (1999)
- (23) Baerlocher, Ch. and Meier, W.M. *Helv. Chim. Acta*, **53**, 1285-1293 (1970)

ANA

Framework Type

Ia $\bar{3}$ d

framework viewed along [001]

Idealized cell constants:	cubic, Ia $\bar{3}$ d, a = 13.6Å	
Coordination sequences and vertex symbols:	T ₁ (48, 2) 4 10 22 39 60 87 118 154 196 242	4-4-6-6-8 ₄ -8 ₄
Secondary building units:	6-2 or 6 or 4	
Loop configuration of T-Atoms:		
Isotypic framework structures:	*Analcime ⁽¹⁻³⁾ [Al-Co-P-O]-ANA ⁽⁴⁾ [Al-Si-P-O]-ANA ⁽⁵⁾ [Ga-Ge-O]-ANA ⁽⁶⁾ [Cs-Na-(H ₂ O)] [Ga-Si-O]-ANA ⁽⁷⁾ [Cs ₁₆][Cu ₈ Si ₄₀ O ₉₆]-ANA ⁽⁸⁾ [K-][B-Si-O]-ANA ⁽⁹⁾ AlPO ₄ -24 ⁽¹⁰⁾ AlPO ₄ -pollucite ⁽¹¹⁾ Ammonioleucite ⁽¹²⁾ Ca-D ⁽¹³⁾ Cs beryllosilicate pollucite ⁽¹⁴⁾	Cs,Fe silicate pollucite ⁽¹⁵⁾ Hsianghualite ⁽¹⁶⁾ Kehoeite ⁽¹⁷⁾ Leucite ⁽¹⁸⁾ Na-B ⁽¹⁹⁾ Pollucite ⁽²⁰⁾ Synthetic analcime ⁽²¹⁾ Synthetic hsianghualite ⁽²²⁾ Synthetic wairakite ⁽²³⁾ Wairakite and additional compositional variants ⁽²⁴⁾
Alternate designation:	Analcite	

References:

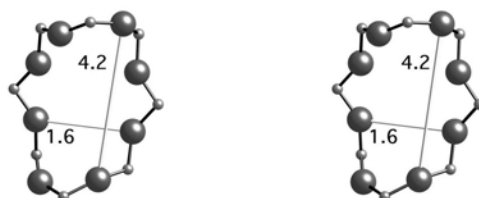
- (1) Taylor, W.H. *Z. Kristallogr.*, **74**, 1-19 (1930)
- (2) Knowles, C.R., Rinaldi, F.F. and Smith, J.V. *Indian Mineral.*, **6**, 127- (1965)
- (3) Ferraris, G., Jones, D.W. and Yerkess, J. *Z. Kristallogr.*, **135**, 240-252 (1972)
- (4) Feng, P.Y., Bu, X.H. and Stucky, G.D. *Nature*, **388**, 735-741 (1997)
- (5) Artioli, G., Pluth, J.J. and Smith, J.V. *Acta Crystallogr.*, **C40**, 214-217 (1984)
- (6) Bu, X., Feng, P., Gier, T.E., Zhao, D. and Stucky, G.D. *J. Am. Chem. Soc.*, **120**, 13389-13397 (1998)

Analcime	Type Material	ANA
----------	---------------	-----

Crystal chemical data: $[\text{Na}^+_{16}(\text{H}_2\text{O})_{16}][\text{Al}_{16}\text{Si}_{32}\text{O}_{96}]$ -ANA
cubic, $Ia\bar{3}d$, $a = 13.73\text{\AA}$ ⁽³⁾

Framework density: 18.5 T/1000 \AA^3

Channels: irregular channels formed by highly distorted 8-rings

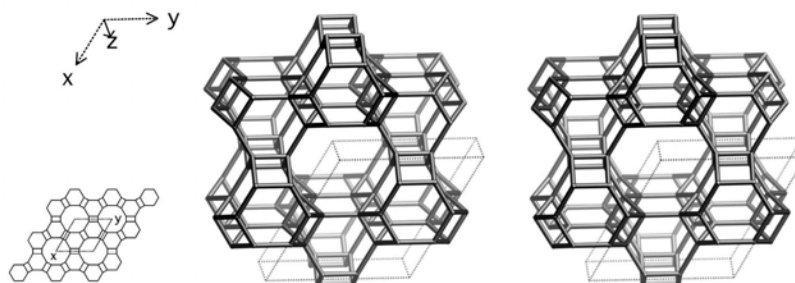


distorted 8-ring viewed along [110]

References (cont.):

- (7) Yelon, W.B., Xie, D., Newsam, J.M. and Dunn, J. *Zeolites*, **10**, 553-558 (1990)
- (8) Heinrich, A.R. and Baerlocher, Ch. *Acta Crystallogr.*, **C47**, 237-241 (1991)
- (9) Millini, R., Montanari, L. and Bellussi, G. *Microporous Materials*, **1**, 9-15 (1993)
- (10) Wilson, S.T., Lok, B.M., Messina, C.A., Cannan, T.R. and Flanigen, E.M. *J. Am. Chem. Soc.*, **104**, 1146-1147 (1982)
- (11) Keller, E.B. *Ph.D. Thesis, ETH, Zürich, Switzerland*, (1987)
- (12) Hori, H., Nagashima, K., Yamada, M., Miyawaki, R. and Marubashi, T. *Am. Mineral.*, **71**, 1022-1027 (1986)
- (13) Ames, L.L. and Sand, L.B. *Am. Mineral.*, **43**, 476-480 (1958)
- (14) Torres-Martines, L.M., Gard, J.A., Howie, R.A. and West, A.R. *J. Solid State Chem.*, **51**, 100-103 (1984)
- (15) Kopp, O.C., Harris, L.A., Clark, G.W. and Yakel, H.L. *Am. Mineral.*, **48**, 100-109 (1963)
- (16) Wen-Hui, H., Saho-Hua, T., Kung-Hai, W., Chun-Lin, C. and Cheng Chi, Y. *Am. Mineral.*, **44**, 1327-1328 (1959)
- (17) McConnell, D. and Foreman Jr., D.W. *Can. Mines*, **12**, 352- (1974)
- (18) Peacor, D.R. *Z. Kristallogr.*, **127**, 213-224 (1968)
- (19) Barrer, R.M. and White, E.A.D. *J. Chem. Soc.*, 1561-1571 (1952)
- (20) Nel, H.J. *Am. Mineral.*, **29**, 443-451 (1944)
- (21) Ghobarkar, H. and Franke, W. *Cryst. Res. Technol.*, 1071-1075 (1986)
- (22) Ghobarkar, H., Schaefer, O. and Knauth, P. *Annal. Chimie, Science Matériaux*, **24**, 209-215 (1999)
- (23) Ghobarkar, H. *Cryst. Res. Technol.*, K90-92 (1985)
- (24) Takeuchi, Y., Mazzi, F., Haga, N. and Galli, E. *Am. Mineral.*, **64**, 993-1001 (1979)

CAN **Framework Type** **P6₃/mmc**



framework viewed along [001] (bottom left: projection down [001])

Idealized cell constants:	hexagonal, P6 ₃ /mmc, a = 12.5Å, c = 5.3Å	
Coordination sequences and vertex symbols:	T ₁ (12, m) 4 10 20 34 54 78 104 134 168 210	4-6-4-6-6-6
Secondary building units:	4-2 or 6 or 4	
Loop configuration of T-Atoms:		
Framework description:	AB sequence of 6-rings	
Isotypic framework structures:	*Cancrinite ^(1,2) [Al-Ge-O]-CAN ⁽³⁾ [Ga-Si-O]-CAN ⁽⁴⁾ [Zn-P-O]-CAN ⁽⁵⁾ Basic cancrinite ^(6,7) Cancrinite hydrate ⁽⁸⁾	Davyne ⁽⁹⁾ ECR-5 ⁽¹⁰⁾ Microsommite ⁽¹¹⁾ Synthetic cancrinite ⁽¹²⁾ Tiptopite ⁽¹³⁾ Vishnevite ⁽¹⁴⁾

References:

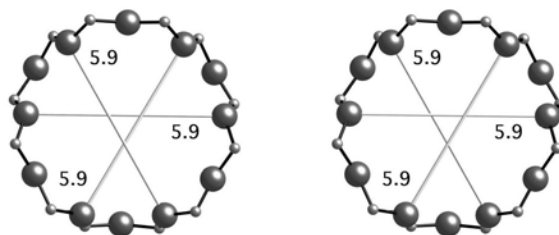
- (1) Pauling, L. *Proc. Natl. Acad. Sci.*, **16**, 453-459 (1930)
- (2) Jarchow, O. *Z. Kristallogr.*, **122**, 407-422 (1965)
- (3) Belokoneva, E.L., Uvarova, T.G. and Dem'yanets, L.N. *Sov. Phys. Crystallogr.*, **31**, 516-519 (1986)
- (4) Newsam, J.M. and Jorgensen, J.D. *Zeolites*, **7**, 569-573 (1987)
- (5) Yakubovich, O.V., Karimova, O.V. and Mel'nikov, O.K. *Crystallogr. Reports*, **39**, 564-568 (1994)
- (6) Barrer, R.M. and White, E.A.D. *J. Chem. Soc.*, 1561-1571 (1952)
- (7) Bresciana Pahor, N., Calligaris, M., Nardin, G. and Randaccio, L. *Acta Crystallogr.*, **B38**, 893-895 (1982)
- (8) Wyart, J. and Michel-Levy, M. *Compt. Rend.*, **229**, 131- (1949)
- (9) Hassan, I. and Grundy, H.D. *Can. Mineral.*, **28**, 341-349 (1990)
- (10) Vaughan, D.E.W. *E. Patent A-190,90* (1986)

Cancrinite**Type Material****CAN**

Crystal chemical data: $[\text{Na}^+_6 \text{Ca}^{2+} \text{CO}_3^{2-} (\text{H}_2\text{O})_2] [\text{Al}_6\text{Si}_6 \text{O}_{24}]$ -CAN
hexagonal, $P6_3$, $a = 12.75\text{\AA}$, $c = 5.14\text{\AA}$ ⁽²⁾

Framework density: 16.6 T/1000 \AA^3

Channels: [001] 12 5.9 x 5.9*



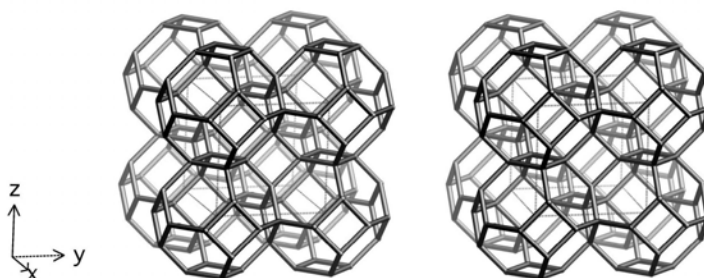
12-ring viewed along [001]

References (cont.):

- (11) Bonaccorsi, E., Comodi, P. and Merlino, S. *Phys. Chem. Mineral.*, **22**, 367-374 (1995)
- (12) Smolin, Y.I., Shepelev, Y.F., Butikova, I.K. and Kobaykov, I.B. *Kristallografiya*, **26**, 63-66 (1981)
- (13) Peacor, D.R., Rouse, R.C. and Ahn, J.-H. *Am. Mineral.*, **72**, 816-820 (1987)
- (14) Hassan, I. and Grundy, H.D. *Can. Mineral.*, **22**, 333-340 (1984)

SOD

Framework Type

Im $\bar{3}m$ 

framework viewed along [100]

Idealized cell constants:	cubic, Im $\bar{3}m$, a = 9.0Å	
Coordination sequences and vertex symbols:	T ₁ (12, $\bar{4}2m$)4 10 20 34 52 74 100 130 164 202	4-4-6-6-6-6
Secondary building units:	6-2 or 6 or 4	
Loop configuration of T-Atoms:		
Framework description:	ABC sequence of 6-rings	
Isotypic framework structures:	*Sodalite ^(1,2) [Al-Co-P-O]-SOD ⁽³⁾ [Al-Ge-O]-SOD ⁽⁴⁾ [Be-As-O]-SOD ⁽⁵⁾ [Be-P-O]-SOD ⁽⁵⁾ [Be-Si-O]-SOD ⁽⁶⁾ [Co-Ga-P-O]-SOD ⁽⁷⁾ [Ga-Co-P-O]-SOD ⁽³⁾ [Ga-Ge-O]-SOD ⁽⁴⁾ [Ga-Si-O]-SOD ⁽⁸⁾ [Zn-As-O]-SOD ⁽⁹⁾ [Zn-Ga-As-O]-SOD ⁽⁷⁾ [Zn-Ga-P-O]-SOD ⁽⁷⁾ [Zn-P-O]-SOD ⁽⁹⁾ [Ca ₈ (WO ₄) ₂][Al ₁₂ O ₂₄]-SOD ⁽¹⁰⁾	AlPO-20 plus numerous compositional variants ^(11,12) Basic sodalite ^(13,14) Bicchulite ⁽¹⁵⁾ Danalite ⁽¹⁶⁾ G ⁽¹⁷⁾ Genthelvite ⁽¹⁸⁾ Hauyn ⁽¹⁹⁾ Helvin ⁽²⁰⁾ Hydroxo sodalite ⁽²¹⁾ Nosean ⁽²²⁾ Silica sodalite ⁽²³⁾ TMA sodalite ⁽²⁴⁾ Tugtupite ^(25,26)

Sodalite	Type Material	SOD
----------	---------------	-----

Crystal chemical data:	[Na ⁺ ₈ Cl ₂] [Al ₆ Si ₆ O ₂₄]-SOD cubic, P4 ₃ n, a = 8.870Å ⁽²⁾
Framework density:	17.2 T/1000Å ³
Channels:	apertures formed by 6-rings only

References:

- (1) Pauling, L. *Z. Kristallogr.*, **74**, 213-225 (1930)
- (2) Loens, J. and Schulz, H. *Acta Crystallogr.*, **23**, 434-436 (1967)
- (3) Feng, P.Y., Bu, X.H. and Stucky, G.D. *Nature*, **388**, 735-741 (1997)
- (4) Bu, X., Feng, P., Gier, T.E., Zhao, D. and Stucky, G.D. *J. Am. Chem. Soc.*, **120**, 13389-13397 (1998)
- (5) Gier, T.E., Harrison, W.T.A. and Stucky, G.D. *Angew. Chem., Int. Ed.*, **30**, 1169-1171 (1991)
- (6) Dann, S.E. and Weller, M.T. *Inorg. Chem.*, **35**, 555-558 (1996)
- (7) Bu, X., Gier, T.E., Feng, P. and Stucky, G.D. *Microporous and Mesoporous Materials*, **20**, 371-379 (1998)
- (8) McCusker, L.B., Meier, W.M., Suzuki, K. and Shin, S. *Zeolites*, **6**, 388-391 (1986)
- (9) Nenoff, T.M., Harrison, W.T.A., Gier, T.E. and Stucky, G.D. *J. Am. Chem. Soc.*, **113**, 378-379 (1991)
- (10) Depmeier, W. *Acta Crystallogr.*, **C40**, 226-231 (1984)
- (11) Wilson, S.T., Lok, B.M., Messina, C.A., Camman, T.R. and Flanigen, E.M. *J. Am. Chem. Soc.*, **104**, 1146-1147 (1982)
- (12) Flanigen, E.M., Lok, B.M., Patton, R.L. and Wilson, S.T. In *Proc. 7th Int. Zeolite Conf.*, (eds. Y. Murakami, A. Iijima and J.W. Ward), pp. 103-112 (1986), Kodansha, Tokyo
- (13) Barrer, R.M. and White, E.A.D. *J. Chem. Soc.*, 1267-1278 (1951)
- (14) Hassan, I. and Grundy, H.D. *Acta Crystallogr.*, **C39**, 3-5 (1983)
- (15) Sahl, K. and Chatterjee, N.D. *Z. Kristallogr.*, **146**, 35-41 (1977)
- (16) Glass, J.J., Jahns, R.H. and Stevens, R.E. *Am. Mineral.*, **29**, 163-191 (1944)
- (17) Shishakova, T.N. and Dubinin, M.M. *Izv. Akad. Nauk SSSR*, 1303- (1965)
- (18) Merlino, S. In *Feldspars and Feldspathoids*, (ed. W.L. Brown), pp. 435-470 (1983), Reidel, Dordrecht
- (19) Loehn, J. and Schulz, H. *N. Jb. Miner. Abh.*, **109**, 201-210 (1968)
- (20) Glass, J.J., Jahns, R.H. and Stevens, R.E. *Am. Mineral.*, **29**, 163-191 (1944)
- (21) Felsche, J., Luger, S. and Baerlocher, Ch. *Zeolites*, **6**, 367-372 (1986)
- (22) Schulz, H. and Saalfeld, H. *Tschermaks Min. Petr. Mitt.*, **10**, 225-232 (1965)
- (23) Bibby, D.M. and Dale, M.P. *Nature*, **317**, 157-158 (1985)
- (24) Baerlocher, Ch. and Meier, W.M. *Helv. Chim. Acta*, **52**, 1853-1860 (1969)
- (25) Sorensen, H. *Am. Mineral.*, **48**, 1178 (1963)
- (26) Hassan, I. and Grundy, H.D. *Can. Mineral.*, **29**, 385-390 (1991)

Curriculum Vitae

NAME: Aphiruk Chaisena

DATE OF BIRTH: November 06, 1966

EDUCATIONAL BACKGROUND:

1986-1989 B.Ed. Chemistry, Rajabhat Institute Chiangmai, Thailand

1993-1995 M.S. Teaching Chemistry, Chiangmai University, Thailand

WORK EXPERIENCE:

1990-1992 Scientist, TCC International (1972), Thailand

1992-1997 Secondary school chemistry teacher, Ministry of Education, Thailand

1997-2000 Lecturer in chemistry, Rajabhat Institute Lampang, Thailand

SCHOLARSHIPS:

2000-2002 Scholarship from Office of Rajabhat Institute Council (ORIC)

2003 Visiting scholarship from Rajabhat Institute Lampang at The
University of Queensland and Queensland University of Technology

PRESENTATION:

“Effectiveness of thermal and acid treatments on some physico-chemical properties of Lampang diatomite”, 29th Congress on science and technology of Thailand, 20-22 October 2003, Khon Kean University

PUBLICATIONS:

1. “Effects of thermal and acid treatments on some physico-chemical properties of Lampang diatomite”, to be published in Suranaree Journal of Science and Technology (accepted)

2. “Synthesis of sodium zeolites from natural and modified diatomite”, to be published in Materials Letters (accepted)